CHAPTER 4

Mineral zoning and P-T-t paths for the early evolution of the central Arunta Block

Summary

Proterozoic high-grade gneisses and granofelses in the Strangways Metamorphic Complex and the Harts Range Group show contrasting P-T-t paths on the basis of mineral compositions and textures.   Rocks in the Strangways Metamorphic Complex preserve evidence for cooling with limited decompression and hydration after a high-temperature, low to moderate-pressure metamorphic peak (>880°C, ≤6.5 kbar) and before a second tectonometamorphic event at moderate temperature and pressure (750-800°C,~7.0 kbar). Rocks from the Harts Range Group preserve mineral compositions and textures that reflect cooling and hydration after the metamorphic peak, but at higher pressures (≥6.5 kbar) than the Strangways Metamorphic Complex.   However, they preserve no evidence for the second metamorphic event. The inferred P-T-t paths for the Strangways Metamorphic Complex and the Harts Range Group appear to have converged near the second tectonometamorphic event in the Strangways Metamorphic Complex, which may reflect southward thrusting of the Harts Range Group onto the Strangways Metamorphic Complex, during a crustal thickening event similar to a collisional style of tectonics. Inferred decompression during cooling in both the Strangways Metamorphic Complex and the Harts Range Group may imply contemporaneous but initially spatially separate peak metamorphism of the same protolith.   If they formed part of the same protolith, the metamorphic geotherm would have been higher to the south.   Thus, detailed analysis of P-T-t paths in ancient granulite facies terrains can reveal relatively subtle differences in the tectonometamorphic history of adjacent areas[4].

4.1 Introduction

The central Arunta Block consists of high-grade, multiply deformed Proterozoic rocks for which an isobaric cooling path after peak metamorphism has been inferred (Warren 1983a; Warren 1983b; Warren and Stewart, 1988). Anticlockwise pressure-temperature-time (P-T-t) paths, involving isobaric cooling from the metamorphic peak, appear to be common in Proterozoic terrains (Harley, 1989). In most high-grade terrains, including the central Arunta Block, the peak metamorphic assemblages occur as coarse-grained granoblastic minerals in layer-parallel foliations. The development of horizontal gneissic (recumbent) foliations during prograde granulite facies metamorphism has been attributed to crustal thickening processes (e.g. Bohlen, 1987). Similarly, upright structures and a penetrative foliation that accompanied low-pressure, high-temperature (LPHT) peak metamorphism in Proterozoic rocks in the Mt Isa inlier and the Broken Hill province may be responses to synmetamorphic crustal thickening (Loosveld and Etheridge, 1990; Hobbs et al., 1984; Clarke et al., 1987). However, the anomalously high geothermal gradients in Proterozoic rocks, associated with LPHT peak metamorphism and layer-parallel foliations have also been explained by models of lithospheric extension or collapse of a thickened crust (Sandiford, 1989; Sandiford and Powell, 1986; Chapter 2). Any tectonic model that attempts to explain the metamorphic history of Proterozoic rocks must reconcile the evidence for crustal thickening with the high geothermal gradients (possibly involving, lithospheric thinning). In order to determine the evolutionary path of a suite of rocks, it is essential that the chronology of deformation and metamorphism be well constrained and the relationship between deformation and metamorphism be determined. It is also important to delineate the relative changes in pressure and temperature between deformations, in order to understand the orogenic processes that may have been responsible for or a consequence of metamorphism. This chapter describes retrograde granulite facies mineral compositional zoning and textures from multiply deformed granofelses and gneisses from the Strangways Metamorphic Complex and the Harts Range Group in order to refine and clarify the early tectonometamorphic-time path and to provide a basis for interpreting the

early-mid Proterozoic tectonic evolution of the central Arunta Block (Chapter 6). The Strangways Metamorphic Complex occurs to the south of north-dipping mylonite zones, which separate it from the Harts Range Group in the north (Fig. 4.1). These mylonite zones preserve evidence for a reverse sense of movement, which postdated peak metamorphism and macroscopic folding of the Strangways Metamorphic Complex and the Harts Range Group.

The effects of a second granulite facies metamorphic event after hydration, cooling and limited decompression from the metamorphic peak are recognized in the Strangways Metamorphic Complex. This second event may have been associated with a widespread compressional deformation unlike, and separate from, the event(s) that were responsible for peak metamorphism (Norman and Clarke, 1990; Chapter 3). Consequently, a simple isobaric cooling history after the metamorphic peak cannot be applied to the Strangways Metamorphic Complex. In contrast, the mineralogy and mineral compositional zoning in the Harts Range Group, appear to reflect slightly higher pressure conditions during and after peak metamorphism. Moreover, the Harts Range Group shows no evidence of the second metamorphic event that affected the Strangways Metamorphic Complex. In this Chapter, it is suggested that the dissimilar P-T-t paths for Strangways Metamorphic Complex and the Harts Range Group may reflect spatially separate but contemporaneous metamorphism/deformation, cooling and decompression of one protolith rather than recording unrelated early-Proterozoic histories. This is despite the Harts Range Group comprising apparent amphibolite facies assemblages, which when analysed in detail, reflect granulite facies conditions. Another implication is that the use of orthopyroxene as a traditional indicator of granulite facies conditions in mafic rocks is not reliable. The second metamorphic event in the Strangways Metamorphic Complex is inferred to represent the effects of a widespread, south-directed compressional tectonic event, which was responsible for juxtaposing and overthrusting the stratigraphically lower Harts Range Group on to the Strangways Metamorphic Complex.
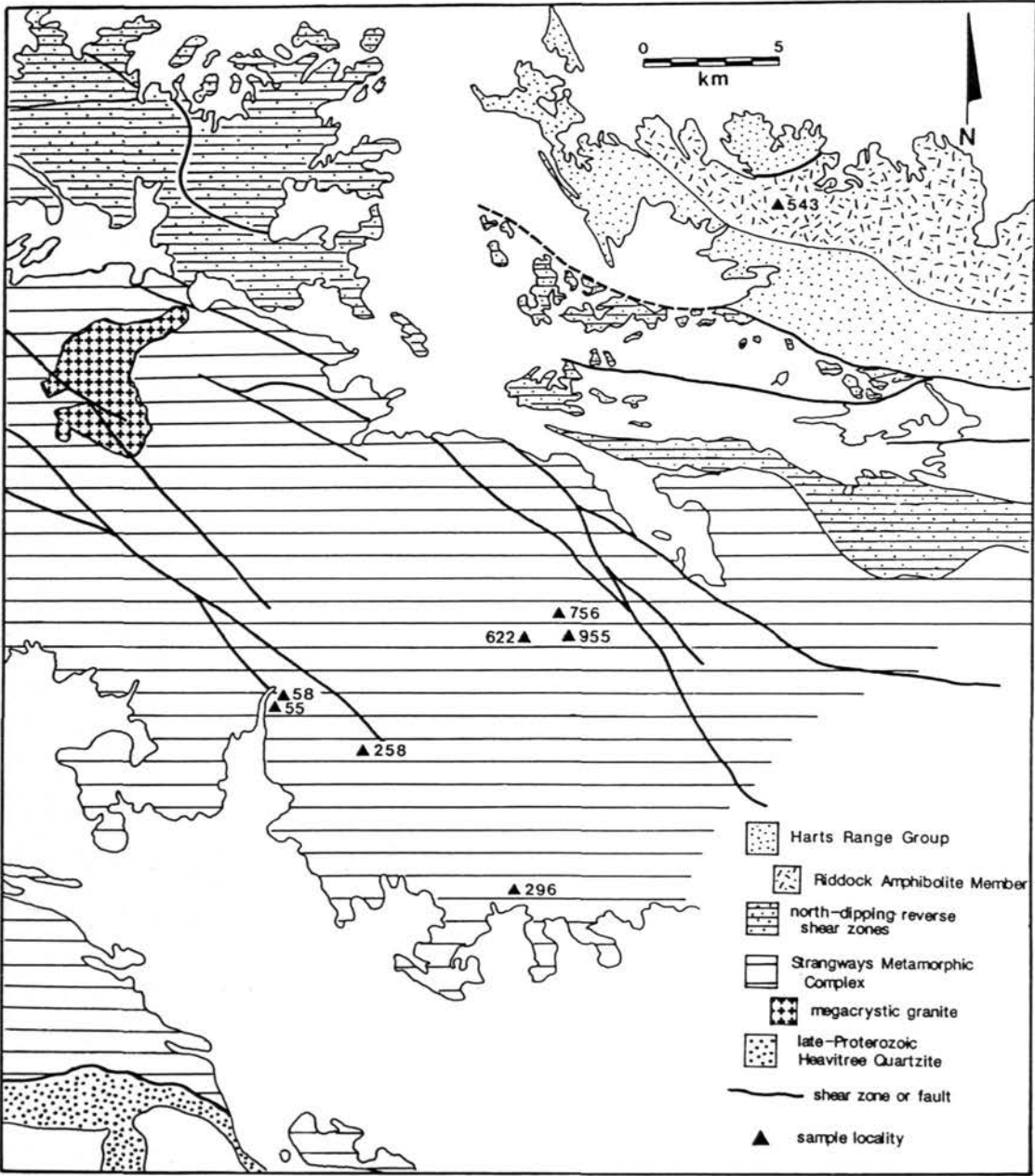
Fig. 4-1 Generalized geology of the central Arunta Block showing sample localities.

The map legend includes:

- Harts Range Group
- Riddock Amphibolite Member
- north-dipping reverse shear zones
- Strangways Metamorphic Complex
- megacrystic granite
- late-Proterozoic Heavitree Quartzite
- shear zone or fault
- ▲ sample locality

Sample localities shown: ▲543, ▲756, 622▲, ▲955, ▲58, ▲55, ▲258, ▲296

4.2 Geological Setting

The gneisses from the Strangways Metamorphic Complex described in this Chapter belong to the Ongeva granulites (Shaw et al., 1984a). Warren (1983a, 1983b) estimated peak metamorphic conditions of 8±1 kbar, 850-920°C and inferred near-isobaric cooling to a normal continental geotherm for rocks from the Strangways Metamorphic Complex. However, the justification for peak metamorphic conditions having been at lower pressures, namely 5.3±1.2 kbar (Norman and Clarke, 1990; Chapter 3) has been outlined in Chapter 3 (also Norman and Clarke, 1990). Oliver et al., (1988) also estimated early low pressure conditions of 6±1 kbar in the Strangways Metamorphic Complex. Evidence for a second distinct granulite facies metamorphism (M$_2$) has been recognized in these and similar rocks (Iyer et al. 1976; Norman and Clarke, 1990; Chapter 3). Norman and Clarke (1990) suggested that this second metamorphic event was associated with a crustal thickening deformation, which increased the lithospheric pressure and produced the macroscopic fold patterns in the Strangways Metamorphic Complex.

The Harts Range Group (Fig. 4.1) consists of folded, interlayered, garnet-bearing mafic gneisses, metapelitic gneisses, calc-silicate rocks and quartz-rich gneisses, which are cut by north-dipping mylonite zones that indicate a south-directed sense of shear. The Harts Range Group (Shaw et al., 1984b) has been subdivided into: (1) the Harts Range meta-igneous complex, which consists of mafic gneisses and plagioclase-rich gneisses; and (2) the Irindina supracrustal assemblage, which consists of quartzites, metapelites and calc-silicates. They have been interpreted as suites of metamorphosed basic igneous and volcano-sedimentary rocks (Sivell and Foden, 1985). The gneisses described in this Chapter belong to the the *Riddock Amphibolite Member* (Shaw et al., 1984b), which is part of the Harts Range meta-igneous complex of Sivell and Foden (1985).

The Riddock Amphibolite Member (Shaw et al., 1984b) forms a large, folded, garnet-bearing, mafic sheet in the Harts Range meta-igneous complex that is continuous for a distance of more than 60 km east of Mount Riddock. Other less continuous mafic layers also occur in the Harts Range meta-igneous complex and the Irindina supracrustal assemblage. The Riddock Amphibolite Member and mafic gneisses contain a tectonometamorphic gneissic foliation (S_2) that is defined by coarse-grained plagioclase-rich±garnet±amphibole leucosome layers and coarse-grained granoblastic layers of clinopyroxene-amphibole-plagioclase±garnet±quartz. S_2 is commonly sub-parallel to compositional boundaries. Due to the intensity of deformation associated with the development of S_2, the compositional layering has probably been rotated into parallelism with S_2. S_2 is folded by east-west trending, upright, tight to isoclinal folds (F_3) with shallow plunges. These folds form the dominant macroscopic fold pattern of rock units in the Harts Range Group (Chapter 6). Lineated amphibole occurs in the axial plane of F_3 folds in the Riddock Amphibolite Member and coarse-grained sillimanite-biotite clots are aligned in the axial planes of F_3 folds in the Irindina gneiss.

The mineral assemblages and mineral zoning of gneisses and granofelses in the Strangways Metamorphic Complex and the Harts Range Group appear to record only the early granulite facies evolution of the central Arunta Block. Near-isothermal decompression after cooling to the kyanite field has been inferred from phyllonitic gneisses similar to those in the Gough Dam Schist Zone (Warren, 1983a). This event probably represents erosion and uplift prior to late-Proterozoic deposition of intracratonic sediments in the Amadeus Basin. All metamorphism and deformation described in this Chapter occurred in the sillimanite stability field and predated shear-zone deformation and the decompression described by Warren (1983a).

4.3   Whole-Rock compositions

Average whole-rock analyses for mafic, felsic and metapelitic gneisses from the Ongeva granulites and metagabbros from the Harts Range Group (Sivell and Foden, 1985; Sivell et al., 1985; Sivell, 1988) are presented in Table 4.1 and shown on AFM,

Table 4.1 Whole-rock analyses from the Ongeva granulites and the Harts Range Group.

wt%	Ongeva granulites				Harts Range Group	
	felsic gneiss (average)	mafic gneiss (average)	ultramafic sample 955	metapelites (average)	metatholeiites[1]* (average)	garnet-bearing metagabbro[2]*
samples	20	11		12	8	
SiO_2	73.20	50.43	49.96	52.69	49.83	50.1
TiO_2	0.41	1.30	0.16	0.89	1.25	1.33
Al_2O_3	12.84	14.79	7.92	23.71	15.26	19.78
Fe_2O_3	1.33	3.22	1.70	5.67	1.40	1.21
FeO	1.39	8.21	2.94	5.43	9.32	8.06
MnO	0.02	0.13	0.15	0.13	0.21	0.23
MgO	0.52	7.24	13.85	3.31	8.48	4.35
CaO	1.31	10.57	22.81	0.83	10.25	11.09
Na_2O	2.21	2.21	0.21	0.95	2.00	2.03
K_2O	5.98	0.73	0.11	5.24	0.42	0.61
P_2O_4	0.07	0.14	0.03	0.05	0.13	0.19
H_2O+	0.32	0.55	0.59	0.82		
H_2O-	0.07	0.05	0.13	0.12		
CO_2	0.06	0.12	0.01	0.17		
TOTAL	99.73	99.69	100.55	99.99	99.59	99.99
X_{Mg}	39.96	61.13	89.36	61.87	49.02	

1. average of analyses from Sivell and Foden (1985), Sivell et al. (1985), Sivell, (1988)
2. From Sivell et al (1985)
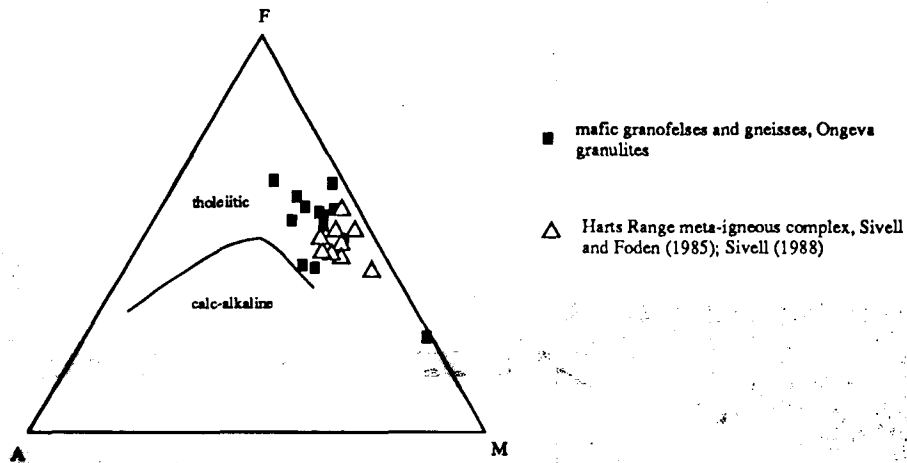* Fe^{2+} calculated assuming initial ratio for Fe of $Fe_2O_3/FeO = 0.15$

Fig. 4.2a AFM (wt%) diagram of mafic gneisses and granofelses from the Ongeva granulites and metagabbros from the Harts Range Group.
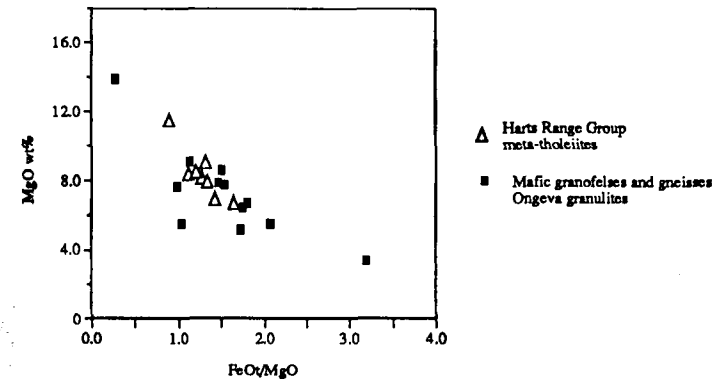A=Na₂O+K₂O; F=FeO+0.8998 Fe₂O₃; M=MgO.

Fig. 4.2b MgO versus FeOT/MgO for mafic gneisses and granofelses from the Ongeva granulites and meta-gabbros from the Harts Range Group.
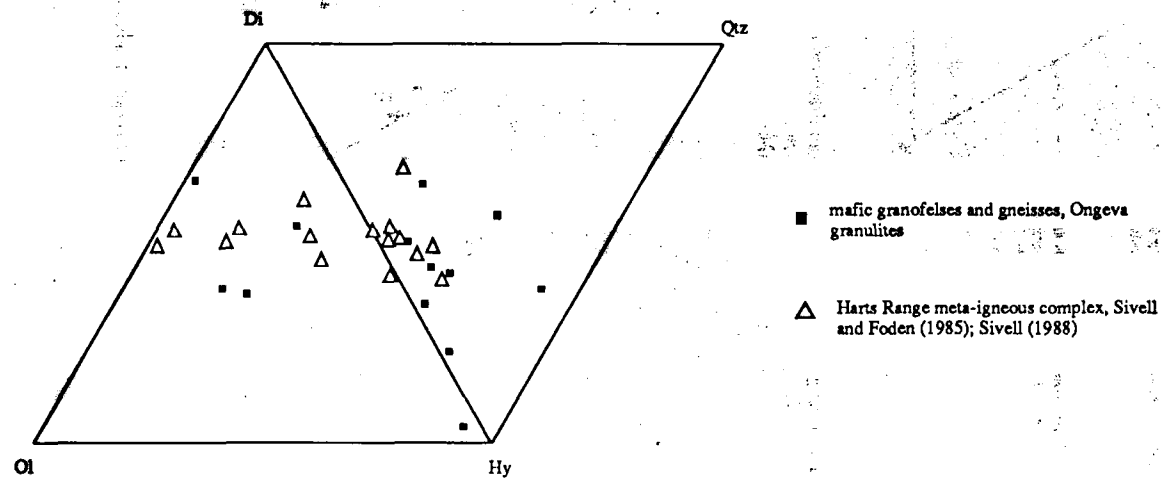
Fig. 4.2c Normative mineralogy of mafic gneisses and granofelses from the Ongeva ganulites and metagabbros from the Harts Range Group, plotted on a diopside-hypersthene-olivine-nepheline-quartz diagram.

A

■ mafic granofelses and gneisses, Ongeva
   granulites

△ Harts Range meta-igneous complex, Sivell
   and Foden (1985); Sivell (1988), Sivell et
   al. (1985)

C   F
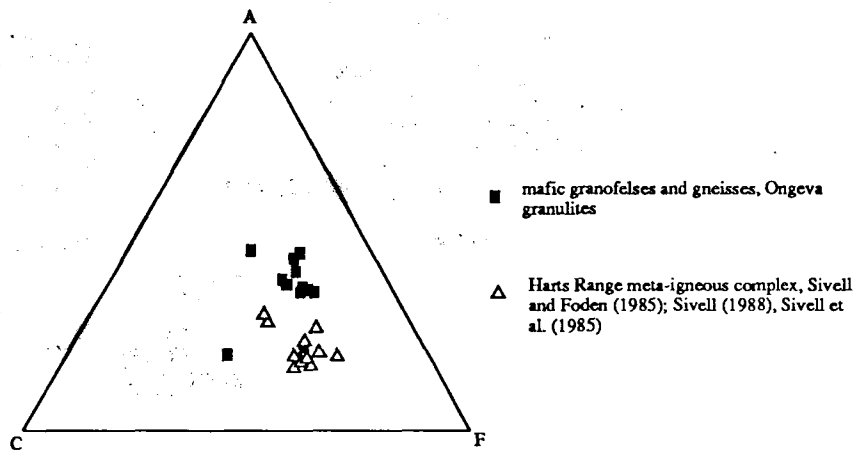
Fig. 4.3a ACF diagram of the molecular compositions of mafic gneisses and granofelses
from the Ongeva granulites and meta-gabbros from the Harts Range Group.
A=Al$_2$O$_3$+Fe$_2$O$_3$-(Na$_2$O+K$_2$O); C=CaO; F=MgO+FeO+MnO
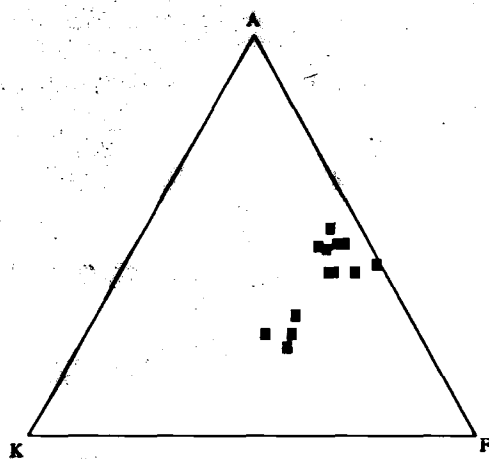

A

K   F

Fig. 4.3b AKF diagram of the molecular compositions of metapelites from
the Ongeva granulites.

135

ACF and AKF diagrams (Figs 4.2 and 4.3). On an AFM (wt%) diagram (Fig. 4.2a), mafic gneisses and an ultramafic rock from the Ongeva granulites plot along a distinct trend that is similar to the field for amphibolites from the Harts Range Group (Sivell et al., 1985). Mafic granofelses and gneisses are common in the Strangways Metamorphic Complex and have a bulk chemical composition very similar to amphibolites studied by Spear (1981), in which the chemical variation of amphiboles with changing P, T and f_{O_2} was examined. The Harts Range metagabbros and mafic rocks from the Ongeva granulites are inferred to be metamorphosed olivine tholeiites and also have similar Fe enrichment trends (Fig. 4.2b). They have similar normative mineralogy (Fig. 4.2c) and Y-Cr contents, which are characteristic of MOR basalts (after Pearce et al., 1984). However, the Harts Range Group metagabbros and mafic gneisses from the Ongeva granulites can be distinguished on a molecular ACF diagram (Fig. 4.3a). The Harts Range Group mafic rocks, including garnet-bearing meta-gabbros, have a lower molecular $Al_2O_3+Fe_2O_3-(Na_2O+K_2O)$ ratio than mafic rocks from the Ongeva granulites, which reflects lower Na contents. In all rocks, the mineral assemblages produced during metamorphism depend mostly on the initial whole-rock compositions. The appearance of garnet in mafic rocks such as quartz tholeiites and alkali olivine basalts (with changing P and T) is well constrained by experimental work (Green and Ringwood, 1967; Wood, 1987; Ito and Kennedy, 1971). Therefore, mafic gneisses from the Harts Range Group and the Ongeva granulites that have similar whole-rock compositions, but different mineral parageneses, reflect different metamorphic histories.

The well-layered felsic gneisses of the Strangways Metamorphic Complex have been interpreted as bimodal igneous suites of extrusive and shallow intrusive rocks that formed in an intra-continental or continental-margin rift setting (Shaw et al., 1979; Shaw et al., 1984a, 1984b; Sivell and Foden, 1985), with minor interlayered tuffs, tephras and arkosic sediments (Chapter 1). Metapelitic gneisses interlayered with these rocks have been interpreted as immature arkosic, continental sediments (Chapter 1).

4.4   Petrography and mineral compositions

The petrography and mineral chemical compositions of gneisses and granofelses from the Ongeva granulites are described, in order to refine our understanding of the early metamorphic evolution of the Strangways Metamorphic Complex. The petrography and mineral chemical compositions of a garnet-bearing mafic gneiss from the Riddock Amphibolite Member is also described, in order to delineate the early metamorphic evolution of the Harts Range Group.   A detailed analysis of the compositions of zoned minerals can provide more information on the metamorphic evolution of the terrains. Although temperature estimates using core and rim mineral compositions give an indication of the relative changes in temperature, accurate absolute estimates of temperature on the basis of zoned profiles are difficult to obtain.   This is because the core composition of many minerals does not reflect peak metamorphism due to continual ionic diffusion between minerals during cooling or because of intra-grain re-equilibration between rim and core compositions.   Nevertheless with care, the nature of mineral zoning together with mineral parageneses, mineral textures and petrogenetic grids can provide important information in delineating the P-T-t path.

Mineral analyses were obtained at Macquarie University using wds and eds systems on a ETEC microprobe at 15 Kev and specimen current of 50 nA. The mineral assemblages and their structural/metamorphic relationships are summarized in Table 3.1. Mineral compositions are presented in Tables 4.2-4.7 at the end of section 4.42 and sample localities are shown in Fig. 4.1.   Mineral zoning profiles are shown in Fig. 4.4. The component composition of pyroxenes was determined using methods outlined by Lindsley (1983) and using the nomenclature of Poldervaart and Hess (1951). Amphibole nomenclature and site occupancy follow Hawthorne (1981).

4.41 Ongeva granulites

mafic granofels (sample 258)

The gneissic layering (S_2) in mafic granofelses is defined by medium to coarse-grained granoblastic orthopyroxene-clinopyroxene-hornblende mesosomes and plagioclase-rich leucosomes that may contain subidioblastic, coarse-grained orthopyroxene. More felsic mafic gneisses may contain quartz and biotite. Garnet is not found in any mafic granofelses or gneisses.

Sample 258 is a mafic granofels that consists of coarse-grained, granoblastic clinopyroxene, orthopyroxene, plagioclase and amphibole. Recrystallized grain boundaries or symplectic intergrowths of fine-grained aggregates between these large grains. Representative microprobe analyses from sample 258 are presented in Table 4.2. The coarse-grained granoblastic clinopyroxene is augite ($X_{En} = 0.43$-0.44) and is zoned with Al^T and Fe^{2+} decreasing, and Mg and Ca increasing, from the core to the rim (Fig. 4.4a). Clinopyroxene may contain orthopyroxene lamellae, which are also chemically zoned along the length of the lamella. The coarse-grained granoblastic orthopyroxene is hypersthene ($X_{En} = 0.53$-0.54) and is zoned with Al^T and Fe^{2+} increasing and Mg and Ca decreasing from the core to the rim (Fig. 4.4a). Coarse-grained green-brown hornblende is ferroan pargasite. Although zoning in hornblende is difficult to recognize, hornblende rims are routinely lower in Al^{iv}, Ti, and Na and higher in Ca. Hornblende also contains a substantial Cl and F content. Coarse-grained plagioclase is labradorite ($X_{An} = 0.55$-0.58) and is not zoned.

On the basis of the mineral textures described in Chapter 3, the granoblastic orthopyroxene-clinopyroxene-plagioclase-hornblende assemblage and zoning profiles represent recrystallization due to M_1 and subsequent metamorphic conditions. The effects of M_2, a second metamorphic event, are characterized by: (1) recrystallized grain boundaries; (2) fine-grained symplectic intergrowths of orthopyroxene-plagioclase±clinopyroxene±hornblende at the interface between M_1 plagioclase and
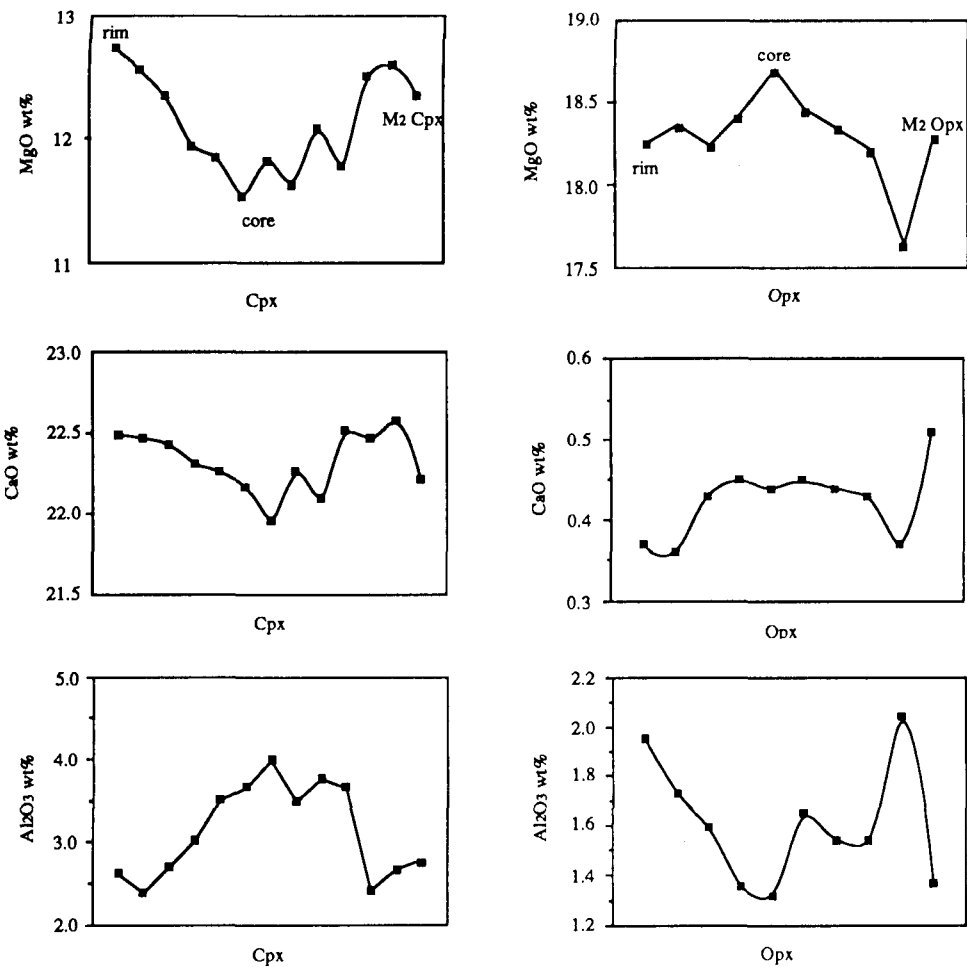
Fig. 4.4a MgO, CaO and Al2O3 (wt%) zoning profiles in clinopyroxene and orthopyroxene from a mafic granofels (sample 258), Ongeva granulites.
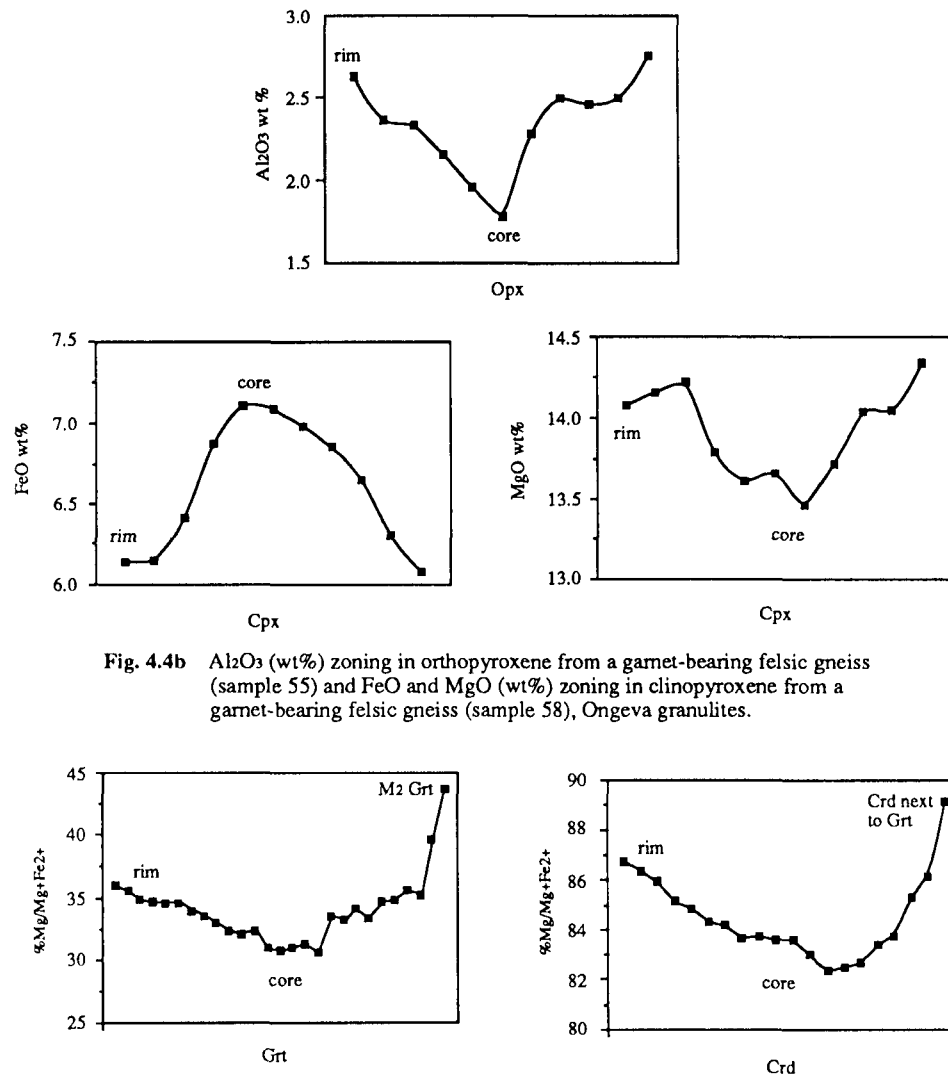
Fig. 4.4b Al2O3 (wt%) zoning in orthopyroxene from a garnet-bearing felsic gneiss (sample 55) and FeO and MgO (wt%) zoning in clinopyroxene from a garnet-bearing felsic gneiss (sample 58), Ongeva granulites.

Fig. 4.4c %XMg (Mg/Mg+Fe2+) zoning in garnet and cordierite from a metapelitic gneiss (sample 622), Ongeva granulites.

Fig. 4.4d Al₂O₃, FeO and MgO (wt%) zoning in clinopyroxene from a calc-silicate rock (sample 756), Ongeva granulites.
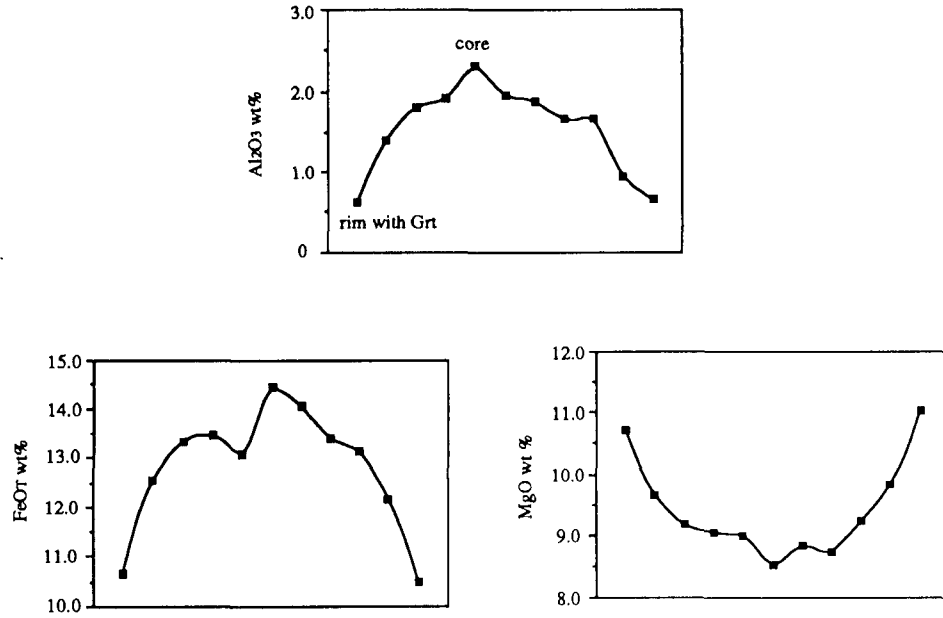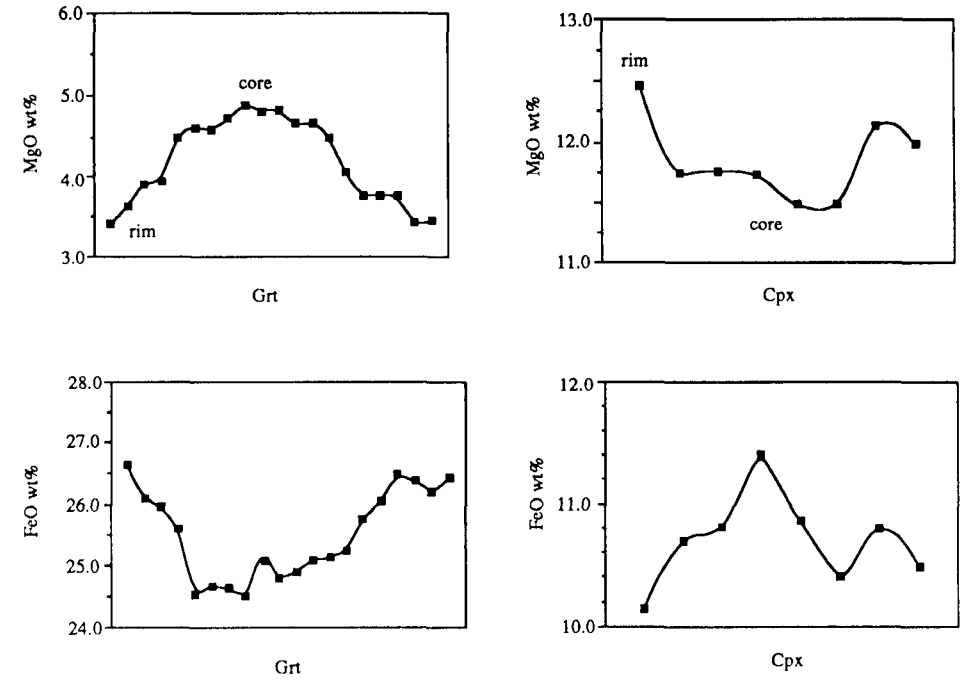
Fig. 4.4e FeO and MgO (wt%) zoning in garnet and clinopyroxene from the Riddock Amphibolite Member (sample 523), Harts Range Group.

hornblende (Figs 4.5a and 4.5b); (3) fine-grained plagioclase-clinopyroxene symplectites at the interface between M_1 clinopyroxene and hornblende; and (4) minor rims of blue-green ferroan pargasite on orthopyroxene. M_2 clinopyroxene and orthopyroxene have different compositions $\frac{from}{}$ M_1 pyroxene rims, but are similar to M_1 pyroxene cores (Table 4.2). M_2 clinopyroxene is augite ($X_{En} = 0.41$) and M_2 orthopyroxene is hypersthene ($X_{En} = 0.52$). Fine-grained M_2 hornblendes have a higher Ti, Al^{iv} and Na content and lower Ca compared with the coarse-grained hornblende rims and are similar in composition to the coarse-grained hornblende cores. The Cl and F content of M_2 hornblende is generally also higher than in the coarse-grained hornblende.

Ultramafic rock (sample 955)

Ultramafic rocks in the Strangways Metamorphic Complex are rare, but where they occur, they usually form boudins within deformed felsic gneisses. Fig. 4.6 shows ultramafic boudins (sample 955) in a hypersthene-bearing felsic gneiss on the limb of a tight to isoclinal F_3 fold. The boudins are intruded by coarse-grained quartz-K-feldspar-biotite pegmatite that probably crystallized after melt in areas of extension on the limbs of the fold. An S_2 leucosome foliation and a biotite S_{2b} foliation in the felsic gneiss are folded by F_3 (Fig. 4.6). The coarse-grained M_1 minerals in the felsic gneiss have been deformed, partly recrystallized and retrogressed. These microstructures may represent the effects of M_2. M_1 plagioclase usually has recrystallized grain boundaries and recrystallized quartz forms a lineated fabric in the axial plane of the F_3 fold. A well-developed quartz stretching lineation is parallel to the fold axis, which implies that recrystallization was synchronous with folding. In contrast, the ultramafic boudins do not show widespread recrystallization and grainsize reduction. Recrystallization of clinopyroxene and grainsize reduction are restricted to narrow, semi-planar zones that cut the boudins. The coarse-grained granoblastic minerals and the mineral composition in the ultramafic rock reflect the effects of M_1 and conditions prior to F_3 folding. Mesoscopic concentric zoning and recrystallization are absent from the ultramafic boudins, which implies that they were not affected by metasomatism during folding.

Fig. 4-5 (a) M_2 orthopyroxene-plagioclase symplectite at the interface of hornblende and M_1 plagioclase. Sample 258. Base of photograph is 1.75 mm.

4.5 (b) M_2 orthopyroxene-plagioclase symplectite at the interface of hornblende and M_1 plagioclase. Sample 258. Base of photograph is 1.75 mm.

4.5 (c) Clinopyroxene-spinel symplectite in an ultramafic rock, Ongeva granulites. Sample 955. Base of photograph is 1.75 mm.

4.5 (d) M_1 garnet and cordierite and M_2 orthopyroxene-sillimanite symplectite, across which, chemical zoning profiles are shown in Fig. 4.4c., Ongeva granulites. Sample 405. Base of photograph is 1.75 mm.

4.5 (e) M_1 cordierite pseudomorphed by M_2 orthopyroxene-sillimanite and sapphirine, Ongeva granulites. Sample 272. Base of photograph is 1.75 mm.
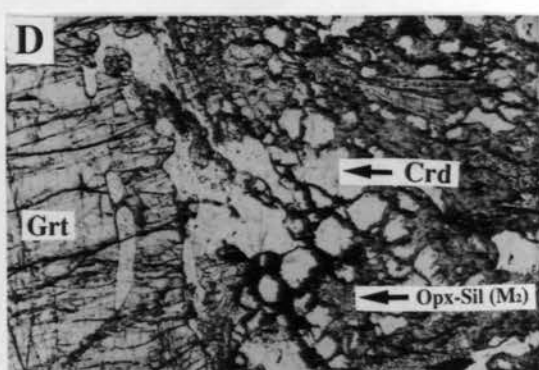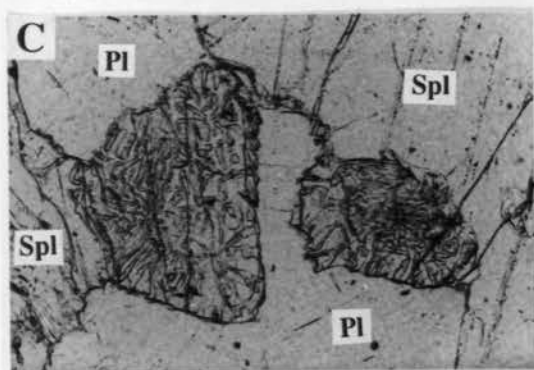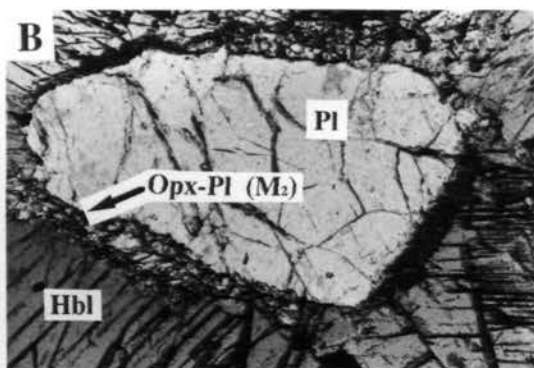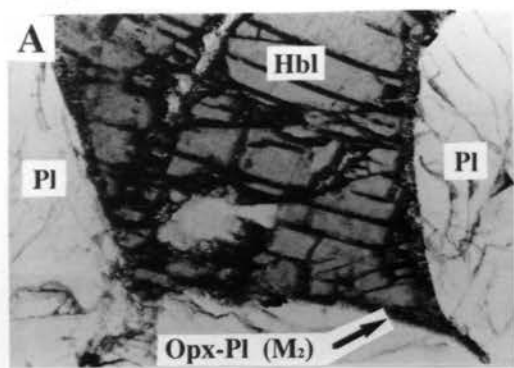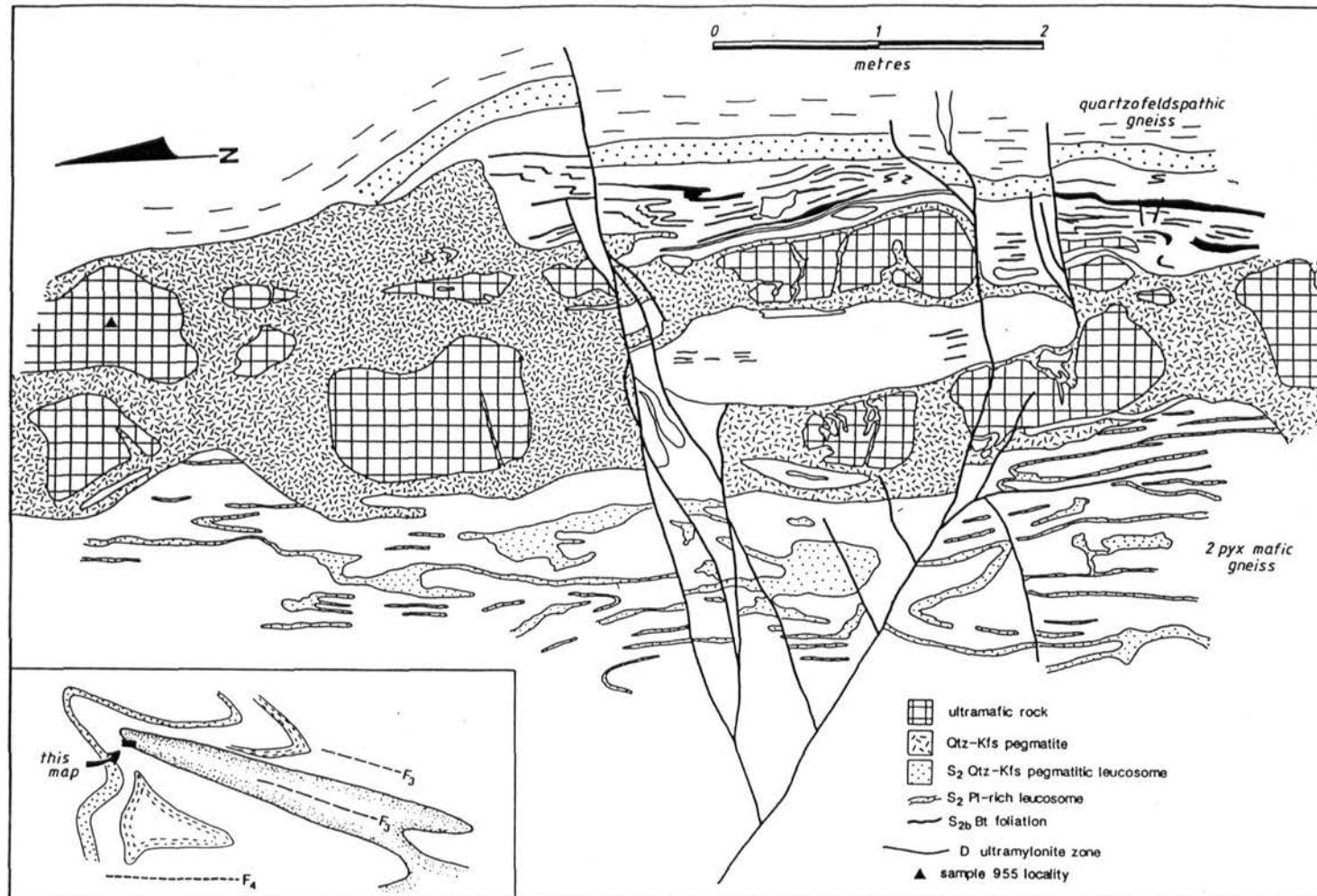
Fig. 4-6 Outcrop sketch of ultramafic boudins on the limb of an F_3 fold.

143

The ultramafic boudins are not foliated and do not contain igneous microstructures. They are composed of coarse-grained, granoblastic clinopyroxene (~70%), hornblende, and minor spinel and plagioclase. Representative microprobe analyses from an ultramafic rock are presented in Table 4.3. Clinopyroxene occurs as coarse-grained granoblastic grains and as symplectic intergrowths with spinel. The coarse-grained clinopyroxene is en⌒ diopside to diopside (X_{En} = 0.38-0.39) and is zoned with Al^T and Fe^{2+} decreasing and Mg increasing towards the rim, similar to the zoning profiles of clinopyroxenes from mafic granofelses. Symplectic intergrowths of spinel and diopside occur between the coarse-grained spinel and diopside, and appear to have replaced granoblastic clinopyroxene (Fig. 4.5b). The symplectic clinopyroxene is diopside and has a similar composition to the granoblastic clinopyroxene cores, with a higher Al content than the granoblastic grain rims. Coarse-grained pale green hornblende with lower-birefringence rims occurs between the clinopyroxene grains. The hornblende is pargasite and the lower-birefringence rims appear to reflect a lower Al content. The spinel is gahnospinel with up to 4.61 wt% Zn and occurs as large grains or in symplectic intergrowths with clinopyroxene. Although Al content decreases slightly towards the rims of the large grains, spinel is not zoned. Medium-grained, granoblastic plagioclase (X_{An} = 0.99) commonly forms a rim around spinel.

Felsic gneisses (samples 58 and 55)

Felsic gneisses vary from equigranular, medium-grained, granoblastic, quartz-rich, K-feldspar-plagioclase-orthopyroxene gneisses and granofelses to garnet-bearing, K-feldspar-quartz-orthopyroxene-biotite migmatites. The proportion of plagioclase varies considerably. Sample 55 is a granoblastic garnet-orthopyroxene-quartz-plagioclase-perthite gneiss and sample 58 is a granoblastic garnet-clinopyroxene felsic gneiss. Representative microprobe analyses from samples 55 and 58 are presented in Table 4.4. Sample 55 also contains minor clinopyroxene, but not in microstructural equilibrium with orthopyroxene. The clinopyroxene occurs with garnet and may represent a small enclave of different bulk composition with an orthopyroxene-bearing felsic gneiss. The gneissic

144

foliation (S_2) in both samples is defined by coarse-grained leucosome layers. In sample 55, polygonal quartz and large equant grains of K-feldspar and plagioclase commonly have smaller equant orthopyroxene grains at the triple junctions. Garnet is poikiloblastic and occurs in S_2 leucosome layers folded by F_3. In sample 58, fine- to medium-grained clinopyroxene occurs between equant coarse-grained quartz and plagioclase. Garnet is composed of fine-grained aggregates, which occur with clinopyroxene. The assemblage garnet-plagioclase-quartz-K-feldspar±orthopyroxene±clinopyroxene represents the effects of peak metamorphism (M_1). The coarse-grained M_1 minerals in samples 55 and 58 have been partly deformed and recrystallized, but do not appear to be as extensively recrystallized and retrogressed as other felsic gneisses in the Ongeva granulites.

In sample 58, clinopyroxene is en diopside to diopside ($X_{En} = 0.47$-0.46) and garnet is almandine-rich ($X_{Alm} = 0.40$, $X_{Pyp} = 0.26$, $X_{Grs} = 0.21$). Clinopyroxene is zoned with Al^T and Fe^T decreasing and Mg slightly increasing towards the grain rims (Fig. 4.4b), similar to clinopyroxene zoning in sample 55. Although garnet appears to have slightly higher X_{Mg} rims than cores, which reflects an increase in Mg and a decrease in Fe towards the grain margins, the garnet-clinopyroxene K_d values (Ellis and Green, 1979) tend to increase towards the grain margins. Plagioclase is bytownite ($X_{An} = 0.89$) and is generally unzoned, but tends to have a higher Na content in the grain margins adjacent to clinopyroxene and garnet.

In sample 55, orthopyroxene is hypersthene ($X_{En} = 0.49$-0.51) and garnet is almandine-pyrope ($X_{Alm} = 0.29$, $X_{Pyp} = 0.27$, $X_{Sps} = 0.23$). Both have high Mn contents. Orthopyroxene is zoned, with Al_2O_3 (wt%) increasing (Fig. 4.4b) and Ca content decreasing slightly towards the rim. Orthopyroxene cores have a low-Al content (1.78 wt%), unlike the composition of the grain margins (up to 2.63 wt%). Zoning in garnet is difficult to recognize because the garnet is generally fine-grained and poikiloblastic. However, the garnet grains appear to have lower X_{Mg} rims, which reflects a decrease in Mg and an increase in Fe towards the margins. Garnet-orthopyroxene K_d values (Harley, 1984a) also increase from the cores to the rims. Minor

clinopyroxene in sample 55 is zoned with Al^T and Fe decreasing and Mg increasing towards the grain rims. Garnet-clinopyroxene K_d values (Ellis and Green, 1979) also increase from the cores to the rims. Plagioclase (X_{An} = 0.93) is generally not zoned, but tends to be more sodic (X_{An} = 0.88) adjacent to orthopyroxene and garnet. Fine-grained biotite occurs with ferro-hastingsitic hornblende as clots around titanomagnetite and as rims on orthopyroxene. Biotite and ferro-hastingsitic hornblende are also aligned oblique to S_2, which may represent S_3 foliation.

Metapelite (sample 622)

Metapelites are characterized by abundant sillimanite, garnet, cordierite and biotite, and commonly grade into garnet-bearing felsic migmatites. Medium to coarse-grained feldspar-quartz±garnet±cordierite leucosome layers delineate a penetrative gneissic foliation (S_2). However, the most obvious foliation (S_{2b}) in the metapelites consists of poorly-lineated, coarse-grained sillimanite, large biotite grains and magnetite, which cuts the main gneissic foliation. An S_1 tectonometamorphic foliation is commonly preserved as folded inclusions trails of fine-grained sillimanite and of spinel-ilmenite in garnet and cordierite porphyroblasts. Cordierite occurs as elongate grains in S_2 or as granoblastic grains with quartz and K-feldspar in the S_2 leucosome foliation. The peak metamorphic (M_1) assemblage in metapelites probably included spinel and quartz with K-feldspar-sillimanite-ilmenite±garnet±cordierite. In cordierite gneisses, coarse-grained cordierite occurring in S_2 is partly replaced by a hypersthene-sillimanite-quartz±magnetite±biotite±sapphirine symplectite (Fig. 4.5c). This symplectite also envelops the coarse-grained S_{2b} sillimanite and represents a second metamorphic paragenesis (M_2) as discussed by Norman and Clarke (1990).

Sample 622 is a coarse-grained cordierite-garnet gneiss, which contains an orthopyroxene-sillimanite-quartz symplectite that partly replaces the cordierite (Fig. 4.5c). Representative microprobe analyses from sample 622 are presented in Table 4.5. Chemical zoning profiles across a large garnet porphyroblast (4 cm diameter) and granoblastic cordierite grains (1.25 cm diameter) are shown in Fig. 4.4c. Both garnet

and cordierite are richer in Mg towards the grain margins. Zoning (X_{Mg} = 0.31-0.37) is most pronounced in the garnet, which increases in Mg (7.65-9.04 wt%) and decreases in Fe (30.67-28.68 wt%) from the grain core to rim. Garnet also contains inclusions of biotite, which increase in X_{Mg} towards the garnet grain rims. Although zoning in cordierite is not well-developed, Mg zoning is evident in grains that are not adjacent to the garnet porphyroblast. Cordierite adjacent to garnet is more homogeneous in composition and has a similar Mg-rich composition to the rims of other grains (Fig. 4.4c).

Garnet porphyroblasts are separated from cordierite by a corona of sillimanite and quartz. This corona is continuous with an orthopyroxene (Al_2O_3 wt% = 5.04-5.9)-sillimanite symplectite that occurs around cordierite grain boundaries (Fig. 4.4c). Orthopyroxene near the garnet porphyroblast has a greater X_{Mg} than orthopyroxene adjacent to cordierite. K-feldspar occurs with garnet and cordierite but is not zoned.

calc-silicate rocks (samples 756 and 296)

A gneissic foliation in calc-silicate rocks is defined by cm-scale quartz-rich and scapolite-wollastonite-clinopyroxene-plagioclase-garnet compositional layers. This layering is parallel to the regional compositional layering (S_1). Sample 756 contains granoblastic clinopyroxene, plagioclase, scapolite and wollastonite. Sample 296 is a quartz-bearing clinopyroxene-garnet-scapolite calc-silicate rock. Minor minerals are calcite, anorthite, sphene and magnetite. Scapolite and wollastonite are commonly recrystallized and partially replaced by anorthite and quartz, respectively, along grain margins. Clinopyroxene and scapolite have coronas of garnet. Reaction textures examined in sample 756 are shown in Fig. 4.7 and representative microprobe analyses from samples 756 and 296 are presented in Table 4.6.

In sample 756, clinopyroxene is salite to diopside (X_{En} = 0.30-0.35) and is zoned with Al^T and Fe^{2+} decreasing and Mg and Ca increasing from core to rim (Fig. 4.4d). Coarse-grained scapolite is meionite (X_{An} = 0.84-0.85) and is zoned with Ca decreasing slightly towards the grain margins. Scapolite commonly contains fine-grained
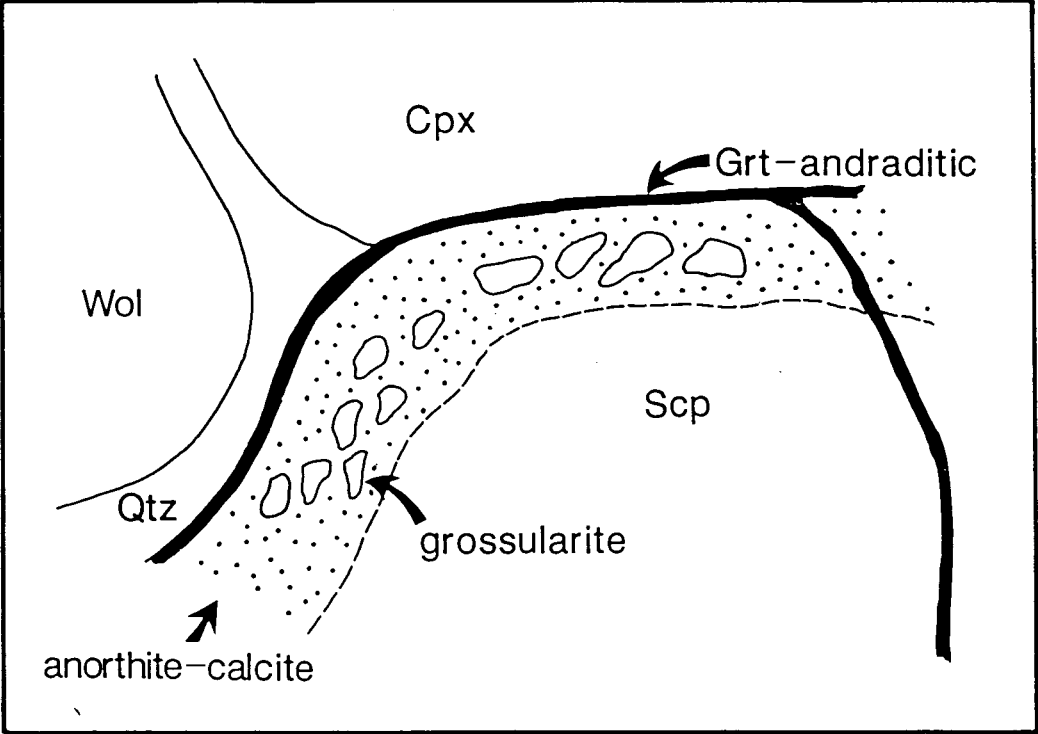
Fig. 4-7 Reaction textures in a calc-silicate rock (sample 756), Ongeva granulites.

148

inclusions of albite. A corona of anorthite (X_{An} = 0.97)±calcite and grossularite (X_{Grs} = 0.98) surrounding scapolite grains now separates scapolite from wollastonite (Fig. 4.7). In other calc-silicate rocks, scapolite is commonly replaced by plagioclase and quartz. A quartz corona surrounding wollastonite now separates wollastonite from scapolite and clinopyroxene (Fig. 4.7). An andraditic garnet (X_{Grs} = 0.72, X_{And} = 0.15) corona occurs between the quartz corona on wollastonite and the corona of anorthite±calcite and grossularite on scapolite (Fig. 4.7). Andraditic garnet (X_{Grs} = 0.72-0.79, X_{And} = 0.27-0.29) also forms coronas on clinopyroxene or occurs as veinlets within clinopyroxene and scapolite. The clinopyroxene adjacent to garnet rims has a low Al content and the garnet may contain Ti. Scapolite may also contain a partial corona of andraditic garnet.

In sample 296, zoned clinopyroxene also contains a corona of andraditic garnet but, in places, the garnet appears as inclusions or as a replacement of clinopyroxene. Minor amphibole also rims clinopyroxene and a corona of K-feldspar occurs between scapolite and quartz.

4.42 Harts Range Group

Riddock Amphibolite Member (sample 543),

Sample 543 consists of coarse-grained granoblastic clinopyroxene, garnet, hornblende and plagioclase, with minor ilmenite and quartz. No igneous microstructures are preserved. Clinopyroxene and garnet are poikiloblastic and contain round inclusions of plagioclase. Unlike rocks from the Ongeva granulites, the coarse-grained M_1 minerals in the Riddock Amphibolite Member do not show recrystallization, grainsize reduction and new grain growth, which have been attributed to M_2 in the Ongeva granulites. Representative microprobe analyses from sample 543 are presented in Table 4.7.

Clinopyroxene and garnet preserve good zoning profiles (Fig. 4.4e). Clinopyroxene is salite (X_{En} = 0.38-0.39) and is zoned, Al^{iv} and Fe^T decreasing and Mg and Ca increasing from the core to the rim. Garnet is almandine-rich (X_{Alm} = 0.47,

X_{Pyp} = 0.13-0.18, X_{Grs} = 0.28-0.29) and decreases in X_{Mg} from the core to the rim, which reflects a decrease in Mg and an increase in Fe^{2+}. Garnet-clinopyroxene K_d values (Ellis and Green, 1979) increase towards the grain margins. Hornblende is pargasitic hornblende. Hornblende rims appear to be lower in Al^{iv}, Ti, and higher in Ca. Unlike hornblende in the Ongeva granulites, hornblende in the Riddock Amphibolite Member generally contains no Cl or F. Plagioclase is andesine-labradorite (X_{An} = 0.49-0.50) and is not zoned.

Table 4.2 Representative microprobe analyses from a mafic granofels (sample 258), Ongeva granulites.

wt%	Cpx core	Cpx rim	Opx core	Opx rim	M₂ Cpx	M₂ Opx	Pl	Hbl core	Hbl rim	M₂ Hbl at Cpx rim	Hbl on Opx
SiO₂	50.90	52.01	52.28	51.29	51.71	51.19	53.31	40.01	39.82	39.54	40.09
TiO₂	0.24	0.24	-	-	0.27	-	-	2.39	2.06	3.10	1.72
Al₂O₃	3.76	2.62	1.32	1.95	2.66	3.16	29.77	13.83	12.26	13.82	13.34
Cr₂O₃	0.23	-	-	-	0.26	-	-	-	-	0.23	-
FeO	10.06	9.48	27.05	28.12	10.07	26.85	-	17.09	15.76	15.65	15.90
MnO	0.31	0.33	0.64	0.51	-	0.67	-	-	0.24	-	-
MgO	12.09	12.74	18.68	18.25	12.34	17.75	-	9.21	9.93	9.12	10.28
CaO	22.10	22.49	0.44	0.37	22.22	0.39	12.09	11.35	11.90	11.77	11.91
Na₂O	0.77	0.95	-	-	0.71	-	4.77	1.76	1.28	1.81	1.38
K₂O	-	-	-	-	-	-	0.14	1.53	2.23	1.81	2.28
F	-	-	-	-	-	-	-	0.69	0.70	0.97	1.37
Cl	-	-	-	-	-	-	-	0.47	0.51	0.55	0.52
TOTAL	100.46	100.86	100.41	100.49	100.24	100.01	100.08	97.39	96.28	96.85	98.11

structural formula

on basis of	6 (O)	6 (O)	6 (O)	6 (O)	6 (O)	6 (O)	32 (O)	23 (O)	23 (O)	23 (O)	23 (O)
Si	1.89	1.92	1.99	1.95	1.93	1.95	9.64	6.04	6.16	6.05	6.08
Ti	0.01	0.01	-	-	0.01	-	-	0.27	0.24	0.36	0.20
Aliv	0.11	0.08	0.01	0.05	0.07	0.05	6.34	1.96	1.84	1.95	1.92
Alvi	0.06	0.03	0.05	0.04	0.05	0.10	-	0.50	0.40	0.54	0.46
Cr	0.01	-	-	-	0.01	-	-	-	-	0.03	-
Fe²⁺	0.23	0.19	0.86	0.89	0.26	0.86	-	2.16	2.04	2.00	2.02
Fe³⁺	0.09	0.10	-	0.01	0.06	-	-	-	-	-	-
Mn	0.01	0.01	0.02	0.02	-	0.02	2.34	-	0.04	-	-
Mg	0.67	0.70	1.06	1.04	0.69	1.01	1.67	2.07	2.29	2.08	2.32
Ca	0.88	0.89	0.02	0.02	0.89	0.02	0.03	1.84	1.97	1.93	1.94
Na	0.06	0.07	-	-	0.05	-	-	0.52	0.38	0.54	0.41
K	-	-	-	-	-	-	-	0.30	0.44	0.35	0.44
TOTAL	4.02	4.00	4.01	4.02	4.02	4.01	20.02	15.66	15.80	15.83	15.79
%X$_{Mg}$*	74.44	78.65	55.21	53.89	72.63	54.01		48.94	52.89	50.98	53.46
Wo	0.42	0.44	0.01	0.01	0.44	0.01					
En	0.43	0.44	0.54	0.53	0.41	0.52					
Fs	0.15	0.12	0.45	0.46	0.15	0.47					

* %Mg/Mg/Fe²⁺

Table 4.3 Representative microprobe analyses from an ultramafic boudin (sample 955), Ongeva granulites.

wt%	Cpx core	Cpx rim	Cpx symplectite	Spl symplectite	Spl core	Spl rim	Pl moat	Hbl core	Hbl rim
SiO_2	52.83	53.63	53.24	-	-	-	42.88	42.49	43.93
TiO_2	-	-	-	-	-	-	-	-	-
Al_2O_3	3.99	1.91	2.93	68.18	65.47	64.73	36.68	16.38	14.71
Cr_2O_3	0.22	-	-	-	-	-	-	-	-
FeO	2.48	1.98	2.24	9.06	9.37	9.18	0.35	3.83	3.86
MnO	0.28	0.33	0.28	0.40	0.23	0.23	-	-	-
MgO	15.95	17.11	16.34	20.17	19.36	19.29	0.33	17.18	18.23
CaO	24.73	24.85	25.26	-	-	-	20.23	12.93	13.23
Na_2O	-	-	-	1.41	2.29	2.17	-	1.58	1.62
K_2O	-	-	-	-	-	-	-	1.85	1.65
F	-	-	-	-	-	-	-	1.89	2.07
Cl	-	-	-	-	-	-	-	0.32	0.32
Zn	-	-	-	2.15	4.09	4.19	-	-	-
TOTAL	100.74	99.81	100.30	101.38	100.81	100.58	100.45	97.60	98.68

structural formula

on basis of	6 (O)	6 (O)	6 (O)	6 (O)	32 (O)	32 (O)	32 (O)	23 (O)	23 (O)
Si	1.92	1.95	1.93	-	-	-	7.93	6.10	6.23
Ti	-	-	-	-	-	-	-	-	-
Al^{iv}	0.08	0.05	0.07	2.97	15.62	15.46	7.99	1.90	1.77
Al^{vi}	0.09	0.03	0.06					0.87	0.69
Cr	0.01	-	-	-	-	-	-	-	-
Fe^{2+}	0.08	0.04	0.06	0.28	1.59	1.56	0.05	0.46	0.46
Fe^{3+}	-	0.02	0.01					-	-
Mn	0.01	0.01	0.01	0.01	0.04	0.04	-	-	-
Mg	0.86	0.93	0.88	1.11	5.85	5.84	0.09	3.67	3.85
Ca	0.96	0.97	0.98	0.01	-	-	4.01	1.99	2.01
Na	-	-	-	0.10	0.90	0.86	-	0.44	0.45
K	-	-	-	-	-	0.03	-	0.34	0.30
TOTAL	4.01	4.00	4.00	4.48	24.00	23.79	20.07	15.77	15.76
%X_{Mg}*	91.49	95.88	93.62	79.86	78.63	78.92		88.86	89.33
Wo	0.43	0.46	0.46						
En	0.52	0.51	0.51						
Fs	0.05	0.03	0.03						

*%$Mg/Mg\mathbb{F}e^{2+}$

Table 4.4 Representative microprobe analyses from felsic gneisses (samples 55 and 58), Ongeva granulites.

sample 55

wt%	Opx core	Opx rim	Grt core	Grt margin	Pl core	Pl next to Grt-Opx	Cpx core	Cpx rim	Grt rim
SiO_2	53.82	54.64	39.22	39.07	45.5	45.29	52.55	53.05	39.9
TiO_2	-	-	-	-	-	-	-	-	-
Al_2O_3	1.78	2.63	21.88	21.72	35.05	35.15	2.95	2.46	21.85
Cr_2O_3	-	-	-	-	-	-	-	-	-
FeO	13.84	13.99	14.48	14.88	0.48	-	6.1	5.68	15.55
MnO	3.73	3.52	10.96	11.2	-	-	1.34	1.41	10.95
MgO	25.57	25.86	7.27	6.81	-	-	14.5	14.75	6.52
CaO	0.37	0.33	7.17	7.37	18.96	18.6	22.53	22.41	7.04
Na_2O	-	-	-	-	0.64	1.39	0.41	0.72	-
K_2O	-	-	-	-	-	-	-	-	-
TOTAL	99.11	100.96	100.97	101.06	100.63	100.43	100.38	100.48	101.81

structural formula

on basis of	6 (O)	6 (O)	12 (O)	12 (O)	32 (O)	32 (O)	6 (O)	6 (O)	12 (O)
Si	1.97	1.96	3	3	8.35	8.33	1.93	1.94	3.03
Ti	-	-	-	-	-	-	-	-	-
Al^{iv}	0.03	0.04	1.97	1.97	7.58	7.62	0.07	0.06	1.96
Al^{vi}	0.05	0.08					0.06	0.05	
Cr	-	-	-	-	-	-	-	-	-
Fe^{2+}	0.42	0.42	0.87	0.88	0.07	-	0.15	0.11	0.99
Fe^{3+}			0.05	0.07			0.04	0.06	-
Mn	0.12	0.11	0.71	0.73	-	-	0.04	0.04	0.71
Mg	1.4	1.39	0.83	0.78	-	-	0.8	0.81	0.74
Ca	0.02	0.01	0.59	0.61	3.73	3.67	0.88	0.88	0.57
Na	-	-	-	-	0.23	0.5	-	0.05	-
K	-	-	-	-	-	-	-	-	-
TOTAL	4.01	4.01	8.02	8.04	19.96	20.12	3.97	4	8
X_{Mg}*	76.92	76.80	48.82	46.99			84.21	88.04	42.77

sample 58

wt%	Cpx core	Cpx rim	Grt core	Grt rim	Pl core	Pl next to Cpx-Grt
SiO_2	52.25	52.26	39.16	39.02	44.87	44.41
TiO_2	0.26	-	0.24	-	-	-
Al_2O_3	2.81	2.31	21.38	22.29	34.98	35.12
Cr_2O_3	-	-	-	-	-	-
FeO	7.31	6.14	20.36	19.64	-	0.33
MnO	0.47	0.5	5.2	5.33	-	-
MgO	13.89	14.08	6.87	7.52	0.25	-
CaO	23.24	23.7	7.89	7.09	18.75	19.12
Na_2O	0.65	0.46	-	-	0.96	1.12
K_2O	-	-	-	-	-	-
TOTAL	100.88	99.74	101.09	100.9	99.81	100.1

structural formula

on basis of	6 (O)	6 (O)	12 (O)	12 (O)	32 (O)	32 (O)
Si	1.91	1.94	3	2.98	8.3	8.23
Ti	0.01	-	0.01	-	-	-
Al^{iv}	0.09	0.06	1.93	2	7.63	7.66
Al^{vi}	0.03	0.04			-	
Cr	-	-	-	-	-	-
Fe^{2+}	0.13	0.14	1.24	1.2	-	0.05
Fe^{3+}	0.09	0.02	0.06	0.06	-	
Mn	0.02	0.02	0.34	0.35	-	-
Mg	0.77	0.78	0.79	0.86	0.07	-
Ca	0.91	0.94	0.65	0.58	2.72	3.79
Na	0.05	0.03	-	-	0.34	0.4
K	-	-	-	-	-	-
TOTAL	4.01	3.97	8.02	8.03	19.06	20.13
X_{Mg}*	85.56	84.78	38.92	41.75		

* $\%Mg/Mg/Fe^{2+}$

Table 4.5 Representative microprobe analyses from a cordierite-garnet gneiss (sample 622), Ongeva granulites.

wt%	Grt core	Grt rim	M₂ Grt	Crd core	Crd rim	Crd core next to Grt	Crd rim next to Grt	Opx near Grt	Opx away from Grt	Bt with Grt %Xmg=30.99	Bt with Grt %Xmg=33.10	M₂ Bt with Sil symp
SiO$_2$	38.21	39.34	39.43	49.17	49.66	49.05	49.25	52.09	51.25	35.86	36.96	37.81
TiO$_2$	-	-	-	-	-	-	-	-	-	5.60	6.22	4.75
Al$_2$O$_3$	21.56	22.41	22.53	33.55	33.79	33.42	33.75	5.41	5.64	14.54	14.95	15.12
Cr$_2$O$_3$	-	-	-	-	-	-	-	-	-	-	-	-
FeO	30.67	28.68	26.35	3.87	3.03	2.88	2.54	18.79	21.03	16.75	13.91	11.58
MnO	0.72	0.64	0.33	-	-	-	-	-	-	-	-	-
MgO	7.65	9.04	11.43	11.12	11.38	11.66	11.86	23.84	22.27	12.47	14.22	16.57
CaO	1.26	0.38	0.52	-	-	-	-	-	-	-	-	-
Na$_2$O	-	-	-	0.31	-	-	0.37	-	-	-	-	-
K$_2$O	-	-	-	-	-	-	-	-	-	9.44	9.36	9.54
Cl										1.57	0.53	0.40
TOTAL	100.07	100.49	100.59	98.02	97.86	97.01	97.77	100.13	100.19	96.23	96.15	95.77

structural formula

on basis of	12 (O)	12 (O)	12 (O)	18 (O)	18 (O)	18 (O)	24 (O)	6 (O)	6 (O)	22 (O)	22 (O)	22 (O)
Si	2.98	3.02	2.98	4.97	5.01	4.98	4.96	1.90	1.89	5.59	5.62	5.66
Ti	-	-	-	-	-	-	-	-	-	0.66	0.71	0.53
Al^{iv}	1.98	2.03	2.01	4.00	4.02	4.00	4.01	0.13	0.11	2.41	2.38	2.34
Al^{vi}								0.10	0.13	0.26	0.30	0.32
Cr	-	-	-	-	-	-	-	-	-	-	-	-
Fe^{2+}	1.94	1.84	1.63	0.26	0.26	0.22	0.14	0.57	0.65	2.18	1.77	1.45
Fe^{3+}	0.06	-	0.04	0.05		0.03	0.07	-		-	-	-
Mn	0.05	0.04	0.02	-	-	-	-	-	-	-	-	-
Mg	0.89	1.04	1.29	1.68	1.71	1.77	1.78	1.30	1.22	2.90	3.22	3.70
Ca	0.11	0.03	0.04	-	-	-	-	-	-	-	-	-
Na	-	-	-	0.06	-	-	0.07	-	-	-	-	-
K	-	-	-	-	-	-	-	-	-	1.88	1.82	1.82
TOTAL	8.01	8.00	8.01	11.02	11.00	11.00	11.03	4.00	4.00	15.88	15.82	15.82
%X$_{Mg}$*	31.45	36.11	44.18	83.58	86.80	88.94	92.71	69.52	65.24	57.09	64.53	71.84

* %Mg/Mg/Fe^{2+}

Table 4.6 Representative microprobe analyses from calc-silicate rocks (samples 756 and 296), Ongeva granulites.

sample 756													sample 296			
wt%	Cpx core	Cpx rim	Grt vein in Cpx	Grt corona between Cpx-Scp	Scp core	Scp margin	Pl on rim of Scp	Grt at Scp margin	Pl inclusion in Scp	Grt vein in Scp	Wo	Grt corona between Wol-Scp	Cpx rim	Grt rim	Hbl on Cpx	Kfs corona
SiO_2	51.56	51.62	37.72	38.45	43.00	45.57	43.70	40.17	67.00	38.59	51.17	39.29	48.55	37.55	34.58	65.01
TiO_2	-	-	0.37	-	-	-	-	-	-	-	-	-	-	-	0.46	-
Al_2O_3	2.32	0.67	9.62	14.83	29.18	31.24	35.99	22.70	19.97	16.81	-	18.20	1.61	11.55	13.26	18.48
Cr_2O_3	-	-	-	0.27	-	-	-	-	-	-	0.34	-	-	-	-	-
FeO	13.07	10.50	16.70	11.06	-	-	-	0.77	0.25	9.01	0.31	7.26	24.62	23.03	31.82	0.34
MnO	0.52	0.61	0.41	0.50	-	-	-	0.30	-	0.41	0.27	0.64	-	0.78	-	-
MgO	9.00	11.04	0.24	-	-	-	-	-	-	0.24	-	-	2.83	0.20	0.68	-
CaO	23.51	24.53	34.59	34.57	20.50	16.37	19.79	37.15	0.70	34.73	47.92	35.04	22.17	27.39	11.22	0.23
Na_2O	0.34	0.36	-	-	1.66	1.14	0.32	-	9.09	-	-	-	0.35	-	-	0.23
K_2O	-	-	-	-	0.54	0.70	0.10	-	0.20	-	-	-	-	-	3.92	15.36
Cl	-	-	-	-	0.23	-	-	-	-	-	-	-	-	-	4.81	-
TOTAL	100.32	99.33	99.65	99.68	95.11	95.02	99.90	101.09	97.21	99.79	100.01	100.43	100.13	100.50	100.75	99.65

structural formula

on basis of	6 (O)	6 (O)	12 (O)	12 (O)	32 (O)	32 (O)	32 (O)	12 (O)	32 (O)	12 (O)	18(O)	12 (O)	6 (O)	12 (O)	23 (O)	32 (O)
Si	1.97	1.96	2.99	2.99	8.50	8.81	8.10	2.99	11.96	2.97	5.96	3.00	1.95	2.98	5.75	12.01
Ti	-	-	0.02	-	-	-	-	-	-	-	-	-	-	-	0.06	-
Al^{iv}	0.30	0.03	0.90	1.36	6.79	7.11	7.86	1.99	4.20	1.53	-	1.64	0.05	1.08	2.25	4.02
Al^{vi}	0.70							-			-		0.02		0.35	
Cr	-	-	-	0.02	-	-	-	-	-	-	0.03	-	-	-	-	-
Fe^{2+}	0.42	0.27	0.02	0.08	-	-	-	0.01	0.04	0.05		0.09	0.77	0.58	2.36	0.05
Fe^{3+}	-	0.06	1.09	0.64			-	0.04	-	0.53	0.03	0.37	0.06	0.95	2.07	
Mn	0.02	0.02	0.03	0.03	-	-	-	0.02	-	0.03	0.03	0.04	-	0.05	-	-
Mg	0.51	0.63	0.03	-	-	-	-	-	-	-	-	-	0.17	0.02	0.17	-
Ca	0.96	1.00	2.94	2.88	4.34	3.39	3.93	2.96	0.13	2.87	5.98	2.86	0.95	2.33	2.00	0.05
Na	0.03	0.03	-	-	0.64	0.43	0.12	-	3.15	-	-	-	0.03	-	1.26	0.08
K	-	-	-	-	0.14	0.17	0.02	-	0.05	-	-	-	-	-	1.02	3.62
TOTAL	4.91	4.00	8.02	8.00	20.41	19.91	20.03	8.01	19.53	7.98	12.03	8.00	4.00	7.99	17.29	19.83
$\%X_{Mg}$*	54.84	70.00	60.00										18.09	3.33	6.72	
X_{Grs}			0.72	0.79				0.98		0.82		0.85	0.59			

* $\%Mg/Mg/Fe^{2+}$

Table 4.7 Representative microprobe analyses from the Riddock Amphibolite Member (sample 543), Harts Range Group.

wt%	Cpx core	Cpx rim	Grt core	Grt rim	Pl core	Pl rim with Grt	Pl rim with Cpx	Hbl core	Hbl rim
SiO_2	51.46	52.61	38.66	38.30	55.79	56.47	56.16	43.13	43.27
TiO_2	0.24	-	-	-	-	-	-	1.63	1.40
Al_2O_3	2.80	1.37	21.86	21.94	28.86	27.69	28.86	12.71	11.72
Cr_2O_3	0.30	-	-	-	-	-	-	-	-
FeO	10.41	10.14	24.79	26.63	-	0.51	-	16.71	16.71
MnO	-	-	0.93	1.65	-	-	-	-	-
MgO	11.48	12.46	4.81	3.41	-	-	-	9.98	10.01
CaO	23.02	23.82	10.84	10.21	10.22	9.71	10.11	11.65	11.96
Na_2O	0.69	0.36	-	-	5.89	6.04	5.63	1.58	1.62
K_2O	-	-	-	-	-	-	-	0.25	0.34
F	-	-	-	-	-	-	-	-	-
Cl	-	-	-	-	-	-	-	-	-
TOTAL	100.41	100.76	101.89	102.15	100.76	100.41	100.75	97.64	97.02

structural formula

on basis of	6 (O)	6 (O)	12 (O)	12 (O)	32 (O)	32 (O)	32 (O)	23 (O)	23 (O)
Si	1.92	1.96	2.95	2.95	9.96	10.12	10.00	6.36	6.46
Ti	0.01	-	-	-	-	-	-	0.18	0.16
Al^{iv}	0.08	0.04	1.97	1.99	6.07	5.85	6.06	1.64	1.54
Al^{vi}	0.05	0.02						0.57	0.53
Cr	0.01	-	-	-	-	-	-	-	-
Fe^{2+}	0.27	0.27	1.46	1.61	-	0.08	-	1.90	2.09
Fe^{3+}	0.06	0.05	0.13	0.11				0.16	-
Mn	-	-	0.06	0.11	-	-	-	-	-
Mg	0.64	0.69	0.55	0.39	-	-	-	2.19	2.23
Ca	0.92	0.95	0.89	0.84	1.96	1.86	1.93	1.84	1.91
Na	0.05	0.03	-	-	2.04	2.10	1.95	0.45	0.47
K	-	-	-	-	-	-	-	0.05	0.07
TOTAL	4.01	4.01	8.01	8.00	20.03	20.01	19.94	15.34	15.46
$\%X_{Mg}$*	70.33	71.88	27.36	19.50				53.55	51.62
Wo	0.46	0.47							
En	0.38	0.39							
Fs	0.16	0.15							

* $\%Mg/Mg+Fe^{2+}$

4.5   Estimates of metamorphic conditions

The results of thermobarometric calculations are presented in Table 4.8 and selected, calculated P-T lines are shown in Fig. 4.8a. Temperature estimates for gneisses in both the Ongeva granulites and Riddock Amphibolite Member indicate cooling from core to rim compositions. Pressure estimates have high uncertainties but generally indicate limited decompression with cooling in both the Ongeva granulites and Riddock Amphibolite Member. Metapelites in the Ongeva granulites preserve mineral compositions that indicate an increase in pressure after cooling during a second metamorphic event.

4.51   Ongeva granulites

Temperature estimates

Two-pyroxene thermometry, using core compositions of clinopyroxene and hypersthene ($Fe^T = Fe^{2+}$) from sample 258 gives temperatures of 795±20°C (Wood and Banno, 1973; Wells, 1977), 738°C (Kretz, 1982) and 850°C (clinopyroxene composition, Lindsley, 1983).   Calculations using estimates of Fe^{3+} (Lindsley, 1983) give similar results to calculations using $Fe^T = Fe^{2+}$. Two-pyroxene thermometry using rim compositions gives temperatures of 750±10 (Wood and Banno, 1973; Wells, 1977) and 645°C and 750°C (Lindsley, 1983). Temperature estimates using the compositions of M_2 pyroxenes, which occur at the triple junctions of M_1 plagioclase, amphibole and orthopyroxene, gives temperatures of 810±17°C (Wood and Banno, 1973; Wells, 1977) and 693-700°C (Kretz, 1982; Lindsley, 1983).

Averaged temperature estimates using Fe-Mg exchange between garnet and clinopyroxene (Ellis and Green, 1979; Krogh, 1988) in sample 58 gives, T = 762±17°C at P = 6.5 kbar for core compositions and T = 727±23°C at P = 6.5 kbar for rim compositions. At similar pressures there is also a slight decrease in temperature. Temperature estimates using Fe-Mg exchange between garnet and orthopyroxene

Table 4.8 P-T estimates using assemblages from the Ongeva granulites and the Riddock Amphibolite Member.

pressure estimates (kbar)

sample	650°C	700°C	750°C	800°C	850°C	assemblage	reference
58 (cores)	6.7	6.8	7.0	7.1	7.2	Cpx-Grt-Pl-Qtz	1
58 (cores)	4.9±1.15	4.9±1.21	5.0±1.27	5.0±1.34	5.0±1.40	Cpx-Grt-Pl-Qtz	2
58 (rims)	6.3	6.5	6.6	6.7	6.8	Cpx-Grt-Pl-Qtz	1
58 (rims)	5.6±1.47	5.5±1.20	5.5±1.18	5.5±1.24	5.5±1.30	Cpx-Grt-Pl-Qtz	2
55 (cores)	6.6	6.6	6.5	6.5	6.5	Opx-Grt-Pl-Qtz	1+3
55 (cores)	7.7	8.0	8.3	8.6	8.9	Opx-Grt-Pl-Qtz	4
55 (cores)	7.6	8.3	8.9	9.5	10.1	Opx-Grt-Pl-Qtz	5
55 (cores)	7.6	7.4	7.3	7.2	7.1	Opx-Grt	6
55 (cores)	4.5±1.09	4.8±1.15	5.1±1.41	5.4±1.76	5.7±2.09	Opx-Grt-Pl-Qtz	2
55 (cores)	4.3	4.3	4.3	4.5	4.6	Cpx-Grt-Pl-Qtz	1+3
55 (rims)	7.0	7.1	7.1	7.1	7.1	Opx-Grt-Pl-Qtz	1+3
55 (rims)	7.8	8.1	8.4	8.7	9.0	Opx-Grt-Pl-Qtz	4
55 (rims)	7.9	8.6	9.3	10.0	10.7	Opx-Grt-Pl-Qtz	5
55 (rims)	2.9	2.5	2.1	1.7	1.4	Opx-Grt	6
55 (rims)	4.6±1.10	4.9±1.39	5.2±1.75	5.5±2.11	5.5±2.11	Opx-Grt-Pl-Qtz	2
55 (rims)	4.0	4.0	4.0	4.0	4.2	Cpx-Grt-Pl-Qtz	1+3
622 (cores)	7.1 (7.6)	6.6 (7.4)	6.1 (7.2)	5.6 (7.0)	5.1 (6.8)	Grt (Crd), aH2O=0.5	7
622 (cores)	7.8 (8.9)	7.4 (8.6)	6.9 (8.4)	6.5 (8.1)	6.0 (7.8)	Grt (Crd)	8
622 (rims)		7.6 (7.6)	7.1 (7.4)	6.6 (7.2)	6.07 (6.9)	Grt (Crd), aH2O=0.5	7
622 (rims)		7.9 (9.0)	7.4 (8.7)	7.0 (8.4)	6.5 (8.1)	Grt (Crd)	8
622 M2			7.2 (7.5)	6.6 (7.3)		Grt (Crd), aH2O=0.5	7
622 M2			8.1 (9.3)	7.7 (9.0)		Grt (Crd)	8
622 M2			6.1±1.9	6.8±1.8		Crd-Grt-Sil-Bi-Opx-Qz	2
543 (cores)	7.5	7.9	8.3	8.7	9.0	Cpx-Grt-Pl-Qtz	1
543 (cores)	8.3	8.6	8.8	8.4	8.7	Cpx-Grt-Pl-Qtz	1+3
543 (cores)	6.14±1.16	6.24±1.06	6.35±0.95	6.45±0.85	6.55±0.75	Grt-Hbl-Pl-Qtz	9
543 (cores)		10.5±1.04				Cpx-Grt-Hbl-Pl-H2O	2
543 (rims)	5.8	6.1	6.4	6.7	7.0	Cpx-Grt-Pl-Qtz	1
543 (rims)	6.4	6.6	6.8	6.2	6.5	Cpx-Grt-Pl-Qtz	1+3
543 (rims)	6.16±0.82	6.28±0.82	6.40±0.86	6.52±0.88	6.63±0.89	Grt-Hbl-Pl-Qtz	9
543 (rims)		9.7±1.9				Cpx-Grt-Hbl-Pl-H2O	2

1 Newton and Perkins (1982)
2 Powell and Holland (1988)
3 Ganguly and Saxena (1984)
4 Perkins and Chipera (1985)
5 Bohlen et al. (1983)
6 Harley (1984)
7 Lonker (1981)
8 Holdaway and Lee (1977)
9 Kohn and Spear (1989)

temperature estimates (°C)

sample	5 kbar	6 kbar	7 kbar	8 kbar	assemblage	reference
258 (cores)	781-801				Cpx-Opx	5,6
258 (cores)	700-738				Cpx-Opx	7,8
258 (rims)	743-758				Cpx-Opx	5,6
258 (rims)	600-645				Cpx-Opx	7,8
258 (M2)	795-827				Cpx-Opx	5,6
258 (M2)	690-700				Cpx-Opx	7,8
58 (cores)	774	777	780	783	Cpx-Grt	1
58 (cores)	740	743	746	750	Cpx-Grt	2
58 (rims)	743	746	749	752	Cpx-Grt	1
58 (rims)	699	702	705	708	Cpx-Grt	2
55 (cores)	700	705	710	715	Opx-Grt	3
55 (rims)	665	670	675	679	Opx-Grt	3
55 (rims)	762	765	768	771	Cpx-Grt	1
55 (rims)	729	732	735	738	Cpx-Grt	2
622		881			Grt(%Xmg=30.99)-Bi	8
622		755			Grt(%Xmg=33.10)-Bi	8
622 (M2)		813			Grt-Bi	8
756		850-860			Scp-Pl	10
543 (cores)	825	826	831	834	Cpx-Grt	1
543 (cores)	805	808	811	814	Cpx-Grt	2
543 (cores)	810				Grt-Hbl	9
543 (rims)	678	680	683	686	Cpx-Grt	1
543 (rims)	640	643	646	649	Cpx-Grt	2
543 (rims)	689				Grt-Hbl	9

1 Ellis and Green (1979)
2 Krogh (1985)
3 Harley (1984)
4 Wood and Banno (1973)
5 Wells (1977)
6 Kretz (1982)
7 Lindsley (1983) - Cpx comp.
8 Ferry and Spear (1978)
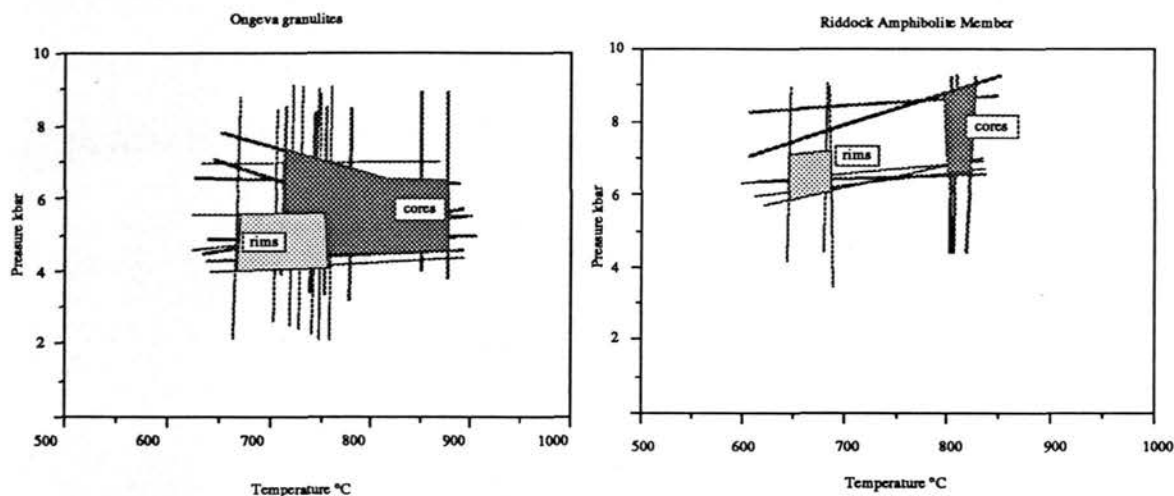9 Graham and Powell (1984)
10 Goldsmith and Newton (197

Fig. 4.8a P-T line estimates using assemblages in samples from the Ongeva granulites, Strangways Metamorphic
Complex and assemblages in the Riddock Amphibolite Member, Harts Range Group.
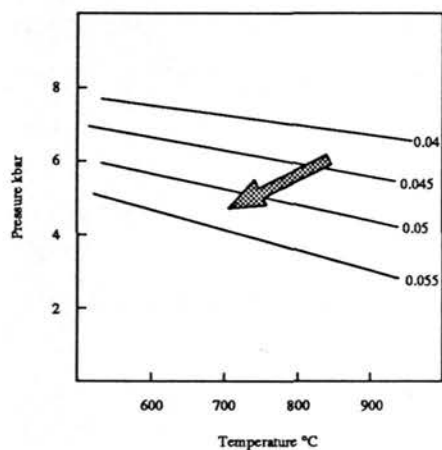

Fig. 4.8b Molecular Al/2 orthopyroxene isopleths in equilibrium
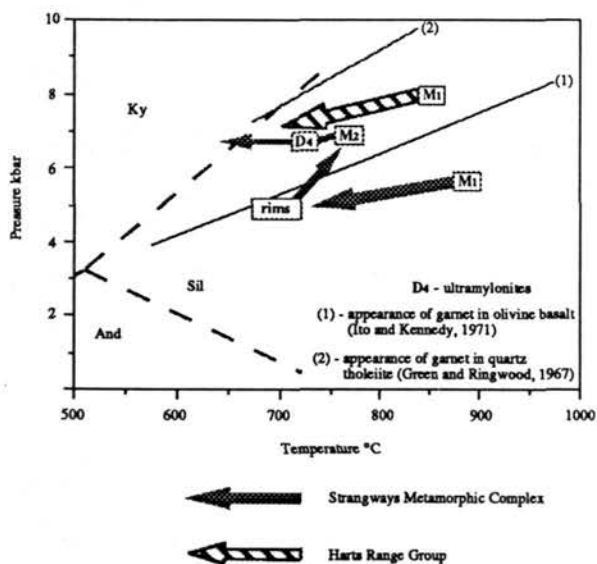with garnet ($X_{Mg} = 0.47$) with changing pressure and
temperature.

Fig. 4.8c Refined P-T-t paths for the early-Proterozoic
history of the central Arunta Block.

159

(Harley, 1984a) in sample 55 give T = 708°C at P = 6.5 kbar for core compositions and T = 673°C at P = 6.5 kbar for rim compositions. Averaged temperature estimates using Fe-Mg exchange between garnet and clinopyroxene (Ellis and Green, 1979; Krogh, 1988) in sample 55 gives T = 750±16°C at P = 6.5 kbar . In sample 55, zoning in garnet with clinopyroxene was not recognized. The clinopyroxene-garnet temperature estimate for sample 55 was calculated using the rim composition of clinopyroxene.

Temperature estimates using Fe-Mg exchange between garnet and biotite (Ferry and Spear, 1978) in sample 622 gives, T = 881°C for core compositions, T = 755°C towards the garnet rim and T = 813°C for M_2 biotite with garnet. Although biotite-garnet temperature estimates indicate cooling during garnet growth, they are probably inaccurate due to garnet re-equilibration during M_2 (see discussion).

In calc-silicate rocks (sample 756), scapolite (X_{An} = 0.84-0.85) occurs with anorthite (X_{An} = 0.97) near the grain boundaries, indicating temperatures of about 850°C (Goldsmith and Newton, 1977) after the metamorphic peak.

Pressure estimates using core compositions

Pressure estimates, using the assemblage garnet-clinopyroxene-plagioclase-quartz (Newton and Perkins, 1982) and core compositions in sample 58 give P = 7.1 kbar at T = 800°C. If the grossular activity of Ganguly and Saxena (1984) for Mn-bearing rocks is used this pressure estimate is reduced. Average pressure calculations (Powell and Holland, 1988; Holland and Powell, 1990) using core compositions from sample 58 and a_{H2O} = 0.1-0.3 give P = 5.0±1.34 at T = 800°C. Pressure estimates using the assemblage garnet-clinopyroxene-plagioclase-quartz (Newton and Perkins, 1982) and the grossular activity of Ganguly and Saxena (1984) for core compositions in sample 55 give P = 4.5 kbar at T = 800°C. Pressure estimates using the assemblage garnet-orthopyroxene-plagioclase-quartz (Newton and Perkins, 1982; Ganguly and Saxena, 1984) and core compositions in sample 55 give P = 6.5 kbar at T = 800°C and average pressure calculations (Powell and Holland, 1988; Holland and Powell, 1990) using a_{H2O}

= 0.1-0.3 give P = 5.4±1.76 $\overset{kbar}{\wedge}$ Higher pressure estimates of P = 7.2-9.5 kbar are indicated by other geobarometers (averaged P-Mg and P-Fe, Perkins and Chipera, 1985; Bohlen et al., 1983; Harley, 1984b). The minerals in sample 55 are Mn-rich, which probably results in overestimates for pressure calculations. Pressure estimates for the assemblage garnet-clinopyroxene-plagioclase-quartz, using an activity of grossular involving the Mn component give significantly lower pressure estimates (~2 kbar) than estimates not using an activity of grossular involving Mn.

The intersection of P-T lines (Fig. 4.8a) gives mean conditions of P = 5.7±0.8 kbar at T = 800°C for core compositions. This does not include the high pressure estimates using Mn-rich minerals in sample 55.

Pressure estimates using rim compositions

Pressure estimates using the assemblage garnet-clinopyroxene-plagioclase-quartz (Newton and Perkins, 1982) for rim compositions in sample 58 yield lower pressures than core compositions, namely P = 6.5 kbar at T = 700°C. However, average pressure estimates (Powell and Holland, 1988; Holland and Powell, 1990) using rim compositions give higher pressures, namely P = 5.5±1.2 kbar but with a high degree of uncertainty.

Pressure estimates using the assemblage garnet-orthopyroxene-plagioclase-quartz (Newton and Perkins, 1982; Ganguly and Saxena, 1984) and rim compositions in sample 55 give P = 7.1 kbar at T = 700°C but average pressure calculations (Powell and Holland, 1988; Holland and Powell, 1990) using a_{H2O} = 0.1-0.3 give P = 4.9±1.39 kbar. Other pressure estimates (Perkins and Chipera, 1985; Bohlen et al., 1983; Harley, 1984b) also give lower pressures for rim compositions at 700°C than core compositions at 800°C. The probable change in pressure with cooling is also reflected by the increase in Al content from the core to the rim of orthopyroxene in microstructural equilibrium with garnet as the solubility of Al_2O_3 in orthopyroxene increases with decreasing pressure at constant temperature (Wood, 1974; Harley, 1984b). Molecular $X_{Al/2}$ isopleths for a zoned orthopyroxene in sample 55 in equilibrium with an almandine garnet

(X_{Mg} = 0.47) are shown in Fig. 4.8b, using the calculations of Harley (1984b). Fig. 4.8b also indicates a P-T path inferred from Al zoning in orthopyroxene.

The intersection of P-T lines (Fig. 4.8a) gives mean conditions of about P = 5.0±0.8 kbar at T = 700°C for rim compositions.

Pressure estimates from garnet and cordierite

Pressure-temperature estimates using garnet and cordierite M_2 compositions (Lonker, 1981) in sample 622 yield, P~7.2 kbar and T = 750°C at a_{H_2O} = 0.5. The high Mg contents of garnet and cordierite coexisting with orthopyroxene, sillimanite and quartz support the high pressure estimates for M_2. However, the intersection of X_{Mg} curves for rim and core compositions does not occur in the garnet-cordierite stability field (Hensen and Green, 1973; Holdaway and Lee, 1977; Lonker, 1981). Both garnet and cordierite contain cores that are lower in X_{Mg}, which indicates that they existed at lower pressures prior to M_2. Garnet core compositions indicate pressures of 5.6-6.5 kbar at 800°C (Lonker, 1981; Holdaway and Lee, 1977). Pressure estimates using cordierite core and rim compositions give pressures within the errors for estimates of M_2, which suggests that cordierite has mostly re-equilibrated at M_2 conditions.

4.52 Harts Range Group

Temperature estimates

Averaged temperature estimates, using Fe-Mg exchange between garnet and clinopyroxene (Ellis and Green, 1979; Krogh, 1988) and core compositions, give T = 816±10°C at P = 6 kbar and T = 822±12°C at P = 8 kbar. Garnet-hornblende exchange thermometry (Graham and Powell, 1984) using core compositions gives T = 810°C for $Fe^T = Fe^{2+}$. Averaged temperature estimates, using Fe-Mg exchange between garnet and clinopyroxene (Ellis and Green, 1979; Krogh, 1988) and rim compositions, yield T = 661±19°C at P = 6 kbar and T = 667±19°C at P = 8 kbar. Garnet-hornblende exchange

thermometry (Graham and Powell, 1984) using rim compositions gives T = 689°C for $Fe^T = Fe^{2+}$.

Pressure estimates

Pressure estimates using the assemblage hornblende-garnet-plagioclase-quartz and core compositions (Kohn and Spear, 1989) give P = 6.6±0.75 kbar at T = 800°C, but pressure estimates using the assemblage garnet-clinopyroxene-plagioclase-quartz (Newton and Perkins, 1982) and the grossular activity of Ganguly and Saxena (1984) give P = 8.4 kbar at T = 800°C. Average pressure calculations (Powell and Holland, 1988; Holland and Powell, 1990) using core compositions gave high pressures (~10 kbar), but with a poor statistical fit. The intersection of P-T lines (Fig. 4.8a) gives mean conditions of about P = 7.7±1.1 kbar at T = 810°C for core compositions.

Pressure estimates using the assemblage hornblende-garnet-plagioclase-quartz and rim compositions (Kohn and Spear, 1989) yield P = 6.3±0.82 kbar at T = 700°C, and pressure estimates using the assemblage garnet-clinopyroxene-plagioclase-quartz (Newton and Perkins, 1982) and the grossular activity of Ganguly and Saxena (1984) give P = 6.6 kbar at T = 700°C. Average pressure calculations (Powell and Holland, 1988; Holland and Powell, 1990) using rim compositions gave high pressures (<10 kbar), which are lower than the estimates using the core compositions, but also with a poor statistical fit. The intersection of P-T lines (Fig. 4.8a) gives mean conditions of about P = 6.6±0.8 kbar at T = 660°C for rim compositions.

4.6 Discussion

Ongeva granulites

The temperature estimates and Ca-Mg-Fe zoning in minerals from mafic rocks in the Ongeva granulites indicate that cooling and ionic diffusion occurred after the metamorphic peak and prior to recrystallization, grainsize reduction and new grain growth during M_2. The Ca content of clinopyroxene increases towards the granoblastic grain margins, which reflects partitioning of Ca between clinopyroxene and orthopyroxene with decreasing temperature (Kretz, 1982). In garnet-clinopyroxene and garnet-orthopyroxene felsic gneisses, continued partitioning and Fe-Mg exchange during cooling and the effect on activities of a significant Mn component result in inaccurate temperature estimates. However, consistently different K_d values between rim and core compositions are consistent with cooling from the metamorphic peak.

In calc-silicate rocks from the Ongeva granulites, the presence of calcite and anorthite on the margins of scapolite represents the breakdown of scapolite as given by the equation: meionite = calcite + anorthite. This breakdown reaction is independent of pressure and X_{CO_2} and occurs with decreasing temperature. It indicates that peak metamorphic temperatures must have exceeded 850°C (Goldsmith and Newton, 1977). The presence of quartz rims on wollastonite in calc-silicate rocks may have resulted from the breakdown of wollastonite with cooling as follows, according to the equation: wollastonite = calcite + quartz, or may have formed as a result of a reaction with anorthite, namely: wollastonite + anorthite = grossular + quartz, which is indicated by the occurrence of grossular with anorthite at scapolite margins. This reaction is temperature-dependent moving from right to left with decreasing temperature and occurs at T = 730°C at P_T = 5 kbar (Boettcher, 1970). It is also restricted to low X_{CO_2} fluid composition. The assemblage scapolite-wollastonite-anorthite-quartz-grossular indicates an internal fluid composition of X_{CO_2} = 0.16-0.20 (Kerrick et al., 1973; Schenk, 1984).

Zoning in coarse-grained hornblende in the mafic rocks is not well developed but the rims are lower in Al^{iv}, Ti , Na and K, which also reflects either cooling or an increasing f_{O_2} (Spear, 1981). Oliver et al. (1988) noted a similar trend in hornblende compositions from mafic rocks 50 km west of this study. In the ultramafic rock hornblende has low-Al rims and occurs between and around granoblastic clinopyroxene. This suggests that hornblende formed after pyroxene, probably due to hydration during cooling. The source of fluid is enigmatic but it could have been derived from the crystallization of felsic partial melts in S_2 and non-confined partial melts late in D_2. The retrograde formation of biotite after orthopyroxene is also thought to involve water from crystallizing partial melts (Warren and Hensen, 1989). Although pressure estimates using M_1 assemblages in metapelitic and felsic rocks appear to give the best results for a low water activity, it is unlikely that the mafic rocks were completely dry and primary hornblende may also have been generated during peak metamorphism.

The presence of zoned M_1 clinopyroxene and hornblende in granoblastic mafic boudins on the limbs of F_3 folds places constraints on the timing of peak metamorphism and subsequent cooling. F_3 folding appears to have been part of a widespread deformation that produced the macroscopic fold pattern in the Ongeva granulites. S_2, S_{2b} and non-confined pegmatites are folded by F_3. This deformation may correlate with a major non-coaxial reworking of the Strangways Metamorphic Complex that Goscombe (1991) has inferred from rocks in the Strangways Range, 75 km northwest of this study. This major deformational event must have occurred after cooling from the metamorphic peak and crystallization of partial melt in S_2. This is contrary to the suggestion of Shaw et al. (1984a) that metamorphism followed folding.

The formation of fine-grained M_2 orthopyroxene at the boundary of coarse-grained hornblende and plagioclase in mafic gneiss from the Ongeva granulites requires an increase in temperature and/or X_{CO_2} (Spear, 1981). Temperature estimates for M_2 pyroxenes indicate that an increase in temperature occurred during M_2. M_2 hornblende has a higher Ti, Al^{iv} and Na content and lower Ca content compared with the coarse-

grained hornblende rims, which may also imply an increase in temperature (Spear, 1981) during M_2. M_2 hornblende in mafic gneisses has a high Cl content similar that of fine-grained M_2 biotite and hornblende in felsic gneisses (Norman and Flood, 1991). The movement of fluid with a high Cl activity in rocks at Mount Schaber is thought to have resulted in strain softening and the production of a macroscopic F_3 sheath fold and partial depletion of Y (Norman and Flood, 1991). In ultramafic rocks from the Ongeva granulites, a clinopyroxene-spinel symplectite has replaced granoblastic M_1 clinopyroxene (Fig. 4.5b) and is similar to symplectic intergrowths of augite and orthopyroxene that form by discontinuous precipitation from clinopyroxene solid solution, with simultaneous grain boundary migration (Boland and Otten, 1985). Spinel forms a host to diopside blebs which suggests that the spinel grain boundary may have swept through the clinopyroxene leaving the symplectite in its wake, in the same manner as described by Boland and Otten (1985). The driving mechanism for grain boundary migration may have been fluid movement and/or grain boundary instabilities during deformation. The symplectic clinopyroxene has a similar composition to M_1 clinopyroxene cores, with a higher Al content than the rims, which suggests that the symplectite formed at higher temperature and/or pressure conditions than M_1 clinopyroxene rims. Formation of the symplectite may represent the effects of M_2.

Pressure estimates from garnet±orthopyroxene±clinopyroxene felsic gneisses in the Ongeva granulites and Al zoning in orthopyroxene in equilibrium with garnet indicate that limited decompression accompanied cooling from the metamorphic peak. Similar zoning in orthopyroxene towards higher Al rims has been found in porphyroclasts from ultramylonitized garnet-orthopyroxene felsic gneisses, which occur in D_4 shear zones that transect the Ongeva granulites (Norman and Vernon, 1991). The recrystallized porphyroclast tails in the ultramylonite contain orthopyroxene with a low-Al content, similar to the clast centres and unlike the clast margins. This suggests that recrystallization in the shear zones occurred at pressures higher than formation of the M_1 orthopyroxene rims in equilibrium with garnet and the limited decompression occurred before ultramylonitization.

Pressure estimates using M_2 assemblages in metapelites from the Ongeva granulites give higher pressures than S_2 assemblages (Norman and Clarke, 1990). Mg-Fe zoning in coarse-grained garnet and cordierite in a metapelite from the Ongeva granulites also indicates that M_2 occurred at higher pressures than the formation of the M_1 and S_2 cores. The zoning in garnet and cordierite probably does not reflect ionic diffusion between garnet and cordierite, but rather the intra-grain re-equilibration between high-Mg rims and lower Mg cores during M_2, based on the movement of the divariant equilibria cordierite = garnet + sillimanite + quartz with changing pressure and the position of the divariant equilibria cordierite + hypersthene = garnet + quartz at M_2 (Hensen and Green, 1973). The higher pressure estimates indicated by the composition of cordierite also probably indicate that cordierite underwent Mg-Fe re-equilibration more readily than garnet. The presence of biotite inclusions in the coarse-grained garnet also suggests that garnet growth occurred during cooling because a prograde M_1 metamorphic path would usually involve dehydration. If the Strangways Metamorphic Complex had followed an isobaric cooling path after peak metamorphism, zoning in garnet would be minimal or garnet compositions would tend towards more Fe-rich rather than more Mg-rich compositions.

In some metapelites, small idioblastic to subidioblastic grains of sapphirine occur with M_2 sillimanite and orthopyroxene that pseudomorph cordierite (Fig. 4.5d). This represents either the breakdown of Mg-cordierite (cordierite = sapphirine + orthopyroxene + sillimanite) or a reaction between cordierite and spinel (cordierite + spinel = sapphirine + orthopyroxene ± sillimanite). The presence of sapphirine in pseudomorphs after cordierite also indicates temperatures of $>762°C$ (Siefert, 1975) during M_2. The presence of spinel inclusions in cordierite (Norman and Clarke, 1990) limits M_1 to low pressures (~4 kbar, Seifert, 1974) and the breakdown reaction of cordierite with spinel to sapphirine and orthopyroxene, which has a flat to negative dP/dT slope (Siefert, 1975), indicates an increase in pressure during M_2.

In calc-silicate rocks from the Ongeva granulites, andraditic garnet rims scapolite and clinopyroxene, and also occurs as inclusions and veinlets in clinopyroxene. Andradite rims postdate the grossular and quartz coronas on scapolite and quartz coronas on wollastonite. The formation of andraditic garnet on scapolite coronas must involve the addition of Fe_2O_3 to grossular, which would increase the stability of grossular-rich garnet at higher temperatures (Boettcher, 1970). Andraditic garnet also appears as inclusions in clinopyroxene, possibly as a result of the partial unmixing of clinopyroxene during an increase in temperature. Clinopyroxene with garnet rims occurs as porphyroclasts in ultramylonites from shear zones that cut the Ongeva granulites (Norman and Vernon, 1991), which suggests that the garnet rims and inclusions formed prior to ultramylonitization. Similar garnet rims in calc-silicate rocks have been described by Warren et al. (1987). They suggested local infiltration of water from shear zones with decreasing temperature as a mechanism to produce the reaction rims. The significant drop in Al content in clinopyroxene adjacent to garnet rims could also reflect the breakdown of the Ca-Tschermak component in clinopyroxene with increasing pressure. The common vein-like occurrence of garnet in clinopyroxene may imply a high fluid (water) vapour pressure during garnet growth. Average pressure estimates using M_2 assemblages in metapelites have a better statistical fit if a moderate water activity is used, and the formation of M_2 minerals in felsic granofelses appears to have involved fluid movement with a high activity of Cl (Norman and Flood, 1991). Evidence for an increase in temperature, pressure and fluid activity during M_2 from other gneisses in the Ongeva granulites suggests that a similar change in metamorphic conditions produced the garnet rims in calc-silicate rocks.

Riddock Amphibolite Member

The temperature estimates and Mg-Fe zoning in clinopyroxene and garnet from the Riddock Amphibolite Member indicate that cooling and ionic diffusion occurred after the metamorphic peak. Although pressure estimates using rim and core compositions have overlapping errors bars, they indicate that limited decompression accompanied

cooling after the metamorphic peak. Unlike the Ongeva granulites, evidence for distinct M_2 assemblages and mineral compositions were not found in the Riddock Amphibolite Member. The whole-rock compositions of mafic gneisses from the Ongeva granulites and mafic gneisses in the Harts Range meta-igneous complex are similar and probably reflect olivine tholeiitic precursors produced in a rift setting. In particular, they both have similar degrees of silica saturation. Garnet-clinopyroxene mafic gneisses have not been found in the Ongeva granulites, but appear to be common in the Harts Range meta-igneous complex. Experiments of dry basalts (Green and Ringwood, 1967; Ito and Kennedy, 1971) indicate that eclogites can form via an intermediate garnet-granulite stage involving the reaction: orthopyroxene + plagioclase = garnet + clinopyroxene. Thus, pressure estimates and the presence of garnet and clinopyroxene in the Riddock Amphibolite Member may imply that peak metamorphism in the Harts Range Group occurred at moderate pressure conditions and at higher pressures than in the Ongeva granulites. Higher pressure and lower temperature conditions in the Harts Range Group than in the Strangways Metamorphic Complex have also been suggested by Oliver et al. (1988). A lack of corona textures indicative of cooling (e.g. orthopyroxne-plagioclase between garnet and clinopyroxene) may reflect a very low water activity in the garnet-clinopyroxene mafic gneisses after peak metamorphism.

4.7   Conclusions

The metamorphic and structural history of the Strangways Metamorphic Complex, the Harts Range Group and the shear zones that dissect the central Arunta block impose constraints on the inferred tectonometamorphic evolution. A tectonic model for the evolution of the central Arunta Block must account for the high heat flow at peak metamorphism, the different geothermal gradients, cooling with decompression after the metamorphic peak, an increase in temperature and pressure during M_2 in the Ongeva granulites, and the high-temperature assemblages preserved in shear zones.

The mineral zoning and reaction history of granulites from the Ongeva granulites are the products of two tectonometamorphic cycles. Peak metamorphism occurred at

conditions of T> 880°C and P≤6.5 kbar and was accompanied by anatexis. The geothermal gradient at peak metamorphism was probably 41-53°C/km. Limited decompression accompanied thermal relaxation after the metamorphic peak, which may imply that crustal thickening was associated with the processes responsible for the high heat flow during peak metamorphism. Decompression and cooling occurred prior to a widespread non-coaxial folding of the Ongeva granulites. The second cycle of metamorphism in the Ongeva granulites resulted in an increase in pressure and temperature after cooling and may have been concomitant with the non-coaxial folding of the Ongeva granulites. Fluid movement with a high activity of Cl accompanied the second metamorphic cycle.

Mineral zoning in the Riddock Amphibolite Member indicates cooling and possible decompression after peak metamorphism at high T (~810°C) and moderate pressures (P = 7.6±1.6 kbar). The geothermal gradient at peak metamorphism was probably 28-41°C/km, i.e. less than the gradient in the Ongeva granulites. Upright folding, with recrystallization of hornblende in the axial plane, occurred after the metamorphic peak. The two inferred P-T-t paths for the Ongeva granulites and the Harts Range Group are dissimilar but appear to have approached each other during M_2 in the Ongeva granulites (Fig. 4.8c). This may imply that the Ongeva granulites and the Harts Range group were juxtaposed at this time either by underthrusting of the Ongeva granulites or overthrusting of the Harts Range Group, as occurs in deformation within zones of continental convergence. The approximately parallel cooling paths, with inferred decompression after the metamorphic peak, for both the Ongeva granulites and the Harts Range group may also imply that the same tectonometamorphic processes responsible for peak metamorphism affected both groups. They possibly formed different parts of the same early-Proterozoic protolith, the suggested geothermal gradients at peak metamorphism reflecting an increase in metamorphic grade southwards.

170

CHAPTER 5

The kinematic history and metamorphic conditions associated with ultramylonitization in the Strangways Metamorphic Complex

Summary

In the early-Proterozoic Strangways Metamorphic Complex, central Australia, discontinuous high-temperature (granulite facies), ductile ultramylonite zones developed during and after a widespread compressional folding deformation (D3) that may have been responsible for a second metamorphic event (M2). The ultramylonite zones form a moderately-dipping extensional system, with extension parallel to an inferred transport axis during D3 folding. Recrystallized assemblages in the ultramylonite zones indicate conditions of P = 7.1±1.3 kbar and T = 770 ± 80°C, similar to M2 conditions. The ultramylonitization represents extension at mid-crustal levels, either between major reverse shear zones during the later stages of the compressional D3/M2 event or as a result of gravitational collapse of a thickened crust on a weak lithosphere. Significant lateral dextral shearing may have also occurred prior to dip-slip movement and may represent lateral escape during compression[5].

[5] Norman, A. R. and Vernon, R. H., 1991. Granulite facies, mid-crustal extension in a Proterozoic collisional orogen, Strangways Metamorphic Complex, central Australia. *Tectonophysics* (submitted).

5.1 Introduction

This Chapter describes and discusses the significance of numerous high-T (granulite facies) high-angle normal ductile shear zones that transect the early-Proterozoic Strangways Metamorphic Complex, south of the Harts Ranges (Fig. 1.0). These shear zones consist of ultramylonite with a well-developed, northeast-plunging stretching lineation. Microstructures preserved in the ultramylonite are similar to high-grade shear fabrics described in the Giles Complex, central Australia (Moore, 1973; Goode 1978), Caledonian thrusts in the Bergen Arcs (Austrheim and Griffin, 1985), mylonites from the Aurela Group granulites, California (Behrmann and Mainprice, 1987) and alpine-type peridotites (Nicolas and Boudier, 1975).

A northeast-side down, normal sense of shear is preserved in most of the ultramylonites and is parallel to a well-developed stretching lineation in the folded country rock. Models involving extensional shear zones have received much attention in recent years. Most work has concentrated on low-angle, simple-shear, normal shear zones (detachments) that separate a high-grade gneissic dome or core complex from lower-grade hanging-wall rocks (Davis and Coney, 1979; Lister and Davis, 1983; Davis et al., 1983; Wernicke, 1985). Horizontal extensions are generally large in these extensional models and heat flows are high. A model of simple-shear lithospheric extension has also been used to explain the high geothermal gradient at peak metamorphism and inferred isobaric cooling paths that are commonly preserved in Proterozoic rocks (Sandiford and Powell, 1986), such as the Arunta Block (Warren and Stewart, 1988).

High-angle to gently dipping normal faults or shear zones also occur in continental rifts (Morley, 1989) and collisional orogens (Burchfiel and Royden, 1985) but are thought to be the result of pure shear extension. Extension in these circumstances is perpendicular to the strike of the orogenic belt or rift system and is generally small, compared with simple-shear models. In collisional orogens, some normal faults, such as those north of the high Himalayas in southern Tibet (Burg et al., 1984) are laterally

extensive (800 km). Upper-crustal normal faults, like those in Tibet, which occur in an over-riding plate and are thought to have formed during gravitational collapse of a topographic front (Burchfiel and Royden, 1985). Collapse of the crust may result if a thinned or normal thickness lithosphere cannot support the thickened crust. Similar upper-crustal, gravitational faults, with crustal extension perpendicular to the orogenic belt also occur in the Andes (Dalmayrac and Molnar, 1981).

In the eastern Alps, extensive normal faults appear to have largely accommodated extension parallel to the strike of the orogen (Selverstone, 1988; Ratschbacher et al., 1989). Orogen-parallel, horizontal extension (continental escape) in the eastern Alps compensated for the crustal thickening, convergence and shortening that was associated with collision. The Red River fault, in southern China, is also thought to have formed due to lateral continental escape, resulting from collisional tectonism in the Himalayas (Tapponnier et al., 1990).

Normal shear zones have also been described from the Rombak Window, Norway and attributed to deformation in the down-going plate during Caledonian subduction (Cashman, 1990). Normal faulting in the direction of subduction has also been recognized in seismic profiles of the Applachian-Ouachita orogenic belt (Lillie, 1985) and the Himalayan foreland of Pakistan (Lillie and Yousef, 1986).

In this Chapter, the overall geometry of shear zones in the Strangways Metamorphic Complex is described and the timing and significance of mylonitization is discussed, taking into account the petrology of the ultramylonites and the tectonometamorphic history preserved in the country rock. The shear zones described in this Chapter represent high-grade (mid-crustal), extensional ultramylonitization, which was probably associated with deformation along a northnortheast-southsouthwest tectonic axis during the development of a collisional orogen in the mid-Proterozoic.

5.2 Critical field Relationships

A pervasive foliation throughout the Strangways Metamorphic Complex is defined by coarse-grained quartz-feldspar-biotite leucosomes in felsic gneisses and coarse-grained orthopyroxene-hornblende-plagioclase leucosomes in mafic gneisses. This foliation has been referred to as S_2 and is subparallel, although locally oblique, to a macroscopic compositional layering (S_1). A coarse-grained sillimanite-biotite-magnetite foliation cuts S_2 in metapelites and has been referred to as S_{2b}. S_1, S_{2a} and S_{2b} are folded by colinear, northeast-plunging D_3 folds that commonly have axes parallel to a well-developed, northeast-plunging quartz stretching lineation (L_3). The shear zones described in this Chapter displace S_2 foliations and cut most folds, although some parallel the folded outcrop pattern.

In the northern part of the Strangways Metamorphic Complex, D_4 shear zones and D_3 folds are cut by a close-spaced, north-dipping, coarse-grained biotite foliation. This foliation forms the pervasive foliation in the Gough Dam Schist Zone (Fig. 1.0). Deformation in the north-dipping, predominantly phyllonitic, Gough Dam Schist Zone has been referred to as D_5. Greenschist facies retrogression is common in the Gough Dam Schist Zone and in the Anamarra granite domain and is probably related to late fluid movement and deformation (uplift). The following structural and mineralogical analysis of shear zones transecting the Strangways Metamorphic Complex has been undertaken where this later retrogression is sparse or nonexistent.

The shear zones trend mostly southeast (Fig. 5.1) and dissect the Strangways Metamorphic Complex into spatially independent units. They are generally discontinuous and consist of ultramylonite with a mylonitic foliation (S_4) parallel to distinct shear zone walls (Fig. 5.2a). The shear zones dip at high to moderate angles (50°-80°) to the northeast and contain a stretching lineation that plunges predominantly to 045. A mylonitic foliation, parallel to the shear zones, may also exist in the country rock, where it is defined by well-lineated, elongate quartz aggregates. However, deformation has been mainly concentrated into the narrow, discrete shear zones. The
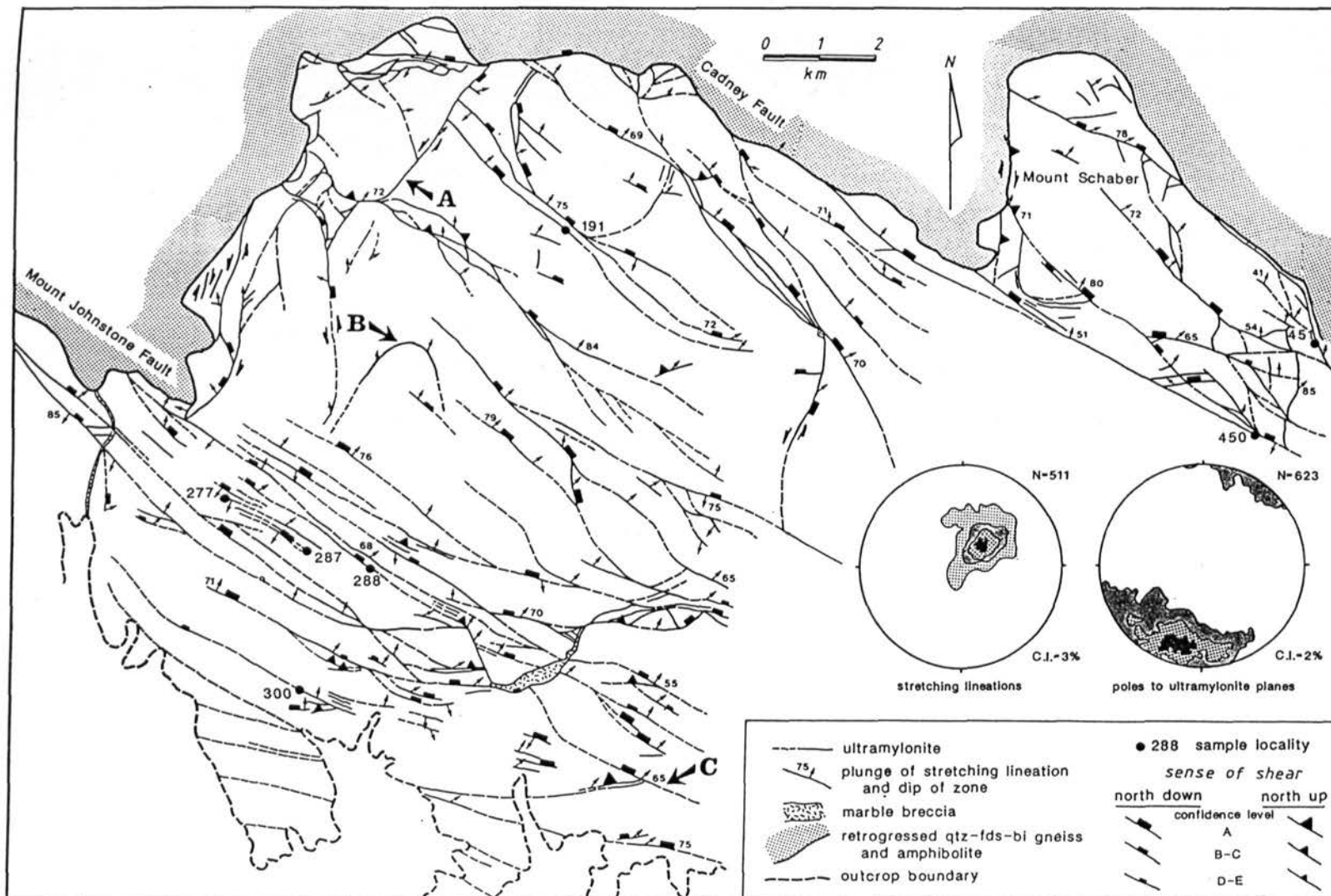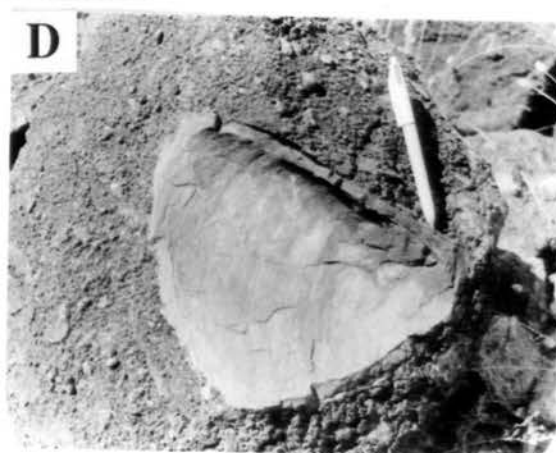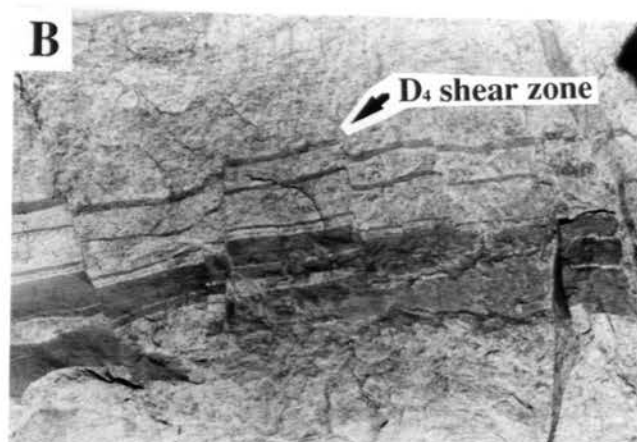
Fig. 5.1 Outcrop pattern of shear zones greater than 0.75 m wide, transecting the Ongeva granulites.

Fig. **5.2** **(a)**   Discontinuous shear zone outcrop.

      5.2 **(b)**   Narrow shear zones and displaced S_2 foliation.

      5.1 **(c)**   Ultramylonite sheath fold in a north-side down shear zone.

      5.1 **(d)**   Marble breccia, containing folded fragments of lineated ultramylonite.

zones are of variable width (1 mm-3 m) and lateral extent. They tend to be wider in the more felsic rocks and narrower and more closely-spaced in the mafic rocks. S_2 commonly bends into and is cut by the zones (Fig. 5.2b).

The shear zones generally bifurcate along strike towards the southeast and down dip, with the acute angle of their intersection towards the west. Any measureable lateral displacement decreases to the southeast and many zones disappear towards the southeast. Some shear zones are laterally isolated, apparently unconnected to a shear zone system.

The ultramylonites contain porphyroclasts in a fine-grained matrix and have an internal monoclinic symmetry, suggesting that deformation was accommodated by predominantly crystal-plastic, non-coaxial, laminar flow, which is typical of most mylonites (e.g. Bell and Etheridge 1973, White et al 1980). Sheath folds (Fig. 5.2c) also occur but are not common. S_4 is defined by fine-grained, thin (<1 mm) compositional layers. Although the shear zones mostly have an anastamosing southeast-trending outcrop pattern and do not appear folded, S_4 has a polar plot distribution pattern similar to the distribution of S_2 that is folded in the country rock (Figs 5.3a, 5.3b). S_4 is distributed about a small circle with a radius of 70° and an axis plunging 80° to 045. Two extensive shear zones (labelled A and B in Fig. 5.1) parallel the folded outcrop pattern, but contain stretching lineations that plunge consistently to the northeast. This implies that ultramylonitization occurred either along folded lithological boundaries or that folding and ultramylonitization, in places, were synchronous.

An L_4 stretching lineation is well developed in the shear zones and is defined by fine-grained ribboned feldspar and quartz and local garnet aggregates. Coarse-grained garnet, hornblende and orthopyroxene in S_2 leucosomes in the country rock are commonly well-lineated in close proximity to the shear zones and are subparallel to the stretching lineation in the ultramylonites. L_4 has a mean plunge of 50° to 045, but has a polar plot distribution (Fig. 5.4a) about two great circles (90/133 and 51/040). L_4 has a similar distribution to a northeast-plunging L_3 stretching lineation measured on S_2 (Fig. 5.4b) and to most D_3 fold axes (Fig. 5.4c). Between some shear zones, D_3 fold axes

(a)

N

(b)

N

Poles to S4 ultramylonitic foliations
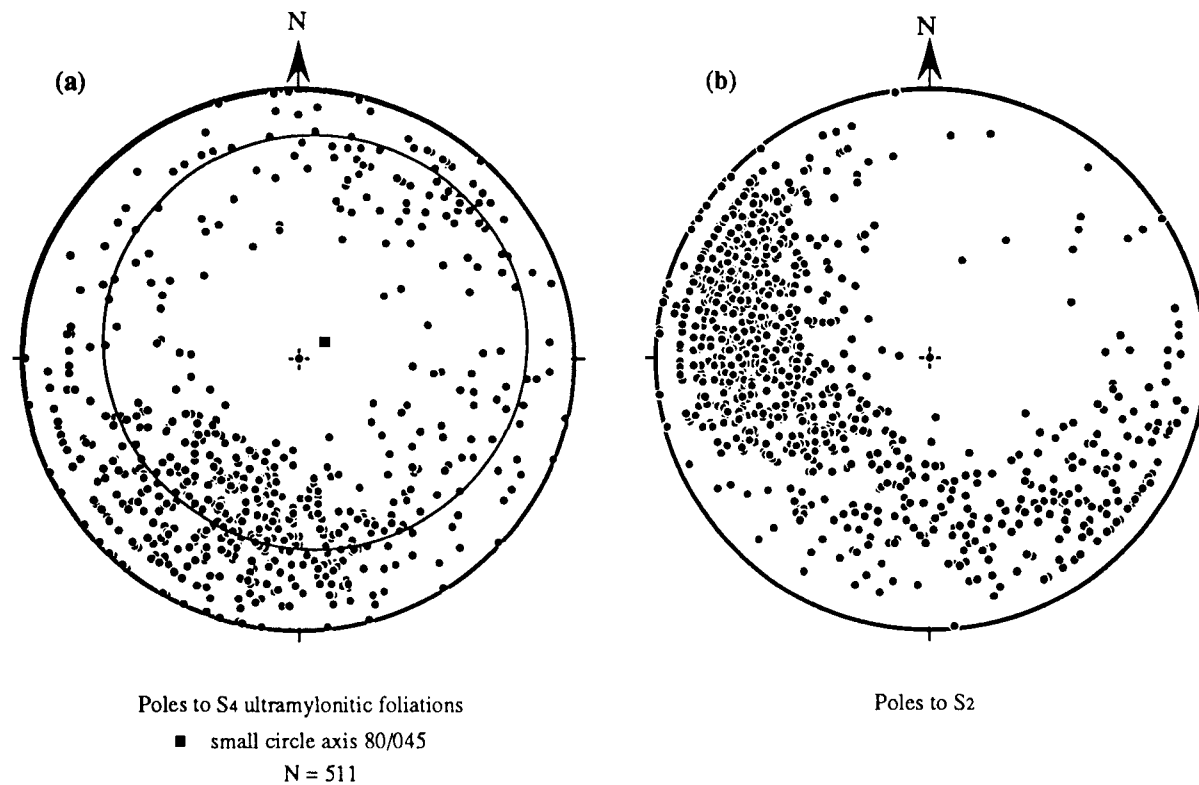
■ small circle axis 80/045

N = 511

Poles to S2

Fig. 5.3 (a) Lower hemisphere, equal area, stereographic projections of poles to ultramylonitic foliations (S4).

5.3 (b) Lower hemisphere, equal area, stereographic projections of poles to S2.
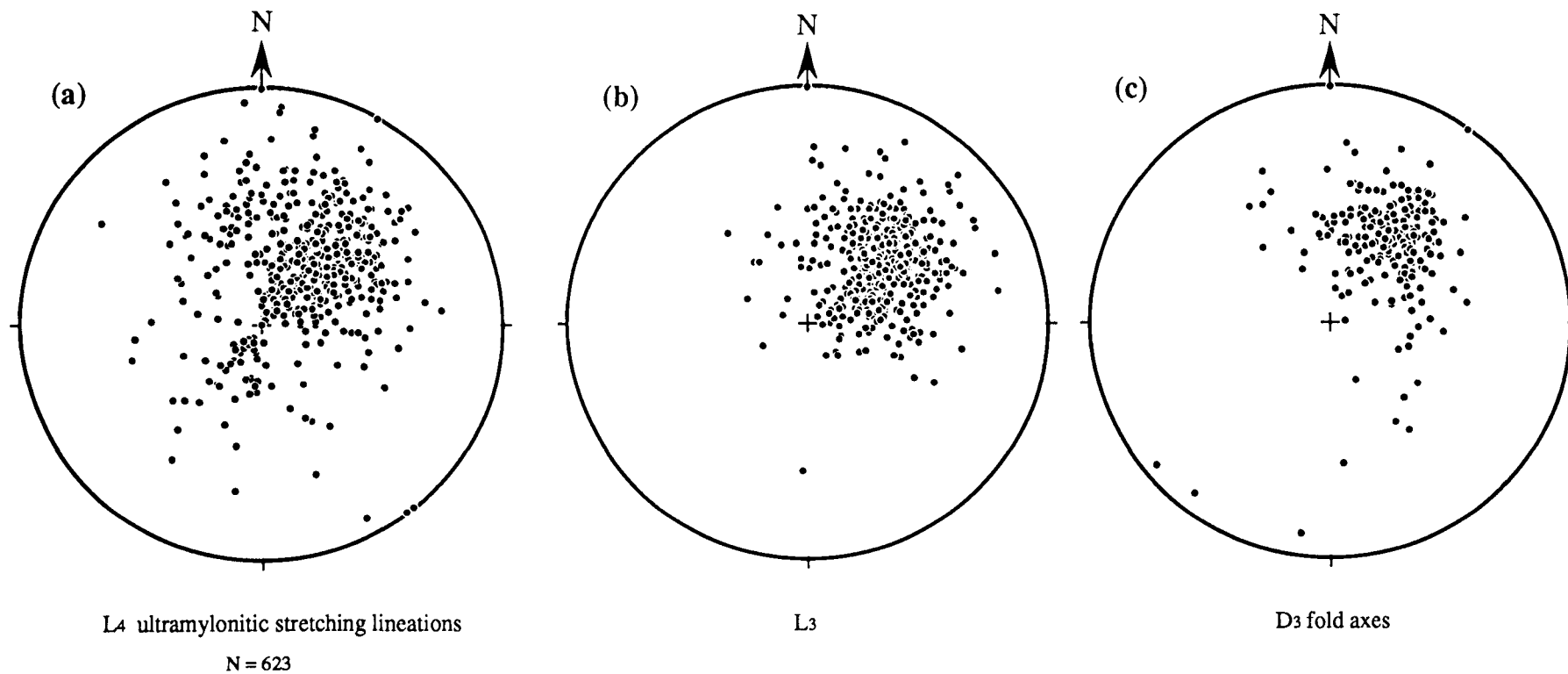
Fig. 5.4 **(a)** Lower hemisphere, equal area, stereographic projections of ultramylonite stretching lineations (L4).

5.4 **(b)** Lower hemisphere, equal area, stereographic projections of L3 in the gneissic country rock.

5.4 **(c)** Lower hemisphere, equal area, stereographic projections of D3 fold axes.

are bent towards the mylonitic extension direction, and fold limbs adjacent to the zones are bent or overturned (Fig. 5.5). The interference of macroscopic D_3 folds is mainly restricted to areas between closely-spaced prominent shear zones, probably reflecting local flattening as a result of space problems encountered during deformation. However, L_3 is rarely observed to be folded and no east-west trending mesoscopic folds refolding D_3 folds between the shear zones were observed, which suggests that little regional-scale shortening has occurred between the shear zones. The similar great circle distribution of D_3 fold axes and L_4 may imply that deformation between some ultramylonite was accompanied by local east-west shear folding.

An unusual marble breccia containing isoclinally and torsionally folded ultramylonite fragments (Fig. 5.2d) occurs along the Mount Johnstone Fault and between lithological boundaries adjacent to shear zones (Fig. 5.1). The folded ultramylonite fragments are fractured and pulled apart, and contain a well-developed, folded stretching lineation. A flow foliation, delineated by coarse-grained recrystallized calcite and minor K-feldspar, diopside, scapolite and quartz clasts, occurs between the ultramylonite fragments. The marble breccia occurs at or near the junction of prominent shear zones and is probably associated with local shortening between the zones. Flattening of calc-silicate rocks interlayered with the mafic and felsic gneissses and 'squeezing' to sites of extension may have accommodated local space-problems during the later part of the ultramylonitic deformation. Rare pseudotachylyte veins also occur in felsic granofelses between narrow shear zones, which form their boundary/generation surfaces. Like the marble breccia, pseudotachylyte probably developed as a result of a local high strain-rate during or after ultramylonitization.

Although the shear zones mostly cut and, in places, displace D_3 folds (Fig. 5.6), the similar distribution of S_2 and S_4 and of L_3, F_3 and F_4 fold axes and L_4 implies that D_3 folding of S_2 and D_4 ultramylonitization were part of the same orogenic cycle.

180

antithetic
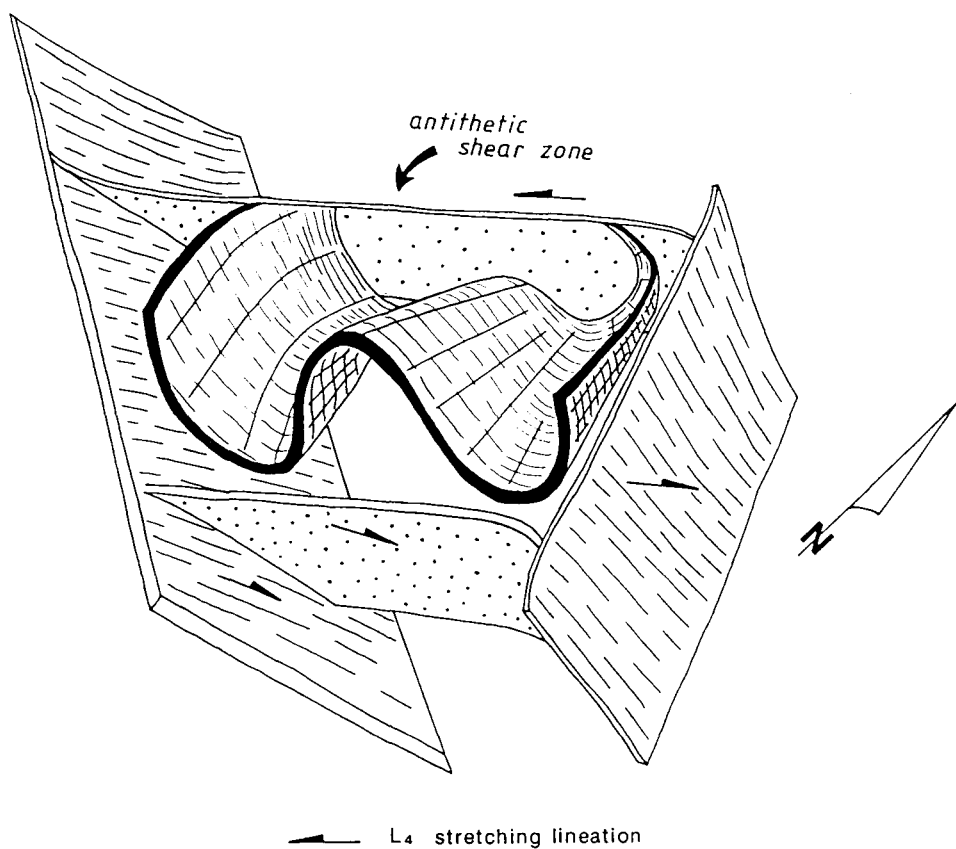shear zone

L₄ stretching lineation

Fig. 5.5 D₃ fold interference adjacent to prominent shear zones and antithetic shear zones. Location is shown in Fig. 5.6.
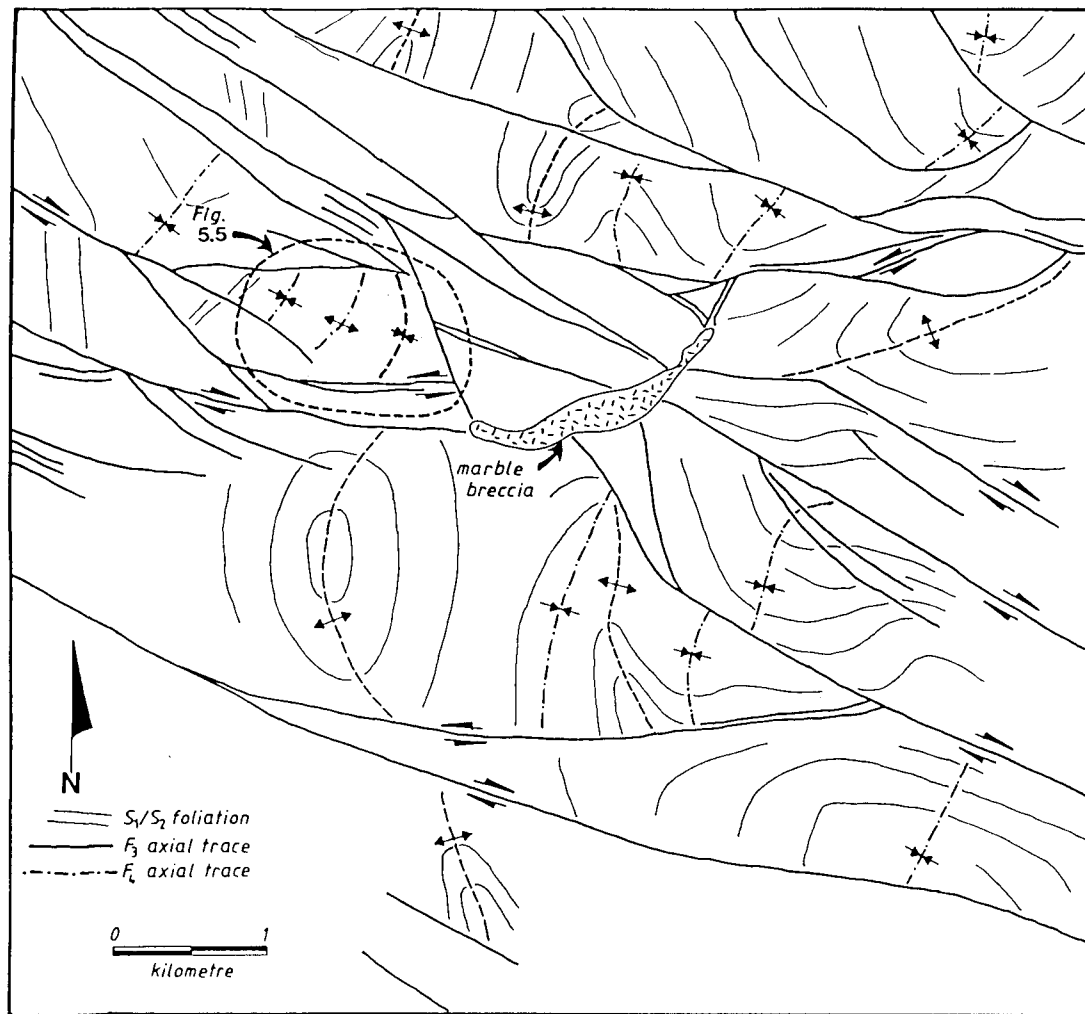
Fig. 5.6 Outcrop fold interference pattern and cross-cutting D_4 shear zones.

5.21 Displacement

There are no apparent metamorphic facies changes across the ultramylonite zones, which suggests that little displacement has occurred. A displacement of 21 m and strain of $\varphi = 6$ were estimated (Ramsay and Graham, 1970) across a rare continuous shear zone (labelled C in Fig. 5.1). However, estimates could be regionally meaningless, as strain has been mostly partitioned into narrow discrete shear zones.

Although L_4 stretching lineations are generally steep and parallel to the shear direction, the displacement of similar rock types across some shear zones indicates that lateral dextral displacement may have also occurred. In places, lateral displacement may have been significant. Displacement of similar rock types across the Cadney fault (Fig. 5.1) indicates that lateral dextral displacement may have been 8 km. To the north of Mount Schaber (Fig. 5.1), dextral displacement of 1 km may have occurred along the southern margin of the Gough Dam Schist Zone. Likewise, the Mount Johnstone Fault (Fig. 5.1), which bisects Strangways Metamorphic Complex, may have also been a zone of dextral displacement. In all these examples, the stretching lineation is steep, implying that the dextral movement predated dip-slip movement.

5.22 Kinematic Indicators

Most shear zones are characterized by a north-dipping foliation, a steep stretching lineation and a north-side down sense of shear. In the field, the sense of shear was determined using criteria described by Simpson and Schmid (1983) and the bending of S_2 folia into the shear zone. In thin section, oblique quartz extinction, a preferred quartz crystallographic preferred orientation determined using a gypsum plate, an oblique fine-grained biotite foliation, and rare "mica fish" (Lister and Snoke, 1984) were useful additional sense of shear indicators.

At each outcrop, a confidence level from A to E was given to the sense of shear determination which was up-graded with slabbing and thin-sectioning of the rock (Fig.

5.1). Confidence level A was used when 4 or more different sense of shear indicators gave the same movement direction (e.g., rotated porphyroclasts, asymmetrical augen, asymmetrical mylonitic folds, an oblique foliation (S-plane), bending of S_2 into the zone) and there was never any contradiction. Confidence level B was used when 3 or more different sense of shear indicators gave the same movement direction. Confidence level C was used when 2 or more different sense of shear indicators gave the same movement direction (one of which was not an asymmetrical fold or the bending of S_2 into the zone). Confidence level D was used when only one reasonable sense of shear indicator was present (e.g. asymmetrical augen). Confidence level E was used when only one sense of shear indicator of dubious quality was present (e.g. bending of S_2 into the zone).

The results of this structural analysis are shown in Table 5.1 and in Fig. 5.1. The sense of shear was determined in samples from 245 outcrops. 79% of the samples preserve a north-side down sense of movement, 38% having a A-B confidence level. Only 8% had a north-side up sense of shear with an A-B confidence level. The most prominent shear zones have a normal sense of shear with a small dextral shear component. Shear zones that have a reverse sense of shear generally link normal shear zones and are referred to as antithetic shear zones (see below).

Table 5.1. Sense of shear determination in shear zones.

category	N-side down	N-side up
A	36	1
B	56	19
C	57	15
D	37	17
E	7	0
TOTAL	193	52

5.23 Antithetic shear zones

Most north-side up shear zones trend eastnortheast and generally connect parallel southeast-trending, north-down shear zones. These reverse shear zones have a sinistral displacement component that is antithetic to the north-down shear zones they connect. Where these zones have been observed, the southerly block is always displaced to the east relative to the northern block. Prominent north-side up sinistral shear zones that join north-side down shear zones are shown in Fig. 5.7. Antithetic shear zones generally occur where the limbs and axial planes of F_3 and F_4 folds have been deformed (Fig. 5.5). Development of the antithetic shear zones was probably synchronous with local shortening that deformed these folds and accommodated a lateral extension component. The stretching lineations associated with the antithetic shear zones and connected normal shear zones also tend to plunge more to the east than elsewhere. Any space problem that may result from the geometry of the shear zones appears to be alleviated by local deformation of F_3 and F_4 folds and by eastnortheast-trending sinistral reverse shear zones, which are antithetic to the overall shear zone system and displace the southern blocks to the east.

5.3 Petrography

5.31 Primary assemblages in S_2

In mafic gneisses, the gneissic layering (S_2) is defined by alternating, medium to coarse-grained orthopyroxene-clinopyroxene mesosomes and thin plagioclase-rich leucosomes, which may also contain subidioblastic, coarse-grained orthopyroxene and hornblende. Hornblende forms up to 70% of the mafic layers and quartz is present in more felsic varieties of mafic gneisses. The main, penetrative S_2 foliation is cut by irregular networks of coarse-grained orthopyroxene-plagioclase-rock that may contain a weak foliation parallel to S_2.
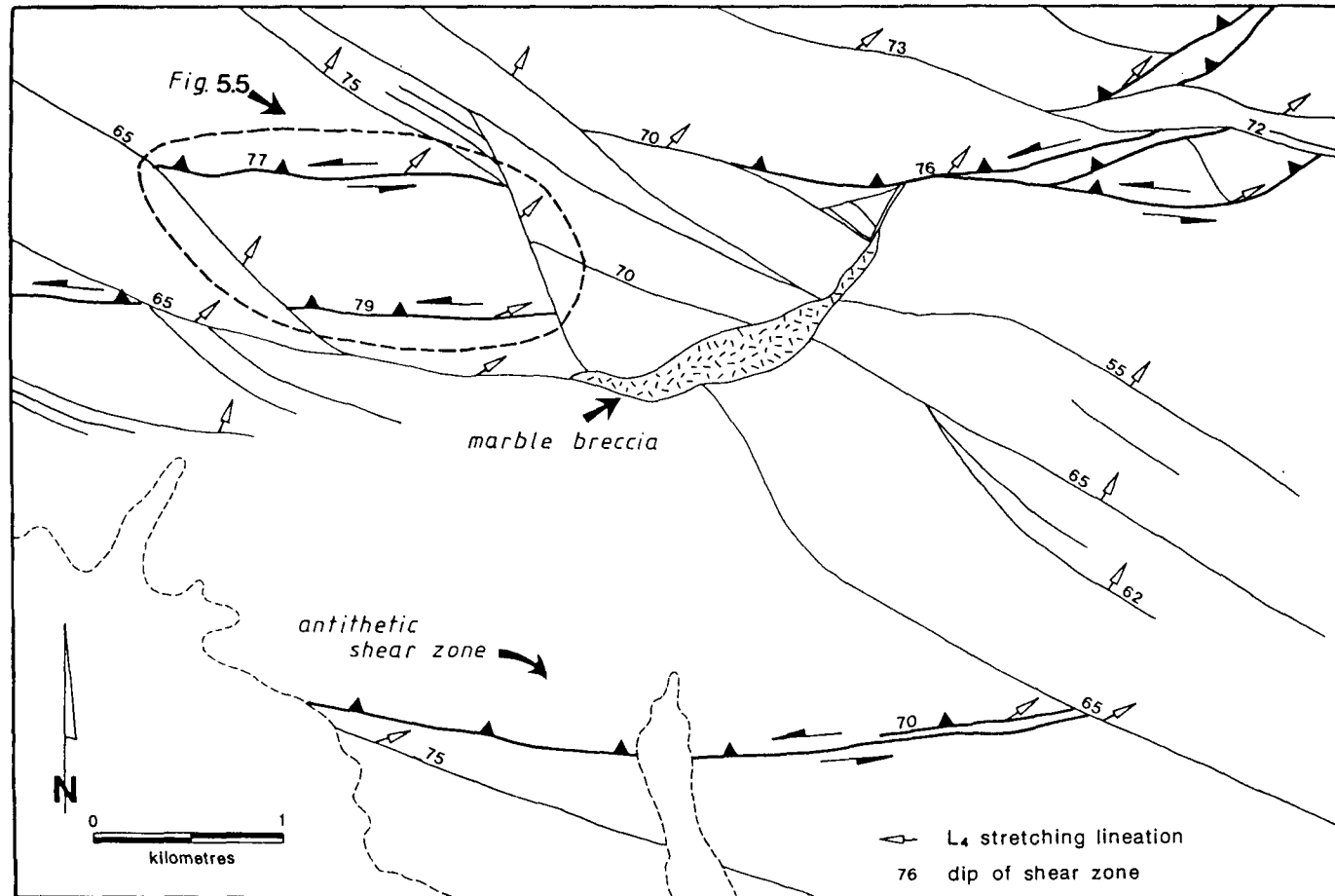
Fig. 5.7 Shear zone geometry, showing ENE-trending antithetic shear zones connecting normal shear zones.

The felsic gneisses vary from equigranular, medium to coarse-grained, quartz-K-feldspar-plagioclase-orthopyroxene granofelses to garnet-orthopyroxene-K-feldspar-quartz--biotite migmatites. The proportion of plagioclase varies considerably (Norman and Flood, 1991; Chapter 1). The gneissic foliation (S_2) is defined mainly by medium to coarse-grained leucosome layers and is cut by irregular, coarse-grained K-feldspar-orthopyroxene pods.

Metapelites are characterized by abundant sillimanite, garnet and biotite, and commonly grade into quartz-feldspar-biotite migmatites. The most obvious foliation in these rocks consists of a poorly-lineated, coarse-grained, sillimanite-biotite-magnetite foliation (S_{2b}) that cuts the medium to coarse-grained K-feldspar-quartz$\pm$biotite$\pm$cordierite$\pm$garnet gneissic S_2 foliation. Garnet occurs as large, elongate, poikiloblastic grains in S_2 or as large grains in coarse-grained, irregular pods of quartz-K-feldspar-biotite that cut S_2.

Calc-silicate rocks contain an S_2 gneissic foliation defined by alternations of medium to coarse-grained quartz-rich layers and granoblastic scapolite-diopside-grossular-anorthite$\pm$wollastonite layers.

The S_2 gneissosity, S_{2b} foliation and the coarse-grained pods are all deformed in the shear zones.

5.32 M₂ assemblages

Fine-grained symplectic aggregates, recrystallized grain boundaries and retrogressed minerals, which are texturally distinct from the coarse-grained minerals in S_2 represent the effects of a second metamorphism (M_2, Chapters 1, 3 and 4). In mafic gneisses, the effects of M_2 are recognized by coronas of granular, subidioblastic orthopyroxene$\pm$clinopyroxene-plagioclase between coarse-grained granoblastic hornblende and plagioclase grains and recrystallized M_1 clinopyroxene grain boundaries. Extensive recrystallization and partial retrogression in felsic gneisses and granofelses probably represents the effects of M_2 (Norman and Flood, 1991, Chapter 1). Quartz is

187

commonly recrystallized into polygonal sub-grains, coarse-grained plagioclase is recrystallized around grain boundaries, and coarse-grained M_1 orthopyroxene is partially retrogressed to magnesio-hastingsite. In places, the recrystallized grains and retrograde minerals form an axial-surface foliation (S_3) to F_3 folds, indicating that recrystallization and partial retrogression accompanied D_3 folding.

In metapelites, granoblastic cordierite has been replaced along its grain boundaries and cleavage planes by fine-grained symplectic aggregates of orthopyroxene-sillimanite-quartz±biotite±magnetite±sapphirine. In places, the symplectite totally pseudomorphs cordierite. New garnet and vermicular magnetite also occur around the margins of coarse-grained elongate garnet grains in S_2.

In calc-silicate rocks, the effects of M_2 are difficult to recognize. However, extensive recrystallization of quartz-rich layers, recrystallized diopside and garnet coronas on diopside and scapolite may represent the effects of M_2 (Chapter 4).

Recrystallized grains and mineral reaction products that represent the effects of M_2 occur between, and appear to be cut by D_4 shear zones, but because of the fine grain-size of both the ultramylonite and M_2 minerals, a clear cross-cutting relationship is difficult to delineate. However, diopside porphyroclasts with M_2 garnet coronas are found in ultramylonitized calc-silicate rocks and garnet porphyroclasts with rims of vermicular M_2 garnet-magnetite are found in ultramylonitized metapelites, which suggests that the D_4 ultramylonitization largely post-dated M_2.

5.33 Ultramylonite textures and assemblages

The ultramylonite consists of a well-foliated, fine-grained recrystallized matrix surrounding porphyroclasts derived from the surrounding high-grade gneisses. The composition of the ultramylonite is usually heterogenous and the mylonitic foliation is defined by different compositional layers, commonly monomineralic. Boudins and thin compositional layers derived from the host gneisses are reworked within the shear zones, resulting in this grain-scale variation in composition (c.f. Vernon, 1974).

Ultramylonitized two pyroxene mafic gneisses

Ultramylonitized mafic two pyroxene-hornblende-plagioclase gneisses (samples 277 and 287) contain recrystallized layers up to 2 mm wide of plagioclase and green-brown to blue-green hornblende that define the mylonitic foliation (S_4, C plane). Plagioclase clasts and recrystallized tails, with delta (δ) rotated shapes or sigma (σ) shapes are common and are useful for determining the sense of shear (Passchier and Simpson, 1986). Hornblende clasts up to 0.4 cm in diameter occur in the finer grained amphibole-rich layers and may also have an asymmetrical shape (Fig. 5.8a).

Orthopyroxene porphyroclasts generally have rounded shapes and recrystallized tails of fine-grained euhedral orthopyroxene or green-brown hornblende (Fig. 5.8b). Fine-grained recrystallized orthopyroxene may also define the mylonitic foliation. Clinopyroxene generally occurs as recrystallized, polygonal grains in monomineralic layers up to 1.5 mm wide, although fine-grained recrystallized clinopyroxene may also occur with granules of orthopyroxene defining the mylonitic foliation. Clinopyroxene porphyroclasts are not common, suggesting that clinopyroxene is more readily recrystallized than orthopyroxene.

Garnet-diopside-scapolite boudins within mafic gneisses may be reworked in the shear zones (sample 287), so that recrystallized orthopyroxene, clinopyroxene, amphibole and plagioclase occur in apparent microstructural equilibrium with the more calcic assemblages, including garnet.

Ultramylonitized felsic gneisses

A well-developed mylonitic foliation (C plane, S_4) is defined by alternating, close-spaced layers of recrystallized quartz, feldspar and fine-grained orthopyroxene granules (Fig. 5.8c; samples 288 and 300). Recrystallized aggregates of garnet may also define a mylonitic foliation. Recrystallized quartz is coarser-grained than recrystallized feldspar and both generally form bands up to 3 mm wide. Quartz usually

Fig. 5.8 (a) δ shaped amphibole porphyroclast and recrystallized amphibole tails. Amphibole, clinopyroxene and plagioclase define the mylonitic foliation. Dextral shear. Sample 277. Base of photograph is 4.4 mm.

5.8 (b) δ shaped orthopyroxene porphyroclast and recrystallized amphibole tails. Amphibole, clinopyroxene and plagioclase define the mylonitic foliation. Dextral shear. Sample 277. Base of photograph is 1.75 mm.

5.8 (c) Mylonitic foliation defined by fine-grained recrystallized orthopyroxene and plagioclase. Dextral shear. Sample 300. Base of photograph is 4.4 mm.

5.8 (d) Garnet porphyroclast with recrystallized tails of garnet and rimmed by biotite. Sample 288. Base of photograph is 1.75 mm.

5.8 (e) Fine-grained neocrystallized sillimanite, parallel to the stretching lineation, defines the mylonitic foliation. Sample 105. Base of photograph is 1.75 mm
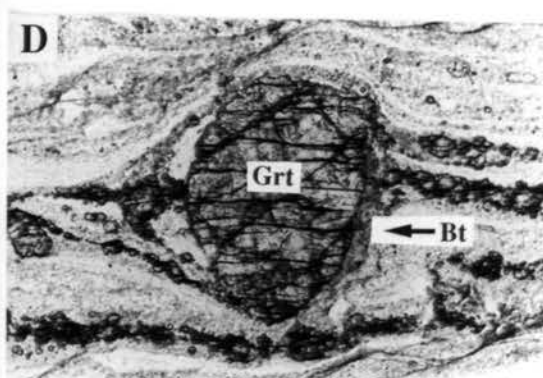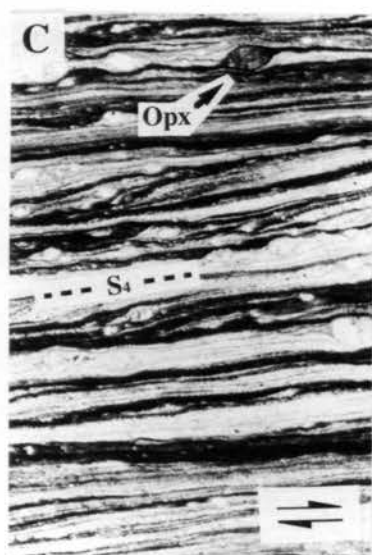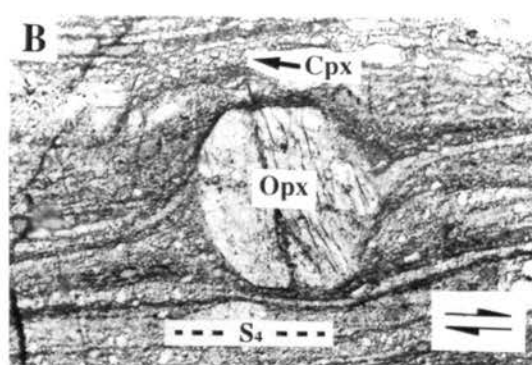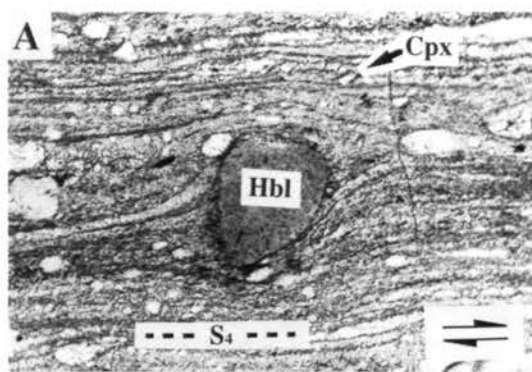
forms a granoblastic mosaic, although grain boundaries oblique to the mylonitic foliation and an oblique crystallographic preferred orientation commonly form a second foliation (S plane), which is consistent with other sense of shear indicators. Plagioclase porphyroclasts, up to 1 cm in diameter, with undulose extinction and recrystallized tails of plagioclase±scapolite, commonly have a δ or σ asymmetrical shape (e.g. Passchier and Simpson, 1986). Totally recrystallized plagioclase clasts are also quite common. Myrmekite commonly replaces K-feldspar adjacent to shear zones, suggesting that it was induced by strain and/or fluid movement during ultramylonitization (Vernon et al., 1983). Orthopyroxene clasts are up to 0.5 cm in diameter and have polygonal recrystallized margins and tails of finer grained (< 0.3 mm) orthopyroxene that define a σ asymmetrical shape. Orthopyroxene clasts may have a chemical zonation (see discussion on mineral composition), with different compositions from that of the recrystallized tails, reflecting different metamorphic conditions between M_1 and ultramylonitization.

In mylonitized garnet-bearing felsic gneisses, almandine-rich porphyroclasts may contain tails of neocrystallized garnet and fine-grained biotite (Fig. 5.8d). Fine-grained biotite after garnet may also form an oblique S foliation that is parallel to a quartz crystallographic preferred orientation. Rarely, the biotite S foliation is kinked and another biotite foliation is present, which may be related to local post-mylonitic deformation or progressive rotation of the stress axes (Platt and Vissers, 1980). Garnet clasts and recrystallized garnet aggregates may occur in the mylonitic foliation, with orthopyroxene clasts and recrystallized granules (sample 288). In the orthopyroxene-garnet ultramylonites, the finer grained orthopyroxene-garnet aggregates may form symplectic intergrowths.

Ultramylonitized metapelitic gneisses

Ultramylonitized metapelitic gneisses are not common, although where they exist, the mylonitic foliation is defined by thin layers of recrystallized quartz, plagioclase and K-feldspar similar to those found in the ultramylonitized felsic gneisses. Fine-grained,

neocrystallized sillimanite and biotite aggregates parallel to the stretching lineation may also define the mylonitic foliation (Fig. 5.8e). Fine-grained biotite commonly forms an oblique foliation (S plane) consistent with other sense of shear indicators. Coarse-grained S_{2b} sillimanite porphyroblasts are common in mylonitized metapelites and are not retrogressed. They generally lie at high angles to the stretching lineation in the foliation, and may have rotated away from the extension direction in the foliation plane during deformation. Cordierite was not found in ultramylonitized metapelites and garnet was not found in microstructural equilibrium with neocrystallized sillimanite. M_2 orthopyroxene-sillimanite assemblages in the country rock are not retrogressed adjacent to shear zones.

Ultramylonitized calc-silicate gneisses

Thin layers, up to 1 mm wide, of granoblastic quartz and scapolite and fine-grained recrystallized plagioclase commonly define the mylonitic foliation (samples 451, 191 and 450) in calc-silicate ultramylonites. Asymmetrical plagioclase porphyroclasts with recrystallized tails of plagioclase and scapolite are common. Recrystallized fine-grained hornblende and hornblende clasts also occur in layers and may define S_4. Clinopyroxene generally occurs as recrystallized polygonal grains in distinct layers. Clinopyroxene clasts are not common, but where they exist, may have garnet coronas. Garnet may also occur as asymmetrical porphyroclasts with neocrystallized tails of fine-grained garnet aggregates (sample 451).

5.34 Marble breccia

An unusual marble breccia containing folded ultramylonite fragments occurs in places between prominent shear zones. The ultramylonite fragments are similar to the ultramylonitized felsic gneisses described above. Coarse-grained calcite that occurs between ultramylonite fragments contains a flow foliation. Large clasts of scapolite, diopside and K-feldspar rimmed by (M_2?) garnet coronas are contained in the marble. These clasts are probably derived from deformed calc-silicate rocks. This marble was

probably ductile during deformation and may have resulted from the flattening and 'squeezing' of calc-silicate rocks during or after the later stages of mylonitization.

5.4   Estimates of P-T conditions from ultramylonite mineral compositions

The composition of recrystallized, microstructurally equilibrated mineral assemblages in ultramylonites have the potential for estimates of metamorphic conditions that existed during D_4 ultramylonitization.   Norman and Clarke (1990) estimated that conditions during M_2, which probably predated ultramylonitization, were P = 7.5±0.8 kbar and T~800°C.   In this paper the recrystallized mineral compositions in ultramylonitized mafic, felsic and calc-silicate gneisses are described and applied to a number of different geothermometers and geobarometers as well as the average pressure approach of Powell and Holland (1988), in order to determine whether metamorphic conditions during D_4 ultramylonitization were distinct from conditions estimated for M_2. Estimates of P-T conditions during D_4 are important for trying to resolve a P-T-t path and the tectonic evolution of the Strangways Metamorphic Complex. Compositional variations between porphyroclasts and their recrystallized tails have been examined to help define relative changes in temperature and pressure from conditions prior to mylonitization to conditions during mylonitization.   In most ultramylonites, the compositions of porphyroclasts probably reflect metamorphic conditions at M_1 or during cooling from the metamorphic peak (D_2). Only recrystallized assemblages in apparent equilibrium and samples containing no retrograde greenschist facies assemblages were used for thermobarometric estimates.

Mineral analyses were obtained at Macquarie University using wds and eds systems on a ETEC microprobe at 15 Kev and specimen current of 50 nA. Mineral compositions in ultramylonitized mafic (samples 277 and 287), felsic (samples 288 and 300) and calcic (samples 287, 191, 450 and 451) gneisses are presented in Tables 5.2, 5.3 and 5.4 at the end of this section. The results of thermobarometric calculations are presented in Table 5.5 and the intersection of calculated P-T lines are shown in Fig.

5.10, also at the end of this section. The intersection of P-T lines is used to calculate the mean metamorphic conditions that existed during ultramylonitization (Fig. 5.10d). Sample localities are shown in Fig. 5.1. The component composition of pyroxenes was determined using methods outlined by Lindsley (1983) and using the nomenclature of Poldervaart and Hess (1951). Amphibole nomenclature and site occupancy follow Hawthorne (1981).

Sample 277 (Opx-Cpx-Hbl-Pl)

Sample 277 is an ultramylonitized two pyroxene-hornblende-plagioclase mafic granofels. Mafic granofelses are common in the Strangways Metamorphic Complex and have a bulk chemical composition very similar to amphibolites studied by Spear (1981), in which the chemical variation of amphiboles with changing P, T and f_{O2} was examined. Orthopyroxene clasts are hypersthene ($X_{En} = 0.63$) and have recrystallized tails of fine-grained hypersthene with a similar composition. Recrystallized hypersthene tails have a higher Al and lower Ca content than the hypersthene clasts. Fe^{3+} is generally higher in recrystallized hypersthene and Mg is lower, although $\%X_{Mg}$ remains constant (62.5-63.5).

Clinopyroxene clasts are rare, but where they exist they have been recrystallized into polygonal grains and occur in medium-grained, granoblastic, monomineralic layers. Clinopyroxene also occurs as fine-grained granules with fine-grained recrystallized hypersthene, defining the mylonitic foliation. There is little variation in clinopyroxene composition, which is endiopside to diopside.

Two pyroxene thermometry, using adjacent recrystallized hypersthene and clinopyroxene ($Fe^T = Fe^{2+}$) gives temperatures of $817\pm20°C$ (Wood and Banno, 1973; Wells, 1977 and Lindsley, 1983-Cpx composition) and $707°C$ (Kretz, 1982). Temperature estimates using the corrections of Kretz (1982) probably represent minimum temperatures. Calculations using estimates of Fe^{3+} (Lindsley, 1983) give similar results.

Hornblende clasts and recrystallized tails are ferroanpargasite. The clasts are green-brown and the recrystallized ferroan pargasite generally is green-blue. It has lower Ti, Al^{IV}, Fe^{2+} and Na and higher Si and Mg content than the clasts.

Plagioclase clasts are commonly totally recrystallized. Plagioclase clasts and recrystallized tails have similar compositions (X_{An} = 0.48-0.51) and commonly form monomineralic layers defining the mylonitic foliation.

Sample 287 (Opx-Cpx-Pl-Hbl, Cpx-Ga-Pl-Qtz-Scap)

Sample 287 is an ultramylonitized mafic gneiss that contains layers of recrystallized garnet-diopside-scapolite. Recrystallized garnet-clinopyroxene and scapolite were probably derived from reworked calc-silicate boudins in the country rock.

Orthopyroxene clasts are hypersthene (X_{En} = 0.61) and have recrystallized tails of fine-grained hypersthene with a similar X_{Mg} (0.61-0.63) that define the mylonitic foliation. However, recrystallized hypersthene tails generally have a higher Al (total) content than the hypersthene clasts and a lower Fe^{2+} content.

Clinopyroxene is generally medium-grained and occurs in monomineralic, granoblastic layers, but also occurs as fine-grained recrystallized granules with recrystallized hypersthene defining the mylonitic foliation. Clinopyroxene clasts and recrystallized tails are augite and may occur in hypersthene-rich layers. Clinopyroxene clasts are not common but where they exist, the recrystallized tails have a lower Al and higher Ca and Fe^{2+} content than clasts.

Two pyroxene thermometry, using recrystallized granules of hypersthene and clinopyroxene ($Fe^T = Fe^{2+}$) gives temperatures of 800±20°C (Wood and Banno,1973; Wells 1977 and Lindsley 1983), similar to temperature estimates for sample 277. Calculations using Fe^{3+} estimates (Lindsley, 1983) give slightly lower (5-10°C) results. Temperature estimates using Kretz (1982) give temperatures that are about 100°C lower.

Hornblende clasts and finer-grained recrystallized hornblende are ferroan-pargasite to ferroan-pargasitic hornblende, respectively. Hornblende occurs with recrystallized hypersthene and in recrystallized garnet-clinopyroxene layers. Most hornblende has totally recrystallized. However, the recrystallized ferroan-pargasitic hornblende tends to have lower Ti, Mg and Na and higher Al^{VI} and Fe^{2+} than the clasts.

Garnet is almandine-rich ($X_{Alm} = 0.52$, $X_{Prp} = 0.24$, $X_{Grs} = 0.29$-0.31) and occurs in layers with recrystallized clinopyroxene (salite). Averaged temperature estimates using Fe-Mg exchange between garnet and clinopyroxene (Ellis and Green, 1979; Krogh, 1988), at P = 6 kbar, give T = $682\pm28°C$.

Plagioclase clasts and recrystallized tails commonly form monomineralic layers defining the foliation. The recrystallized plagioclase tails commonly have a more anorthitic composition ($X_{An} = 0.76$) than the clasts. Fine-grained granoblastic scapolite is also common in the recrystallized tails of plagioclase clasts. The scapolite is Cl-bearing, contains little SO_3 and is meionite ($X_{An} = 0.70$-0.72). Recrystallized plagioclase and scapolite compositions indicate temperatures of >700°C, (Goldsmith and Newton, 1977) during mylonitization. Minor recrystallized quartz may also define the foliation.

Pressure estimates using equilibrium compositions of garnet-clinopyroxene-plagioclase-quartz (Newton and Perkins, 1982) give P = 5.4 kbar at T = 600°C and P = 5.9 kbar at T = 800°C.

Recrystallized ferroan pargasitic hornblende may also occur in the garnet-salite layers. Garnet-hornblende exchange thermometry (Graham and Powell, 1984) gives T = 700°C for $Fe^T = Fe^{2+}$ and T = 708°C for estimates of Fe^{3+}. Pressure estimates using this assemblage hornblende-garnet-plagioclase-quartz (Kohn and Spear, 1989) give P = 6.1 ± 1.56 at T = 600°C and P = 6.5 ± 1.2 kbar at T = 800°C. Average pressure calculations (Powell and Holland, 1988; Holland and Powell, 1990) using compositions

196

of recrystallized clinopyroxene, garnet, ferroan-pargasitic hornblende and plagioclase give slightly higher pressures and show a significant dependence on water activity, best results (σfit minimized) being obtained with a_{H2O} = 0.5-0.7. An average pressure calculation using a_{H20} = 0.7 gives P = 7.2±1.5 kbar at 700°C and P = 7.5±1.6 at T = 750°C.

Average pressure calculations using recrystallized orthopyroxene, ferroan-pargasitic hornblende plagioclase and quartz also show a significant dependence on water activity, best results also being obtained with an a_{H2O} = 0.5-0.7. An average pressure calculation using a_{H2O} = 0.7 at 700°C gives P = 6.4±1.7 kbar and P = 7.8±1.8 at T = 750°C.

The intersection of P-T lines calculated for sample 287 are shown in Fig. 5.10a. Estimated mean conditions during ultramylonitization, using the intersection of P-T lines, is P = 6.6±1.0 kbar and T = 740±50°C.

Sample 288 (Opx-Ga-Pl-Qtz, Hbl-Ga, Cpx)

Sample 288 is an ultramylonitized orthopyroxene-garnet felsic gneiss that contains minor boudins of mafic two pyroxene granofels. Recrystallized fine-grained, euhedral to subhedral orthopyroxene and garnet form granular layers that define the mylonitic foliation and may also appear as symplectic intergrowths on a back-scatter electron image. Orthopyroxene clasts up to 0.5 cm in diameter and fine-grained recrystallized tails are hypersthene (X_{En} = 0.49-0.51). The clasts are commonly zoned, with Al (total) increasing and Ca decreasing slightly towards the rim. X_{Mg} in hypersthene clasts has an opposite zoning profile to Al content (Fig. 5.9), which reflects a decrease in Mg and an increase in Fe towards the clast margin. The recrystallized hypersthene tails have a low-Al content (0.82 wt%) similar to the clast centres and unlike the composition of the clast margins (up to 1.68 wt%). X_{Mg} in the recrystallized tails is generally similar to or higher than in the clast centres and unlike that in the clast margins. This implies that the
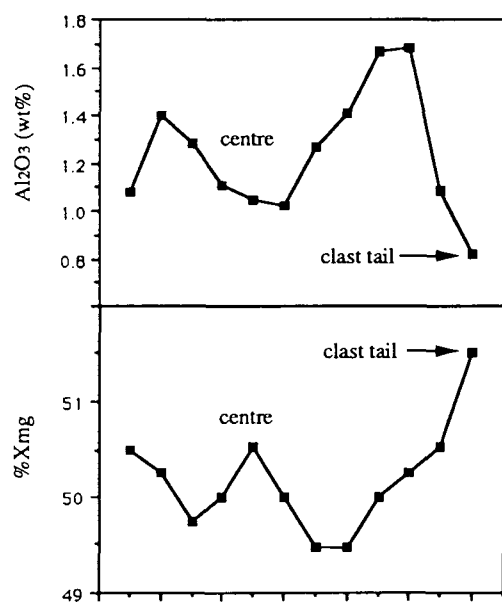
Fig. 5.9 Zoning profiles across a hypersthene porphyroclast from sample 288.

zoning profiles across hypersthene clasts are not related to diffusion processes during mylonitization, but reflect previous metamorphic conditions.

Garnet is almandine-rich (X_{Alm} = 0.59-0.62, , X_{Grs} = 0.20, X_{Prp} = 0.14) and shows no difference in composition between the fine-grained garnet intergrown with recrystallized hypersthene and larger garnet clasts. Pressure estimates obtained using recrystallized hypersthene and garnet compositions (Harley, 1984a) give P = 7.9 at T = 650°C and P = 6.45 kbar at T = 800°C. Temperature estimates using Fe-Mg exchange between hypersthene and garnet (Harley, 1984b) give T = 533-556°C between 4-9 kbar, which is significantly lower than temperatures estimated using two pyroxene thermometry and garnet-clinopyroxene thermometry in samples 277 and 287 and garnet-hornblende thermometry in sample 288.

Plagioclase clasts and recrystallized tails occur in the hypersthene-garnet layers and also as monomineralic layers defining the mylonitic foliation. Plagioclase clasts are andesine (X_{An} = 0.41) and the recrystallized tails are oligoclase (X_{An} = 0.28). Polygonal medium-grained quartz may also define the mylonitic foliation.

Recrystallized plagioclase, quartz, hypersthene and garnet occur in apparent equilibrium and can also be used to estimate pressure. Pressure estimates vary from 8.0±0.7 kbar (Perkins and Chipera, 1985) to 7.1 kbar (Newton and Perkins, 1982) at T = 700°C. Average pressure calculations (Powell and Holland, 1988; Holland and Powell, 1990) using recrystallized hypersthene, garnet, plagioclase and quartz give, P = 6.1±0.8 kbar at T = 500°C and P = 9.1±2.2 kbar at 700°C.

A thin layer, up to 0.5 cm wide, of clinopyroxene-hornblende-garnet also occurs in sample 288 and probably represents a mylonitized mafic layer or mafic boudin within the felsic gneiss. The clinopyroxene is salite and occurs as medium-grained polygonal grains. The larger hornblende grains are magnesian hastingsite and have the same composition as the smaller recrystallized grains. Minor almandine-rich garnet (X_{Alm} =

199

0.59) also occurs in the salite-hastingsite layer in microstructural equilibrium with the hastingsite.

Garnet-hornblende Fe-Mg exchange thermometry (Graham and Powell, 1984) gives T = 779°C for $Fe^T = Fe^{2+}$ and T = 669°C if Fe^{3+} is estimated. Pressure estimates using the assemblage hornblende-garnet-plagioclase-quartz (Kohn and Spear, 1989) give P = 7.1±2.3 at T = 600°C and P = 7.8±1.4 kbar at T = 800°C.

Average pressure calculations (Powell and Holland, 1988; Holland and Powell, 1990), using recrystallized clinopyroxene, hastingsite, plagioclase and quartz, show a significant dependence on water activity, best results (σfit minimized) being obtained with a_{H2O} = 0.1-0.3. An average pressure calculation using a_{H2O} = 0.1 at 700°C gives P = 6.4±1.8 kbar for a suggested temperature of T = 675°C.

The intersection of P-T lines (Fig. 5.10b), calculated using assemblages from sample 288, gives mean conditions of P = 7.3±0.8 kbar and T = 655±95°C.

Sample 300 (Opx-Pl-Qtz)

Recrystallized fine-grained polygonal orthopyroxene forms granular layers that define the mylonitic foliation. Orthopyroxene clasts and recrystallized tails are hypersthene (X_{En} = 0.5) but the hypersthene in the tails commonly has a lower Al content. The clasts are generally zoned with low-Al cores, compositionally similar to the recrystallized tails, and Al content increasing towards the rim. Ca content tends to increase with increasing Al content. Plagioclase clasts are anorthite to andesine and the recrystallized tails are more albitic in composition (X_{An} = 0.41). Polygonal medium-grained quartz and fine-grained plagioclase monomineralic layers also define the mylonitic foliation.

Sample 450 (Cpx-Pl-Scap-Hbl)

Clinopyroxene occurs as clasts and recrystallized tails defining the foliation. The clinopyroxene clasts are augite, whereas the recrystallized tails have lower Al and Fe

and higher Ca and Mg than the clasts and are salite in composition. Hornblende clasts and recrystallized tails are ferroanpargasite and occur with clinopyroxene. The ferroanpargasite in the tails are lower in Ti, Al^T and Na+K and higher in Si, Mg and Ca than in the clasts. Scapolite ($X_{An} = 0.62$) occurs as granoblastic, polygonal grains in monomineralic layers or with fine-grained, recrystallized plagioclase ($X_{An} = 0.41$) in the mylonitic foliation. Recrystallized plagioclase tails are more albitic ($X_{An} = 0.55$) than plagioclase clasts ($X_{An} = 0.61$).

Sample 191 (Cpx-Ga-Hbl-Scap-Pl-Qtz)

Clinopyroxene clasts and recrystallized tails define the mylonitic foliation. The clasts are augite and have higher Al_2O_3 and FeO and lower MgO and CaO than the recrystallized tails, which are augite to salite. Garnet is almandine-rich ($X_{Alm} = 0.53$, $X_{Grs} = 0.29-0.31$) and occurs with recrystallized clinopyroxene. Recrystallized garnet tends to have a lower grossular content and higher pyrope content than garnet clasts, but the compositional difference is minor. Garnet-clinopyroxene thermometry (Ellis and Green, 1979; Krogh, 1988) at P = 6 kbar gives T = 718±16°C. Plagioclase clasts and recrystallized tails generally occur as monomineralic layers also defining the foliation. Plagioclase clasts are more anorthitic ($X_{An} = 0.68$) than their recrystallized tails ($X_{An} = 0.45$). Fine-grained Cl-bearing scapolite also occurs with plagioclase in the recrystallized tails. Granoblastic quartz occurs in layers or with recrystallized plagioclase. Pressure estimates using equilibrium compositions of garnet-plagioclase-clinopyroxene-quartz (Newton and Perkins, 1982) give P = 5.5 kbar at T = 600°C and P = 6.8 kbar at T = 800°C.

Hornblende clasts and recrystallized hornblende are magnesian hastingsite and also occur in the garnet-clinopyroxene layers. The recrystallized hastingsite tails are higher in Si and lower in Al^T and Ti than the clasts. Garnet-hornblende thermometry (Graham and Powell, 1984) gives T = 779°C for $Fe^T = Fe^{2+}$ and T = 623°C for estimates of Fe^{3+}. The assemblage hornblende-garnet-plagioclase-quartz (Kohn and Spear, 1989) gives P = 6.5±1.95 at T = 600°C and P = 7.1±1.2 kbar at T = 800°C. Average pressure

calculations (Powell and Holland, 1988; Holland and Powell, 1990) using recrystallized clinopyroxene, garnet, hornblende, plagioclase and quartz show a significant dependence on water activity. Pressures decrease with increasing a_{H_2O}, but σfit is minimized for low a_{H_2O} = 0.1-0.3. An average pressure calculation using a_{H_2O} = 0.3 at 700°C gives P = 6.5±1.5 kbar.

The intersection of P-T lines (Fig. 5.10c) calculated using assemblages from sample 191, gives mean conditions of P = 7.0±1.1 kbar and T = 740±40°C.

Sample 451 (Cpx-Ga-Pl-Kfs-Qtz)

Clinopyroxene is ferroaugite and occurs as clasts and fine-grained recrystallized tails defining the foliation. The clast cores tend to have higher Al (total) and Fe^{2+} and lower Mg than the recrystallized diopside that occurs in the mylonitic foliation. Garnet is grossular-rich and occurs with recrystallized clinopyroxene. The grossular content is greater and almandine content is lower in the clasts (X_{Grs} = 0.59, X_{Alm} = 0.26) than in the recrystallized tails (X_{Grs} = 0.51, X_{Alm} = 0.38). The andradite content is low, but decreases slightly in the tails, suggesting that the oxidation state during mylonitization was not significantly different from conditions prior to mylonitization. The recrystallized garnet composition lies on the limit for garnet compositions used to calibrate the garnet-clinopyroxene thermometer (Ellis and Green, 1979) and may be unreliable for temperature estimates. Garnet-clinopyroxene thermometry using the recrystallized garnet composition (Ellis and Green, 1979; Krogh, 1988) at P = 6 kbar, gives T = 698-796°C.

Plagioclase clasts and tails may also define the foliation and have similar compositions (X_{An} = 0.92-0.94), suggesting that the clasts have re-equilibrated during mylonitization. Fine-grained Cl-bearing scapolite (X_{An} = 0.79) also occurs with anorthite in the recrystallized tails of plagioclase clasts, indicating temperatures of about 750-800°C (Goldsmith and Newton, 1977) during mylonitization.

Average pressure calculations (Powell and Holland, 1988; Holland and Powell, 1990), using recrystallized clinopyroxene, garnet, plagioclase and quartz, have a poor σfit, suggesting that this assemblage is unreliable for pressure estimates. However, the geobarometer of Newton and Perkins (1982) gives P = 5.6 kbar at T = 750°C using Fe^T = Fe^{2+} and P = 6.6 kbar, if Fe^{3+} is estimated.

5.41 Interpretation

The intersection of all P-T lines (Fig. 5.10d), derived using the above recrystallized assemblages, gives an estimate of the mean metamorphic conditions during ultramylonitization, namely P = 7.1±1.3 kbar and T = 770±80°C.

Ultramylonitized pelitic/are characterized by neocrystallization of sillimanite and biotite, and and ultramylonitized felsic gneisses by recrystallization of orthopyroxene and almandine-rich garnet in rocks of appropriate composition. Nowhere is kyanite, gedrite or cordierite recognized in the shear zones. Although the lack of these minerals may be a function of bulk composition, their absence may also imply that deformation occurred at higher temperatures than the kyanite-gedrite stability field and higher pressures than the cordierite stability field.

Pressure estimates show a significant dependence on water activity. Water activity estimates are very variable and are strongly dependent on the country rock composition during ultramylonitization. Best results for for felsic and calc-silicate ultramylonites were obtained using a low water activity, $a_{H2O}\sim0.1$. However, best results for mafic ultramylonites were obtained using $a_{H2O}\sim0.7$.

Ultramylonitized mafic gneisses and granofelses are characterized by recrystallized clinopyroxene with lower Al and higher Ca and Fe^{2+} than clinopyroxene clast centres, and recrystallized orthopyroxene with higher Al and lower Ca and Mg than orthopyroxene clast centres. This indicates lower temperatures during recrystallization of the clasts (Lindsley, 1983). Recrystallized clinopyroxene in microstructural equilibrium with garnet in calc-silicate ultramylonites also has lower Al and higher Ca than the clasts,

Table 2. Represenative microprobe analyses from ultramylonitized mafic gneisses.

wt%	sample 277								sample 287										
	Opx clast	Opx in tail	Cpx at Opx margin	Cpx polygonal	Pl clast	Pl in tail	Hbl clast	Hbl recryst	Opx clast	recryst Opx	Cpx clast	recryst Cpx	Hbl clast	recryst Hbl	Pl clast	recryst Pl	Scap	Grt	Cpx adj to Grt
SiO_2	52.67	51.92	52.22	52.34	55.4	55.13	40.65	41.6	53.19	53.15	51.76	51.65	42.27	42.26	51.23	49.14	46.61	39.13	52.59
TiO_2	-	-	-	-	-	-	2.04	1.8	-	-	0.47	-	1.79	1.76	-	-	-	-	-
Al_2O_3	1.22	1.43	1.83	1.87	28.54	28.14	12.73	12.34	1.37	1.79	2.77	2.43	12.59	13.14	31.44	32.67	28.5	21.88	2.45
Cr_2O_3	-	-	0.23	0.4	-	-	0.23	-	-	-	0.33	-	-	-	-	-	-	-	-
FeO	23.67	23.98	7.66	7.99	-	0.37	15.43	15.16	23.66	22.94	8.43	8.73	13.12	13.45	-	-	0.49	25.41	7.97
MnO	0.4	0.34	-	-	-	-	0.23	-	0.39	0.32	-	-	-	-	-	-	-	0.9	-
MgO	22.05	21.3	14.53	13.97	0.35	-	10.87	11.19	21.79	21.81	13.55	13.43	12.52	11.66	-	-	0.29	6.49	13.66
CaO	0.3	1	22.75	22.97	10.4	10.35	11.92	11.94	0.31	0.57	22.46	22.89	12.17	11.54	13.91	15.88	15.73	7.4	23.05
Na_2O	-	-	0.75	0.6	5.6	5.76	1.56	1.44	-	-	0.89	0.57	2.25	1.85	3.68	2.73	3.12	-	0.64
K_2O	-	-	-	-	0.19	0.21	2.24	2.18	-	-	-	-	0.76	0.78	-	-	1.24	-	-
Cl	-	-	-	-	-	-	0.84	0.8	-	-	-	-	0.28	0.33	-	-	0.26	-	-
TOTAL	100.31	99.97	99.97	100.14	100.48	99.96	98.74	98.45	100.71	100.58	100.66	99.7	97.75	96.77	100.26	100.42	96.24	101.21	100.36

Structural analysis

	sample 277								sample 287										
on basis of	6(O)	6(O)	6(O)	6(O)	32(O)	32(O)	23(O)	23(O)	6(O)	6(O)	6(O)	6(O)	23(O)	23(O)	32(O)	32(O)	32(O)	12(O)	6(O)
Si	1.96	1.95	1.93	1.94	9.93	9.96	6.1	6.23	1.98	1.97	1.91	1.93	6.24	6.26	9.29	8.95	9.03	3	1.94
Ti	-	-	-	-	-	-	0.23	0.2	-	-	0.01	-	0.2	0.2	-	-	-	-	-
Al^{IV}	0.04	0.06	0.07	0.06	6.03	5.99	1.9	1.77	0.03	0.03	0.1	0.08	1.76	1.74	6.71	7.01	6.51	1.97	0.06
Al^{VI}	0.02	0.01	0.01	0.02			0.35	0.4	0.04	0.05	0.03	0.03	0.43	0.56			-	-	0.05
Cr	-	-	0.01	0.01	-	-	0.03	-	-	-	0.01	-	-	-	-	-	-	-	-
Fe^{2+}	0.71	0.71	0.12	0.17	-	0.06	1.94	1.9	0.74	0.71	0.16	0.18	1.62	1.67	-	-	0.08	1.59	0.19
Fe^{3+}	0.02	0.05	0.12	0.08	-	-	-	-	-	-	0.1	0.09	-	-	-	-	-	0.03	0.06
Mn	0.01	0.01	-	-	-	-	0.03	-	0.01	0.01	-	-	-	-	-	-	-	0.06	-
Mg	1.22	1.19	0.8	0.77	0.09	-	2.43	2.5	1.21	1.21	0.74	0.75	2.75	2.58	-	-	0.08	0.74	0.75
Ca	0.01	0.04	0.9	0.91	2	2	1.91	1.92	0.01	0.02	0.89	0.91	1.92	1.83	2.7	3.1	3.27	0.61	0.91
Na	-	-	0.05	0.04	1.95	2.02	0.45	0.42	-	-	0.06	0.04	0.64	0.53	1.3	0.96	1.17	-	0.05
K	-	-	-	-	0.04	0.05	0.43	0.42	-	-	-	-	0.14	0.15	-	-	0.31	-	-
TOTAL	3.99	4.02	4.01	4	20.04	20.08	15.8	15.76	4.02	4	4.01	4.01	15.7	15.52	20	20.02	20.45	8	4.01
X_{Mg}*	0.63	0.63	0.87	0.82			0.56	0.57	0.62	0.63	0.82	0.81	0.63	0.61				0.32	0.80
Wo	0.01	0.02	0.44	0.45					0.01	0.01	0.44	0.44							0.45
En	0.63	0.62	0.49	0.46					0.61	0.62	0.46	0.45							0.44
Fs	0.36	0.36	0.07	0.1					0.38	0.37	0.1	0.11							0.11

* $Mg/Mg+Fe^{2+}$

Table 5.3 Represenative microprobe analyses from ultramylonitized felsic gneisses.

	sample 288									sample 300		
wt%	Opx in tail	Opx clast centre	Opx clast rim	Grt with recyst Opx	Pl clast	Pl in tail	Cpx polgonal	Grt with amph	Hbl with Grt	Opx clast	Opx in tail	Opx clast 30 um from rim
SiO_2	51.4	51.6	51.27	37.79	58.4	57.63	51.88	38.03	38.73	50.39	52.12	50.17
TiO_2	-	-	-	-	-	-	-	-	1.75	-	-	-
Al_2O_3	0.82	1.11	1.08	21.22	26.28	26.45	1.56	21.17	13.49	1.25	0.96	1.57
Cr_2O_3	-	-	-	-	-	-	-	0.21	-	-	-	-
FeO	29.93	29.86	29.68	29.52	0.28	0.63	11.91	29.35	20.84	30.97	29.99	30.72
MnO	0.45	0.78	0.6	1.61	-	-	0.39	1.33	-	0.43	0.41	0.4
MgO	17.61	16.82	17.05	3.57	-	-	11.7	3.98	7.28	16.98	16.97	17.24
CaO	0.42	0.51	0.46	7.1	8.16	6.07	22.41	7.26	11.45	0.39	0.27	0.33
Na_2O	-	-	-	-	6.51	8.63	0.65	-	0.94	-	-	-
K_2O	-	-	-	-	0.17	0.25	-	-	2.8	-	-	-
Cl									1.5			
TOTAL	100.63	100.68	100.14	100.81	99.8	99.66	100.5	101.33	98.78	100.41	100.72	100.43

Structural analysis

	sample 288									sample 300		
on basis of	6 (O)	6 (O)	6 (O)	12 (O)	32 (O)	32 (O)	6 (O)	12 (O)	23 (O)	6(O)	6 (O)	6 (O)
Si	1.97	1.98	1.98	2.97	10.46	10.39	1.95	2.97	5.98	1.94	2	1.93
Ti	-	-	-	-	-	-	-	-	0.2	-	-	-
Al^{IV}	0.03	0.02	0.02	1.97	5.55	5.62	0.06	1.95	2.02	0.06	0.04	0.07
Al^{VI}	0.01	0.03	0.03				0.01		0.43	-	-	-
Cr	-	-	-	-	-	-	-	0.01	-	-	-	-
Fe^{2+}	0.93	0.96	0.96	1.85	0.04	0.1	0.28	1.81	2.13	0.94	0.96	0.99
Fe^{3+}	0.03	-	-	0.09			0.09	0.11	0.56	0.06	-	-
Mn	0.02	0.03	0.02	0.11	-	-	0.01	0.09	-	0.01	0.01	0.01
Mg	1.01	0.96	0.98	0.42	-	-	0.65	0.46	1.68	0.98	0.97	0.99
Ca	0.02	0.02	0.02	0.6	1.57	1.17	0.9	0.61	1.89	0.02	0.01	0.01
Na	-	-	-	-	2.26	3.01	0.05	-	0.28	-	-	-
K	-	-	-	-	0.04	0.06	-	-	0.55	-	-	-
TOTAL	4.02	4	4.01	8.01	19.92	20.35	4	8.01	15.72	4.01	3.99	4
X_{Mg}*	0.52	0.50	0.51	0.19			0.70	0.20	0.44	0.51	0.50	0.50
Wo	0.01	0.01	0.01				0.45			0.01	0.01	0.01
En	0.51	0.49	0.49				0.38			0.5	0.49	0.51
Fs	0.48	0.5	0.5				0.17			0.49	0.5	0.48

* $Mg/Mg+Fe^{2+}$

Table 5.4 Represenative microprobe analyses from ultramylonitized calc-silicate rocks.

	sample 450								sample 451							sample 191									
wt%	Cpx clast	Cpx tail	Hbl clast	recryst Hbl	Pl clast	Pl tail	Scap	recryst Pl	Grt clast	recryst Grt	Cpx clast	recryst Cpx	Pl clast	Pl in tail	Scap in tail	Cpx clast	recryst Cpx	Grt clast	recryst Grt	Pl clast	Pl in tail	Scap in tail	Scap polygonal	Hbl clast	recryst Hbl
SiO_2	52.16	52.54	40.42	41.67	55.46	54.92	49.46	57.5	38.24	38.24	47.9	48.47	44.84	44.66	46.49	50.15	50.48	37.82	38.09	50.94	56.21	50.85	48.73	38.58	39.29
TiO_2	-	-	1.65	1.14	-	-	-	-	-	0.23	-	-	-	-	-	0.28	-	-	-	-	-	-	-	1.75	0.93
Al_2O_3	2.11	0.97	13.26	12.79	29.35	28.93	26.51	27.21	18.4	19.01	3.4	2.66	35.39	35.24	28.23	2.56	2.04	20.92	21.1	31.39	27.93	27.72	27.66	13.55	13.29
Cr_2O_3	0.22	-	-	0.27	-	-	-	-	-	-	-	0.23	-	-	-	0.25	-	-	-	-	-	-	-	-	-
FeO	9.53	8.82	17.15	17.16	-	-	-	0.4	18.79	22.3	19.4	19	0.24	0.39	0.34	14.41	13.67	26.8	26.01	0.24	0.26	0.39	0.39	21.4	21.9
MnO	0.43	0.29	0.26	-	-	-	-	-	1.35	0.87	-	0.34	-	-	-	0.25	0.31	2.31	2.98	-	-	-	-	-	-
MgO	13.09	13.65	9.14	9.97	-	-	0.24	-	0.47	0.65	5.92	6.67	-	-	-	9.67	10.19	2.06	2.3	-	-	0.23	0.3	7.01	6.98
CaO	22.04	23.54	11.7	11.97	11.36	11.31	15.22	8.44	23.61	19.43	22.73	22.51	18.69	19.04	18.1	22.33	22.81	11.25	10.64	13.81	9.59	13.08	16.68	11.4	11.6
Na_2O	0.55	0.39	1.48	1.32	4.03	5.07	5.12	6.61	-	-	0.45	0.51	0.86	0.71	3.1	-	0.58	-	-	3.57	6.23	4.72	3.9	0.96	1.01
K_2O	0.12	-	1.82	1.44	-	-	0.59	-	-	-	-	-	-	-	0.54	-	-	-	-	0.14	0.22	0.59	0.66	2.44	2.29
SO_3	-	-	-	-	-	-	-	-	-	-	-	-	-	-	0.03	-	-	-	-	-	-	0.04	-	-	-
Cl	-	-	1.29	1	-	-	0.96	-	-	-	-	-	-	-	0.48	-	-	-	-	-	-	0.44	0.67	0.98	1.38
TOTAL	100.25	100.2	98.17	98.73	100.2	100.23	98.1	100.16	100.86	100.5	100.03	100.39	100.02	100.04	97.31	99.9	100.08	101.16	101.12	100.09	100.44	98.06	98.99	98.07	98.67

Structural analysis

on basis of	6(O)	6(O)	23(O)	23(O)	32(O)	32(O)	32(O)	32(O)	12(O)	12(O)	6(O)	6(O)	32(O)	32(O)	32(O)	6(O)	6(O)	12(O)	12(O)	32(O)	32(O)	32(O)	32(O)	23(O)	23(O)
Si	1.94	1.95	6.15	6.23	9.92	9.87	9.39	10.29	2.98	3.01	1.87	1.88	8.28	8.26	8.94	1.93	1.92	2.97	2.99	9.26	10.08	9.53	9.22	5.96	6.05
Ti	-	-	0.19	0.13	-	-	-	-	-	-	0.01	-	-	-	-	0.01	-	-	-	-	-	-	-	0.2	0.11
Al^{IV}	0.06	0.04	1.85	1.78	6.19	6.13	5.93	5.73	1.69	1.76	0.13	0.12	7.69	7.67	6.39	0.07	0.08	1.93	1.95	6.72	5.9	6.12	6.17	2.04	1.95
Al^{VI}	0.03	-	0.52	0.48	-	-	-	-	-	-	0.03	0.01	-	-	-	0.04	0.01	-	-	-	-	-	-	0.42	0.47
Cr	0.01	-	-	0.03	-	-	-	-	-	-	-	0.01	-	-	-	0.01	-	-	-	-	-	-	-	-	-
Fe^{2+}	0.24	0.20	2.18	1.99	-	-	-	0.06	0.86	1.24	0.51	0.47	0.04	0.06	0.06	0.45	0.32	1.63	1.63	0.04	0.04	0.06	0.06	1.32	1.24
Fe^{3+}	0.06	0.08	-	0.15	-	-	-	-	0.36	0.23	0.12	0.15	-	-	-	0.01	0.12	0.13	0.08	-	-	-	-	1.44	1.57
Mn	0.01	0.01	0.03	-	-	-	-	-	0.09	0.06	-	0.01	-	-	-	0.01	0.01	0.15	0.2	-	-	-	-	-	-
Mg	0.73	0.76	2.07	2.22	-	-	0.07	-	0.06	0.08	0.35	0.39	-	-	-	0.55	0.58	0.24	0.27	-	-	0.06	0.08	1.61	1.6
Ca	0.88	0.94	1.91	1.92	2.18	2.18	3.09	1.62	1.97	1.64	0.95	0.94	3.7	3.77	3.73	0.92	0.93	0.95	0.89	2.69	1.84	2.63	3.38	1.89	1.92
Na	0.04	0.03	0.44	0.38	1.4	1.77	1.88	2.29	-	-	0.03	0.04	0.31	0.25	1.16	-	0.04	-	-	1.26	2.17	1.72	1.43	0.29	0.3
K	0.01	-	0.35	0.27	-	-	0.14	-	-	-	-	-	-	-	0.13	-	-	-	-	0.03	0.05	0.14	0.16	0.48	0.45
TOTAL	4.01	4.01	15.69	15.58	19.69	19.95	20.50	19.99	8.01	8.02	4	4.02	20.02	20.01	20.41	4	4.01	8	8.01	20	20.08	20.26	20.5	15.65	15.66
X_{Mg}*	0.75	0.79	0.49	0.53					0.07	0.06	0.41	0.45				0.55	0.64	0.13	0.14					0.55	0.56
Wo	0.43	0.46									0.43	0.43				0.43	0.44								
En	0.43	0.43									0.23	0.26				0.31	0.36								
Fs	0.14	0.11									0.34	0.31				0.26	0.2								

* $Mg/Mg+Fe^{2+}$

Table 5.5 P-T estimates using ultramylonite assemblages.

pressure estimates (kbar)

sample	400°C	450°C	500°C	550°C	600°C	650°C	700°C	750°C	800°C	assemblage	reference
288A	5.7	5.9	6.2	6.4	6.7	6.9	7.1	7.4	7.6	Opx-Grt-Pl-Qtz	1
288A	4.7±0.72	5.4±0.77	6.1±0.82	6.8±0.98	7.6±1.38	8.3±1.77	9.1±2.16			Opx-Grt-Pl-Qtz	2
288A	5.2±1.5	5.7±1.3	6.1±1.2	6.6±1.1	7.0±1.0	7.5±0.8	8.0±0.7	8.4±0.6	8.9±0.5	Opx-Grt-Pl-Qtz	3
288A					6.8	7.6	8.4	9.2	10	Opx-Grt-Pl-Qtz	4
288A	10.23	9.82	9.37	8.89	8.41	7.91	7.42	6.93	6.45	Opx-Grt	5
288A	6.4±3.32	6.6±2.66	6.8±2.79	7.0±2.52	7.1±2.26	7.3±1.99	7.5±1.73	7.7±1.46	7.8±1.35	Grt-Hbl-Pl-Qtz	6
288A				2.7±1.45	3.9±1.58	5.1±1.70	6.4±1.82	7.7±1.93	9.0±2.05	Grt-Hbl-Cpx-Pl	2
287	4.8	5	5.1	5.2	5.4	5.5	5.6	5.8	5.9	Cpx-Grt-Pl-Qtz	1
287	5.8±2.45	5.9±2.12	6.0±1.79	6.0±1.65	6.1±1.56	6.2±1.47	6.3±1.38	6.4±1.29	6.5±1.21	Grt-Hbl-Pl-Qtz	6
287				6.2±2.28	6.6±1.59	6.9±1.41	7.2±1.48	7.5±1.56	7.8±1.63	Cpx-Grt-Hbl-Pl	2
287				2.7±1.32	3.9±1.45	5.2±1.56	6.4±1.67	7.8±1.78		Opx-Grt-Hbl-Pl	2
191	4.2	4.5	4.9	5.2	5.5	5.8	6.2	6.5	6.8	Cpx-Grt-Pl-Qtz	1
191	5.9±3.11	6.0±2.81	6.2±2.51	6.30±2.22	6.5±1.95	6.6±1.90	6.8±1.75	6.9±1.6	7.1±1.45	Grt-Hbl-Pl-Qtz	6
191				2.7±1.21	4.0±1.31	5.2±1.40	6.5±1.50	7.8±1.59	9.1±1.68	Cpx-Grt-Hbl-Pl	2
451	4.9	5	5.1	5.2	5.3	5.4	5.5	5.6	5.6	Cpx-Grt-Pl-Qtz	1

1 Newton and Perkins (1982)
2 Powell and Holland (1988)
3 Perkins and Chipera (1985)
4 Bohlen et al. (1983)
5 Harley (1984)
6 Kohn and Spear (1989)

temperature estimates (°C)

sample	4 kbar	5 kbar	6 kbar	7 kbar	8 kbar	9 kbar	assemblage	reference
288A	533	538	542	547	551	556	Opx-Grt	1
288A				779			Hbl-Grt	2
287				801			Opx-Cpx	3
287				798			Opx-Cpx	4
287				661			Opx-Cpx	5
287				780±20			Opx-Cpx	6
287	701	704	706	709	712	715	Grt-Cpx	7
287	648	651	654	657	660	663	Grt-Cpx	8
287				700			Hbl-Grt	2
277A				817			Opx-Cpx	3
277A				826			Opx-Cpx	4
277A				708			Opx-Cpx	5
277A				830±20			Opx-Cpx	6
191	728	731	734	736	739	742	Grt-Cpx	7
191	696	699	702	705	708	711	Grt-Cpx	8
191				779			Hbl-Grt	2
451	791	793	796	798	801	803	Grt-Cpx	7
451	693	695	698	700	703	706	Grt-Cpx	8
451				750-800			Pl-Scap	9

1 Harley (1984)
2 Graham and Powell (1984)
3 Wood and Banno (1973)
4 Wells (1977)
5 Kretz (1982)
6 Lindsley (1983)
7 Ellis and Green (1979)
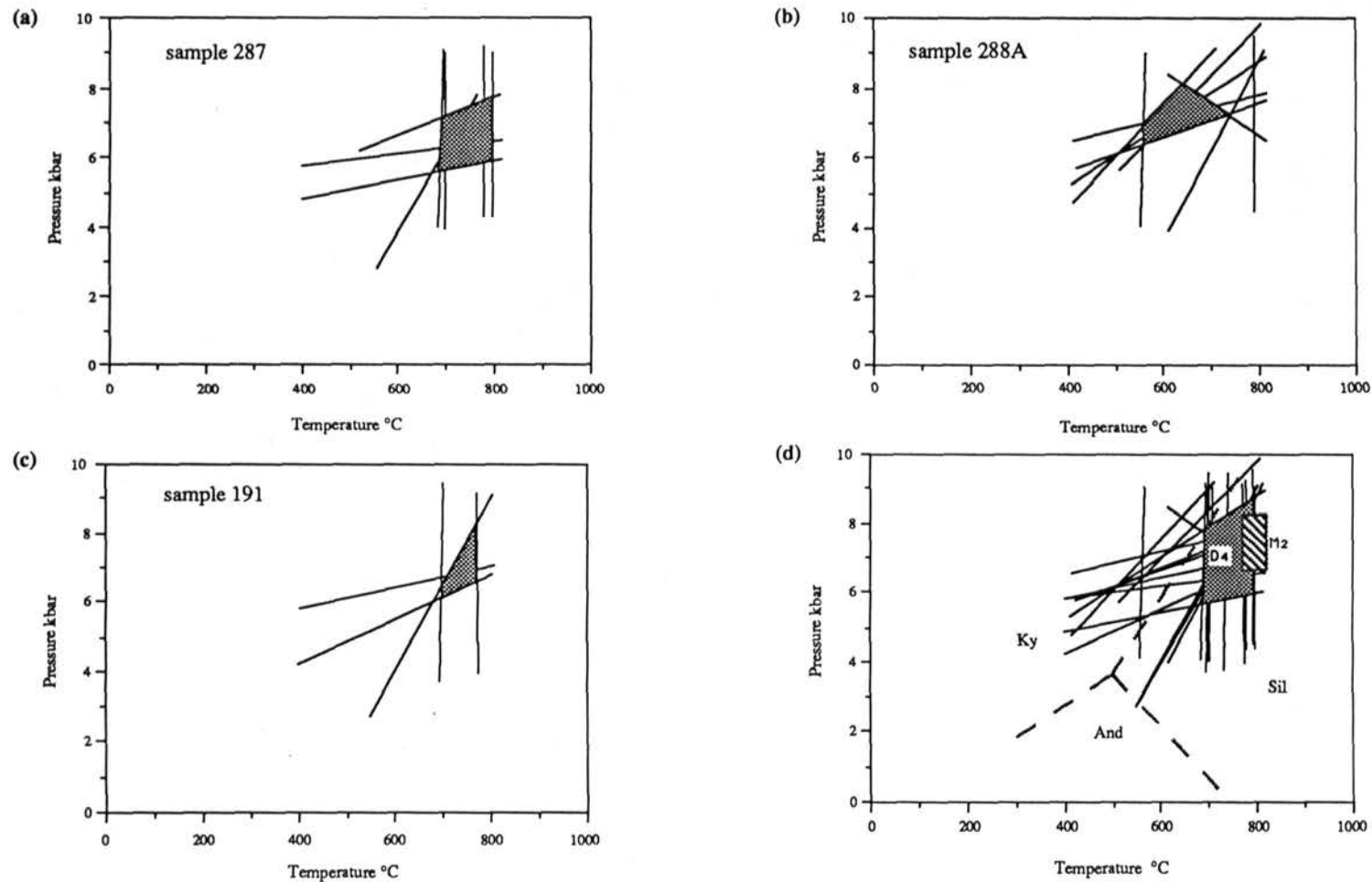8 Krogh (1985)
9 Goldsmith and Newton (1977)

Fig. 5.10 (a) P-T lines estimate using assemblages in samples 287.
    5.10 (b) P-T lines estimate using assemblages in sample 288A.
    5.10 (c) P-T lines estimate using assemblages in sample 191.
    5.10 (d) P-T lines from (a), (b), (c) and area of best fit for
        ultramylonitization and M₂.

which also probably reflects lower temperatures during ultramylonitization. Recrystallized hornblende in mafic and calc-silicate ultramylonites generally has lower Ti, Al^{IV}, Fe and Na+K and a higher Si and Mg than the clasts. This probably reflects lower temperatures and/or increased f_{O_2} during mylonitization (Spear, 1981).

Plagioclase clasts and recrystallized tails commonly form monomineralic layers defining the mylonitic foliation. Plagioclase clasts are generally totally recrystallized, but where they are not totally recrystallized, the recrystallized tails are more albitic than the clasts, probably reflecting cooler conditions during mylonitization. Fine-grained Cl-bearing scapolite also may occur in the recrystallized tails of plagioclase clasts, owing to the breakdown of plagioclase, indicating temperatures probably in excess of 700°C (Goldsmith and Newton, 1977) during mylonitization.

Temperature estimates from porphyroclast compositions are generally higher than those from the recrystallized assemblages, although accurate temperature estimates could not be determined because of zoning in some clasts. Similarly, pressure estimates using porphyroclasts are inaccurate. Orthopyroxene clasts in ultramylonitized felsic gneisses are commonly zoned in Al, Fe and Mg content. This zonation appears to be unrelated to the composition of the recrystallized tails and probably reflects previous metamorphic conditions, thus indicating relatively rapid re-equilibration and a high strain-rate during ultramylonitization.

5.5 Discussion

The microstructures and assemblages preserved in the foliated gneisses and the shear zones of the Strangways Metamorphic Complex are related to processes that occurred prior to uplift of the block to the earth's surface, as no microstructures indicative of substantial isothermal decompression (e.g. reaction coronas) have been observed. M_2 metamorphism, D_3 folding and D_4 ultramylonitization in the Strangways Metamorphic Complex post-date the main granulite facies event (M_1) and were probably unlike the processes that produced M_1, which was characterized by low-pressure, high-

temperature metamorphism typical of many Proterozoic terrains (Norman and Clarke, 1990; Chapters 3 and 4). The timing of M_2/D_3 and D_4 is not known, except that they post-date cooling from the metamorphic peak and predate widespread retrogression along D_5 shear zones that bound the Strangways Metamorphic Complex. An estimated cooling rate of 1-5°C/Ma from peak metamorphism appears to be common in granulite terrains (Bohlen, 1991). Using a cooling rate of <5°C/^{Ma} would suggest that the D_4 shear zone deformation (at 700°C) occurred between 200 Ma and 40 Ma after the metamorphic peak (at 900°C) and between 100 Ma and 20 Ma after M_2 (at 800°C). D_4 ultramylonitization occurs within the erosional time constant (20-110 my) for erosion of an overthrust continental crust (England and Richardson, 1977) after M_2. This suggests that D_4 may have been part of the same orogenic cycle responsible for M_2.

The Strangways Metamorphic Complex was probably brought to the surface during movement along north-dipping retrogressed mylonite zones that bound the complex. However, it is not known whether rotation of F_3/F_4 fold axes, stretching lineations and north-dipping D_4 shear zones occurred during uplift of the complex along these mylonite zones. Any block rotation along north-dipping listric reverse faults would increase the dip of D_3/D_4 structures and an initial sub-horizontal to low angle attitude of L_3, F_3/F_4 fold axes and D_4 shear zones cannot be dismissed. Deformation in the D_4 shear zones occurred in the sillimanite stability field. Kyanite occurs in the retrogressed D_5 shear zones (Warren, 1983a) that bound the Strangways Metamorphic Complex but is not found in any of the D_4 shear zones described in this paper. M_2 assemblages in the Strangways Metamorphic Complex indicate an increase in pressure to P = 7.5±0.8 kbar during M_2 (Norman and Clarke, 1990; Chapters 3 and 4) and there is no evidence that the terrain cooled to a normal crustal geotherm prior to D_4 ultramylonitization. Granulite facies conditions also existed during D_4 ultramylonitization (P = 7.1±1.3 kbar and T = 770±80°C) and were similar to conditions during M_2, except for slightly lower temperatures and possibly slightly lower pressures.

The D_4 shear zones zones generally cut F_3/F_4 folds and have a normal sense of displacement subparallel to a northeast-plunging stretching lineation (L_3) and F_3/F_4 fold axes in the country rock. L_3 and F_3/F_4 fold axes are inferred to be parallel to the transport axis during D_3 (Chapter 2). D_3 may represent a crustal thickening, the effects of which are recognized by the texturally distinct 'up-pressure' M_2 assemblages (Norman and Clarke, 1990; Chapter 3). The similar metamorphic conditions during M_2 and D_4 ultramylonitization may imply that D_3 and D_4 were part of the same orogenic cycle. The colinearity of stretching lineations in the shear zones, and the inferred northnortheast-northeast tectonic transport axis during D_3 would also suggest that D_4 ultramylonitization was a continuation of D_3. A decrease in displacement along D_4 shear zones to the southeast and easterly extension associated with antithetic shear zones suggest that minor dextral extension also occurred during D_4 ultramylonitization.

5.6   Conclusions

Granulite facies ultramylonite zones cutting the Strangways Metamorphic Complex form a moderately-dipping extensional system that is unlike simple-shear detachment systems that are characteristic of large lithospheric extension. The high-angle shear zones are similar to normal faults and shear zones that occur in active A- and B-type convergence zones (c.f. Burchfiel and Royden, 1985; Dalmayrac and Molnar, 1981) as a response to crustal thickening. A prerequisite for collapse in terrains of thickened continental crust is crustal shortening to produce topographic relief and a crustal load that cannot be supported by the lithosphere. Evidence for gravitational collapse has mostly been described from the over-riding plate in a convergence zone, at upper crustal levels. Evidence for gravitational collapse at mid-crustal levels has not previously been described and may not be expected to occur because of high confining pressures. Crustal thickening during D_3, as evidenced by an increase in pressure during M_2, may provide the conditions necessary for extension that occurred at mid-crustal levels during ultramylonitization. Crustal thickening must have been significant, if the lithospheric pressure became greater than the confining pressures and gravitational collapse occurred.

Alternatively, the Strangways Metamorphic Complex may have behaved as a rigid block, with deformation concentrated into narrow high-angle normal shear zones (Etchecopar, 1977) between active north-dipping reverse shear zones. The normal displacement in the shear zones would have occurred in the footwall and be reverse to the overall sense of shear.

The displacement of similar rock types across prominent shear zones indicates that km-scale, lateral dextral displacement may have occurred in the Strangways Metamorphic Complex prior to dip-slip normal movement. Significant lateral displacement may have been the result of east-west lateral extension or transpression during a major crustal reworking event (D_3/M_2) along a northnortheast-southsouthwest axis, similar to continental escape that has been inferred in some collisional orogens (Selverstone, 1988; Ratschbacher et al., 1989).